T H E U N I V E R S I T Y O F A L B E R T A

RELEASE FORM

NAME OF AUTHOR Iain Douglas Calder

TITLE OF THESIS Measurements of the Temperature and Frequency Dependence of Longitudinal Sound in Hexagonal-Close-Packed Helium-4

DEGREE FOR WHICH THESIS WAS PRESENTED Doctor of Philosophy

YEAR THIS DEGREE GRANTED 1977

THE UNIVERSITY OF ALBERTA

MEASUREMENTS OF THE TEMPERATURE AND FREQUENCY DEPENDENCE OF LONGITUDINAL SOUND IN HEXAGONAL-CLOSE-PACKED HELIUM-4

by

© IAIN DOUGLAS CALDER

A THESIS

SUBMITTED TO THE FACULTY OF GRADUATE STUDIES AND RESEARCH

IN PARTIAL FULFILMENT OF THE REQUIREMENTS FOR THE DEGREE

OF DOCTOR OF PHILOSOPHY

IN

LOW TEMPERATURE PHYSICS

DEPARTMENT OF PHYSICS

EDMONTON, ALBERTA

FALL 1977

THE UNIVERSITY OF ALBERTA

FACULTY OF GRADUATE STUDIES AND RESEARCH

The undersigned certify that they have read, and recommend to the Faculty of Graduate Studies and Research for acceptance, a thesis entitled "MEASUREMENTS OF THE TEMPERATURE AND FREQUENCY DEPENDENCE OF LONGITUDINAL SOUND IN HEXAGONAL-CLOSE-PACKED HELIUM-4", submitted by Iain Douglas Calder in partial fulfilment of the requirements for the degree of Doctor of Philosophy in Low Temperature Physics.

ABSTRACT

The velocity and attenuation of longitudinal sound propagating in single crystals of hcp He^4 at a molar volume of 17.4 cm^3 were measured between 0.25 K and melting, and at frequencies of 5, 15 and 25 MHz. All samples showed an extremely large dispersion and in most cases a large velocity anomaly extending from between 1 and 1.8 K down to the lowest temperatures. At higher frequencies the anomaly was reduced in magnitude and it shifted to lower temperatures. The anomaly was usually positive, but in two cases it was negative and in two other cases was not present at all. The attenuation was 0.01 cm^{-1} or less near melting and increased up to 100 times by the lowest temperature, except for the two crystals without velocity anomalies; these showed no dramatic rise in attenuation. The attenuation increased with frequency. Several theories involving second sound, zero sound, dislocations and superfluidity are invoked in order to explain the effects. None was successful.

ACKNOWLEDGEMENTS

I wish to express my deep gratitude to my supervisor, Professor J. P. Franck, for his generous support and direction.

The expert technical assistance and advice of Allan O'Shea was invaluable. I wish also to thank Mrs. Ruth Nelson for her efficient and accurate typing of the manuscript for this thesis.

A special thanks goes to my wife Jane for her continual support and encouragement.

Awards of scholarships from the National Research Council and from the Province of Alberta are gratefully acknowledged.

TABLE OF CONTENTS

LIST OF TABLES

LIST OF FIGURES

CHAPTER 1

INTRODUCTION

Solid helium was originally studied with the expectation that it would prove to be the simplest and most ideal of all solids. For some physical properties these hopes have been at least qualitatively realized, but in other respects the behaviour of solid helium deviates dramatically from that of more normal solids.

Most of these unusual effects can be attributed to the quantum nature of helium. Because the atoms are very light, and interact only through a weak Van der Waals potential, they possess a very large zero point energy and experience such large excursions from their lattice sites that the wave functions of neighbouring atoms overlap to a significant extent. The symmetry of the wave functions then becomes important so that liquid He^3, a fermi particle (2 protons, 1 neutron and 2 electrons) has markedly different properties from liquid He^4, a bose particle (2 protons, 2 neutrons, 2 electrons). The localization of the atoms on lattice sites in the solid reduces the overlap so that the differences between the two isotopes are more subtle in the solid state.

Since it has a lower boiling point than any other substance, helium can be purified to an extremely high degree with simple techniques. Only disorder-type

defects will then be present. As well, single crystals of solid helium are relatively easy to grow, and it is a dielectric. For these several reasons, research on solid helium is largely free of the many spurious effects which plague the study of other more complex solids. Transport properties in particular may be observed under the nearly ideal conditions which are difficult and expensive to attain in other crystals. A lightly damped second sound mode may be propagated while the thermal conductivity exhibits the pronounced umklapp maximum and well-defined Poiseuille flow region typical of very pure dielectrics.

Solid helium has an extraordinarily high compressibility, enabling observations to be taken over a wide range of molar volumes (the volume is halved with the application of 1500 bar of pressure). Of thermodynamic interest is the fact that solid helium's high compressibility allows its properties to be measured at an essentially constant volume.

The present work may be considered in part to be the third stage of a long term project to measure the temperature, volume and frequency dependence of the attenuation of sound in solid helium. I believe the data contained in this work to be the first reliable measurements of attenuation, particularly at higher temperatures.

The most important goal of this work is to examine in greater detail the anomalous behaviour of the sound velocity which was discovered in this laboratory by Franck

and Hewko (1973) and further investigated by Wanner and Mueller (1974) and Wanner et al. (1976). The original aims were to observe the anomaly with much greater precision and to extend the measurements to lower temperatures. The high quality of the ultrasonic transducers used enabled me to successfully excite and observe the third and fifth harmonics of the fundamental frequency. This allowed not only the dispersion in solid helium to be measured for the first time in the long wavelength limit, but also the frequency dependence of the attenuation and the velocity anomaly.

Preliminary results of this work have already been published elsewhere (Calder and Franck (1977)).

CHAPTER 2

THEORY

For the study of classical lattice dynamics and sound propagation I have found particularly useful books by Maradudin et al. (1971), Born and Huang (1954), Musgrave (1970) and Reissland (1973), with supporting material from Nye (1957). There are available numerous useful reviews of quantum lattice dynamics including those by Guyer (1969), Koehler (1975) and Glyde (1976).

The most recent reviews of the properties of solid helium are the works of Wilks (1967), Keller (1969), Trickey et al. (1972) and Glyde (1976). Theories of the various contributions to the temperature dependence of the sound velocity and attenuation can be found in Bhatia (1967), Truell et al. (1969) and especially Maris (1971).

2.1 Classical Lattice Dynamics

It is obvious from numerous experiments like the present one that sound does propagate in bulk solid helium in the long wavelength limit. With this observation in mind, we can confidently go ahead and use the relations of continuum mechanics as developed in section 2.3 in order to relate the velocity of sound to such macroscopic properties of the crystal as the elastic constants. However in order to use acoustic modes effectively as probes of the properties of a solid on the atomic scale, we need

a microscopic theory of lattice dynamics. Although classical lattice dynamics are totally inadequate to describe solid helium, even with anharmonic corrections, a brief outline still serves as a useful introduction to the methods required when dealing with solid helium.

Each atom sits in the potential well created by all other atoms in the crystal. If the atoms make only very small excursions from their equilibrium positions, then the potential may be expanded into the harmonic form:

$$V = V_o + \tfrac{1}{2} \left. \frac{\partial^2 V}{\partial u^j_{s\ell}\, \partial u^{j'}_{s'\ell'}} \right|_0 u^j_{s\ell}\, u^{j'}_{s'\ell'} \qquad (2.1\text{-}1)$$

where there is summation over repeated indices and $u^j_{s\ell}$ represents the scalar displacement of atom s in unit cell ℓ in the direction j. Higher order terms may be added to (2.1-1) to give anharmonic corrections. The total kinetic energy, for atoms of mass M_s is:

$$T = \tfrac{1}{2} M_s\, \dot{u}^j_{s\ell}\, \dot{u}^j_{s\ell}. \qquad (2.1\text{-}2)$$

The equations of motion can then be easily found from Lagrange's equations giving,

$$M_s \ddot{\underline{u}}_{s\ell} = - \underline{\underline{D}}_{s\ell;s'\ell'} \cdot \underline{u}_{s'\ell'} \qquad (2.1\text{-}3)$$

where $$D^{jj'}_{s\ell;s'\ell} \equiv \left.\frac{\partial^2 V}{\partial u^j_{s\ell}\, \partial u^{j'}_{s'\ell'}}\right|_0 \qquad (2.1\text{-}4)$$

and henceforward there is no summation over s only.

Assuming only central forces are present, and using the Bloch condition,

$$\underline{u}_{s\ell}(t) = e^{i\underline{q}\cdot\underline{\ell}}\, \underline{u}_{so}(t), \qquad (2.1\text{-}5)$$

we find,

$$M_s \ddot{\underline{u}}_{s\underline{q}}(t) = - \underline{\underline{D}}_{ss'}(\underline{q})\cdot \underline{u}_{s'\underline{q}}(t), \qquad (2.1\text{-}6)$$

where $\underline{q}$ is the wave vector and,

$$\underline{\underline{D}}_{ss'}(\underline{q}) \equiv \sum_{\underline{h}} \underline{\underline{D}}_{ss';\underline{h}} e^{i\underline{q},\underline{h}} . \qquad (2.1\text{-}7)$$

Assume a plane wave solution:

$$\underline{u}_{s\underline{q}}(t) \equiv \underline{u}_{s\underline{q}} e^{i\omega t} \qquad (2.1\text{-}8)$$

so we have finally,

$$[\underline{\underline{D}}_{ss'}(\underline{q}) - M_s\omega^2(\underline{q})\delta_{ss'}\underline{\underline{I}}]\cdot \underline{u}_{s'\underline{q}} = 0 \qquad (2.1\text{-}9)$$

where $\delta_{ss'}$ is the Kronecker delta and $\underline{\underline{I}}$ the identity matrix. One can now find ω as a function of $\underline{q}$ by solving the secular equation,

$$|\underline{\underline{D}}_{ss'}(\underline{q}) - M_s\omega^2(\underline{q})\delta_{ss'}\underline{\underline{I}}| = 0. \qquad (2.1\text{-}10)$$

This equation has 3n solutions where n is the number of particles in one unit cell and the three refers to j = 1, 2, 3, the three polarizations of the vibrations. The group velocity is defined as,

$$\underline{c}_j = \underline{\nabla}_{\underline{q}}\cdot\omega_j(\underline{q}), \qquad (2.1\text{-}11)$$

but usually what one measures is the phase velocity $\underline{v}_j$, defined by,

$$\omega_j(\underline{q}) = \underline{v}_j(\underline{q})\cdot\underline{q} \quad . \qquad (2.1\text{-}12)$$

In the case where there is no dispersion, the phase velocity is identical with the group velocity.

In the long wavelength limit (i.e. for small $\underline{q}$), $\underline{\underline{D}}_{ss'}(\underline{q})$ in (2.1-10) can be expanded in powers of $\underline{q}$ (Maradudin et al (1971)) and (2.1-10) can, after some lengthy algebra, be written in the form,

$$|(C_{\alpha\beta\lambda\mu} + C'_{\alpha\lambda\beta\mu})q_\lambda q_\mu - \rho\omega_j^2\delta_{\alpha\beta}| = 0, \qquad (2.1\text{-}13)$$

where C and C' are complicated functions of the derivatives of $D_{ss'}(\underline{q})$. Equation (2.1-13) provides a link between lattice dynamics and the continuum model

discussed in section 2.3.

We can gain further insight into classical lattice dynamics by forming the Hamiltonian of the system in the harmonic approximation from (2.1-1) and (2.1-2) and diagonalizing it to give:

$$H = \tfrac{1}{2} \sum_{\underline{k}j} [|p(\underline{k}j)|^2 + \omega^2(\underline{k}j)|q(\underline{k}j)|^2] \qquad (2.1\text{-}14)$$

where

$$u^{\alpha}_{s\ell} = \xi(s\ell\alpha;\underline{k}j)\ q(\underline{k}j), \qquad (2.1\text{-}15)$$

$$\dot{u}^{\alpha}_{s\ell} = \xi(s\ell\alpha;\underline{k}j)\ p(\underline{k}j), \qquad (2.1\text{-}16)$$

and $$\omega^2(\underline{k}j) = D^{\alpha\alpha'}_{s\ell;s'\ell'}\ \xi^*(s\ell\alpha;\underline{k}j)\xi(s'\ell'\alpha';\underline{k}'j')\delta_{\underline{k}-\underline{k}'}\ , \qquad (2.1\text{-}17)$$

with $$\xi(s\ell\alpha;\underline{k}j) = M_s^{-\frac{1}{2}}\ e_{\alpha}(\underline{k}j)e^{-i\underline{k}\cdot\underline{\ell}s}\ . \qquad (2.1\text{-}18)$$

Using (2.1-18) in (2.1-17) along with the Bloch theorem once again we find:

$$[\underline{\underline{D}}(\underline{k}j) - m\omega^2(\underline{k}j)\underline{\underline{I}}]\underline{u}(\underline{k}j) = 0, \qquad (2.1\text{-}19)$$

as in equation (2.1-9).

Equation (2.1-14) then gives the Hamiltonian for a harmonic oscillator so that the quantized lattice modes, or phonons, obey Bose-Einstein statistics.

2.2 The Lattice Dynamics of Solid Helium

In most normal crystals the harmonic approximation used in equation (2.1-1) is a good one. As long as the kinetic energy of a particle is only a small fraction of the depth of the potential well, then the particle remains very near to the bottom of the potential well, where (2.1-1) is valid. Small excursions from $(\partial V/\partial u) = 0$ can usually be accounted for with small anharmonic corrections to equation (2.1-1).

The interatomic forces for helium are the Van der Waals forces, which are very weak for the tightly bound electronic shell around helium atoms. A simple approximation is the Lennard-Jones potential:

$$V(r) = 4\varepsilon \left[(\sigma/r)^{12} - (\sigma/r)^{6}\right], \qquad (2.2\text{-}1)$$

as shown by the dashed curve of figure 1. From the virial coefficients of helium gas, it is found that the helium potential has a very shallow well of $\varepsilon = 10.2$ K and a very extended hard core with $\sigma = 2.556$Å. If (2.2-1) is used in equation (2.1-10), then the sound velocity predicted by (2.1-10) is four times larger than that found experimentally. Classical lattice dynamics also predict a molar volume too small by half and a compressibility thirty times too small. On the other hand, heat capacity and thermal conductivity behave quite normally, so that some sort of long range correlations

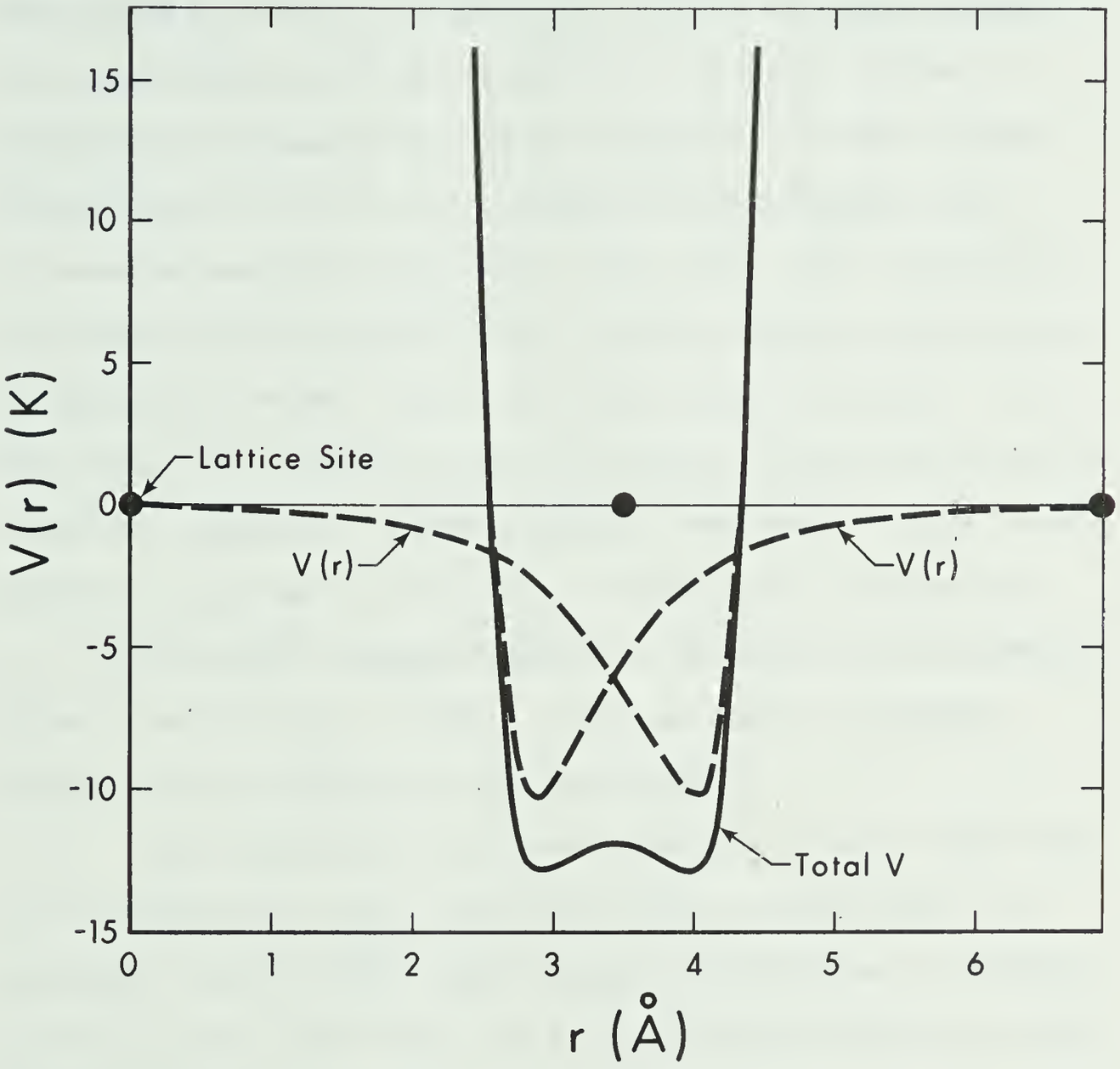

Figure 1 Interatomic potential well in solid helium-4 at 17.4 cm^3/mole.

must be present.

At P = 0, T = 0, the kinetic energy of a solid arises solely from the zero point energy ε_o. In the case of helium $\varepsilon_o \simeq V(r_o)$, where $r_o = 2^{1/6} \cdot \sigma$, so that solidification will only take place with the application of a substantial pressure (at least 25 bar). If the helium atoms were to sit at the bottom of the potential well created by neighbouring atoms, then the large excursions resulting from the zero point dynamic energy would bring neighbouring atoms' hard cores into close contact. Thus the atoms move farther apart so that we have the situation shown in figure 1. In this model, the atoms sit at local potential maxima so that their vibrational frequencies $\omega \sim 2\pi(V''(r)/m)^{\frac{1}{2}}$ become imaginary, as first calculated by DeWette and Nijboer (1965). Thus we have a complete breakdown of classical lattice dynamics.

Any successful lattice dynamical theory must take into account not only the long range correlations, or phonons, but also the short range correlations of neighbouring atoms which move in a cooperative manner in order to minimize wave function overlap.

The method which allows the simplest physical interpretation (Nosanow (1964, 1966), Fredkin and Werthamer (1965)), assumes the wavefunction proposed by Jastrow (1955):

$$\Psi = \prod_i \phi_i(r_i - \ell_i) \prod_{i<j} f(r_i - r_j), \qquad (2.2\text{-}2)$$

where $\phi_i(r_i)$ are the single particle wave functions localized at lattice sites ℓ_i, while $f(r_i - r_j)$ is a Jastrow function describing the short range correlation between particles i and j. A useful analytic form for $f(r)$ is:

$$f(r) = e^{-KV(r)} \qquad (2.2\text{-}3)$$

where K is a variational parameter. Now ϕ_o is so close to a Gaussian that we let

$$\phi_i(r_i) = e^{-Ar_i^2/2} \qquad (2.2\text{-}4)$$

and if Ψ is used in the first term of a cluster expansion for the energy E (i.e. in a variational approach),

$$E \simeq \frac{\int \Psi H \Psi}{\int \Psi^2} \quad , \qquad (2.2\text{-}5)$$

then we find

$$E = \tfrac{1}{4}\hbar \sum_{\underline{k},\lambda} \omega_{\underline{k},\lambda} + \sum_{i<j} \int \Phi^2 \, V_{eff.}(r_{ij}) \qquad (2.2\text{-}6)$$

where

$$\Phi = \prod_i \phi_i(r_i) \quad . \qquad (2.2\text{-}7)$$

$V_{eff}(r_{ij})$ is an effective potential given, for two-body interactions, by,

$$V_{eff}(r_{ij}) \simeq f^2(r_{ij})[V(r_{ij}) - \frac{\hbar^2 K}{2m} \nabla^2 V(r_{ij})]. \tag{2.2-8}$$

Then K and A are varied to minimize E.

Now the long range correlations must be properly accounted for by using self-consistent phonon theory (Nosanow and Werthamer (1965), De Wette et al. (1967)). This is essentially a Hartree method in which the frequency ω becomes a variational parameter so we set

$$\frac{\partial E}{\partial \omega_{\underline{k}\lambda}} = \frac{\hbar}{4} + \sum_{i<j} V_{eff}(r_{ij}) \frac{\partial \Phi^2}{\partial \omega_{\underline{k}\lambda}} = 0 \quad . \tag{2.2-9}$$

Then $\omega_{\underline{k}\lambda}$ are given by the determinant of the dynamical matrix

$$D_{\alpha\beta}(\underline{k}) = \frac{1}{m} \sum_{ij} (e^{-i\underline{k}\cdot\underline{r}_{ij}} - 1) \left\langle \frac{\partial^2 V_{eff}(r_{ij})}{\partial u_{i\alpha} \partial u_{j\beta}} \right\rangle , \tag{2.2-10}$$

$$\text{i.e. } |D_{\alpha\beta} - \omega^2 \delta_{\alpha\beta}| = 0. \tag{2.2-11}$$

Equation (2.2-11) resembles equation (2.1-10) very closely. Only the dynamical matrix is defined differently than in equation (2.1-7) so that the second derivatives of the potential are now averaged in order to account for

long range correlations, while an effective potential is used to allow short range correlations. With these renormalized force constants we have a quasiharmonic result in which we can still speak of phonons as good excitations in solid helium.

Several improvements have been made by using higher order terms in the cluster expansion of equation (2.2-5) (Hetherington et al. (1967)), by using a fully correlated wave function rather than a Gaussian approximation (Koehler (1967)) and by including higher order anharmonic terms in equation (2.1-1) (Koehler (1968), Koehler and Werthamer (1972)). Other recent developments in the dynamics of quantum crystals are discussed by Glyde (1976) and Koehler (1975). Most of these have been applied only to He^3.

2.3 Wave Propagation in Ideal Elastic Solids

An excellent reference work upon which I have relied heavily for the contents of this section is the book by Musgrave (1970).

If $u_i(x_j)$ is the displacement in the i direction as a function of x_j, the position within a continuous elastic medium, then for small values of the displacement we define the strain tensor as

$$\varepsilon_{ij} \equiv \tfrac{1}{2}\left(\frac{\partial u_i}{\partial x_j} + \frac{\partial u_j}{\partial x_i}\right) \quad . \qquad (2.3\text{-}1)$$

As well, the stress σ_{ij} is defined as the force per unit area acting in the i direction upon a surface with normal in the j direction. For small strains Hooke's law holds so that in general:

$$\sigma_{ij} = c_{ijk\ell}\, \varepsilon_{k\ell} \,, \tag{2.3-2}$$

where the elements of the tensor $c_{ijk\ell}$ are called the elastic stiffness constants, and from dynamic considerations,

$$c_{ijk\ell} = \frac{\partial^2 V}{\partial \varepsilon_{ij} \partial \varepsilon_{k\ell}} \bigg|_0 \,. \tag{2.3-3}$$

By symmetry arguments the number of independent elastic constants can be substantially reduced. Using the Voigt notation where $c_{ijk\ell}$ becomes a 6x6 matrix and index pairs become single indices according to the prescription 11 → 1, 22 → 2, 33 → 3, 23 or 32 → 4, 31 or 13 → 5, 12 or 21 → 6, c_{ij} for a crystal with hexagonal symmetry is:

$$c_{ij} = \begin{bmatrix} c_{11} & c_{12} & c_{13} & 0 & 0 & 0 \\ c_{12} & c_{11} & c_{13} & 0 & 0 & 0 \\ c_{13} & c_{13} & c_{33} & 0 & 0 & 0 \\ 0 & 0 & 0 & c_{44} & 0 & 0 \\ 0 & 0 & 0 & 0 & c_{44} & 0 \\ 0 & 0 & 0 & 0 & 0 & \tfrac{1}{2}(c_{11}-c_{12}) \end{bmatrix} . \tag{2.3-4}$$

The force on an infinitesimal volume is

$$\frac{\partial \sigma_{ij}}{\partial x_j} = \rho \ddot{u}_i, \tag{2.3-5}$$

so that upon substituting (2.3-1) and (2.3-2) into (2.3-5), we find,

$$c_{ijk\ell} \frac{\partial^2 u_k}{\partial x_\ell \partial x_j} - \sigma \ddot{u}_i = 0. \tag{2.3-6}$$

If we assume a plane wave form for u_k:

$$u_k = A_k \exp i\,(\underline{q}\cdot\underline{x} - \omega t), \tag{2.3-7}$$

then

$$|c_{ijk\ell}\, q_j q_\ell - \rho\omega^2 \delta_{ik}| = 0 \tag{2.3-8}$$

is the resulting secular equation from which $\omega(\underline{q})$ may be obtained. Equation (2.3-8) is identical to equation (2.1-10). Several authors including Zener (1936), Gold (1950) and Musgrave (1954) have solved equation (2.3-8) explicitly for the hexagonal case. They find that the velocity surfaces have cylindrical symmetry about the c-axis so that all velocities may be expressed in terms of a single angle γ between the c-axis and the direction of propagation. There are three mutually perpendicular polarizations: a pure transverse mode T_1, a quasi-

traverse (i.e. predominantly transverse) mode T_2 and a quasi-longitudinal mode L. These phase velocities v are given by

$$\rho v_{T_1}^2 = \tfrac{1}{2}(c_{11}-c_{12})\sin^2\gamma + c_{44}\cos^2\gamma \qquad (2.3\text{-}9)$$

$$\rho v_{T_2}^2 = \tfrac{1}{2}[(c_{11}+c_{44})\sin^2\gamma + (c_{33}+c_{44})\cos^2\gamma - \phi(\gamma)] \qquad (2.3\text{-}10)$$

$$\rho v_L^2 = \tfrac{1}{2}[(c_{11}+c_{44})\sin^2 + (c_{33}+c_{44})\cos^2\gamma + \phi(\gamma)], \qquad (2.3\text{-}11)$$

where $\phi^2(\gamma) = (c_{11}-c_{44})^2\sin^4\gamma + (c_{33}-c_{44})^2\cos^4\gamma +$

$$+ 2\sin^2\gamma\cos^2\gamma[(c_{11}-c_{44})(c_{44}-c_{33}) + 2(c_{13}+c_{44})^2]. \qquad (2.3\text{-}12)$$

The velocities for a molar volume of 17.4 cm^3 are illustrated in figure 2, using the elastic constants calculated in appendix 1.

Without loss of generality we may set the azimuthal angle equal to 90°, so that the polarizations are given by

$$p_{T_1} = (1, 0, 0) \qquad (2.3\text{-}13)$$

$$(P_{L,T_2})_1 = 0 \qquad (2.3\text{-}14)$$

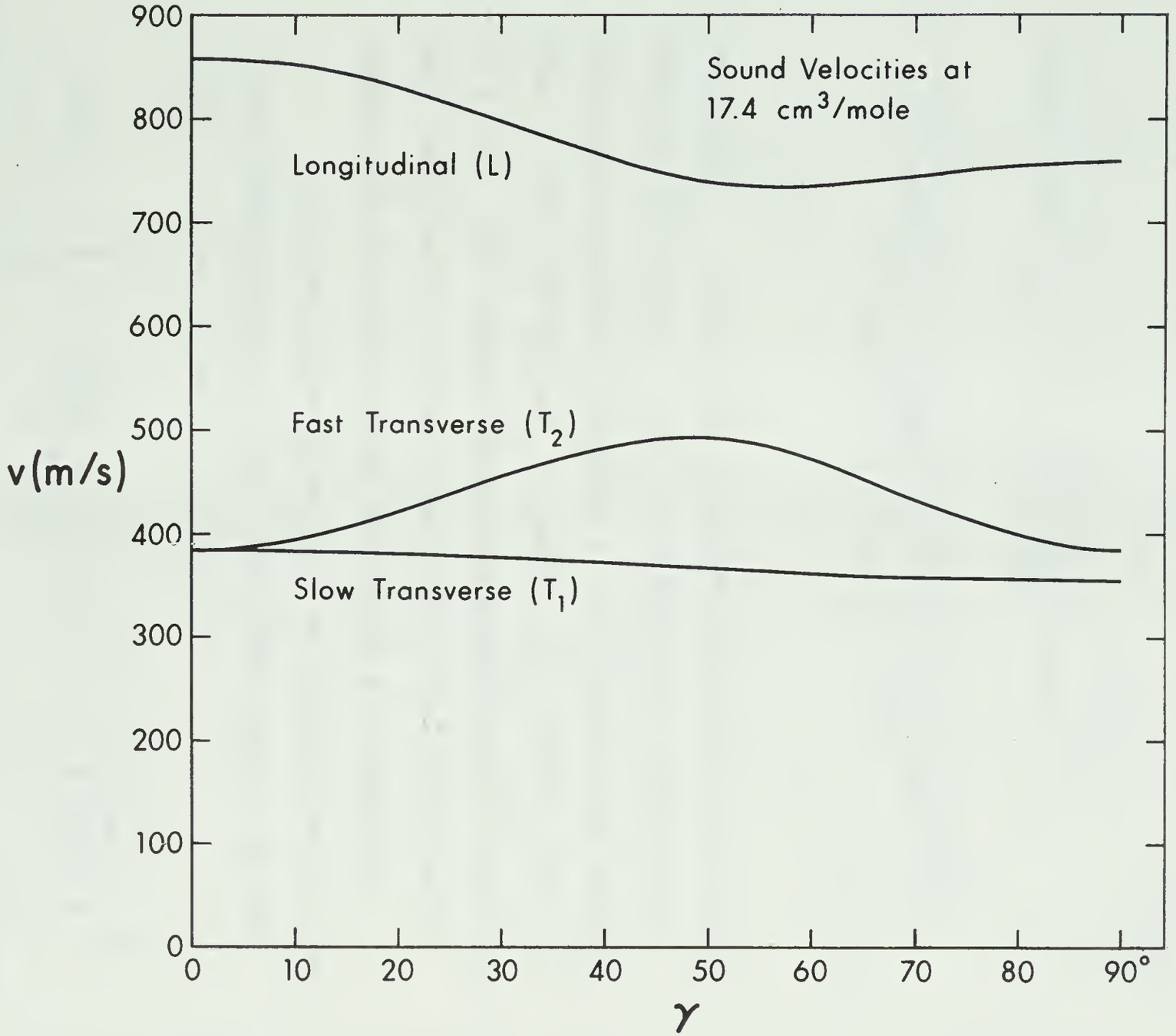

Figure 2 Orientation dependence of the sound velocity at 17.4 cm^{3}/mole.

$$(p_{L,T_2})_2 = f(\rho v^2, c_{ij}, \gamma)/[1 + f^2(\rho v^2, c_{ij}, \gamma)]^{\frac{1}{2}} \tag{2.3-15}$$

$$(p_{L,T_2})_3 = [1-(p_{L,T_2})_2^2]^{\frac{1}{2}} = [1 + f^2(\rho v^2, c_{ij}, \gamma)]^{-\frac{1}{2}} \tag{2.3-16}$$

where $$f(\rho v^2, c_{ij}, \gamma) = \tfrac{1}{2}\left(\frac{c_{11}+c_{12}}{c_{13}+c_{44}}\right) \tan\gamma \; x$$

$$x \; \frac{\rho v^2 - c_{44}\sin^2\gamma - [c_{33} - 2(c_{13}+c_{44})^2/(c_{11}+c_{12})]\cos^2\gamma}{\rho v^2 - c_{44}\cos^2\gamma - \tfrac{1}{2}(c_{11}-c_{12})\sin^2\gamma} \; . \tag{2.3-17}$$

The angle δ which the direction of polarization makes with the direction of pure transverse or longitudinal vibration is shown in figure 3 as a function of orientation γ for the T_2 and L modes at a molar volume of 17.4 cm^3. The angle between the polarization vector and the c-axis is $\gamma-\delta$, since the c-axis, the polarization vector and the propagation direction are coplanar.

In general the direction of propagation of sound is not perpendicular to the transducer but is at some angle Δ from the normal direction:

$$\cos \Delta_{T_1} = \left\{ 1 + \frac{[(c_{11}-c_{12})^2 - 4c_{44}^2]^2 \sin^2\gamma\cos^2\gamma}{[(c_{11}-c_{12})^2 \sin^2\gamma + 4c_{44}^2\cos^2]^2} \right\}^{-\frac{1}{2}} \tag{2.3-18}$$

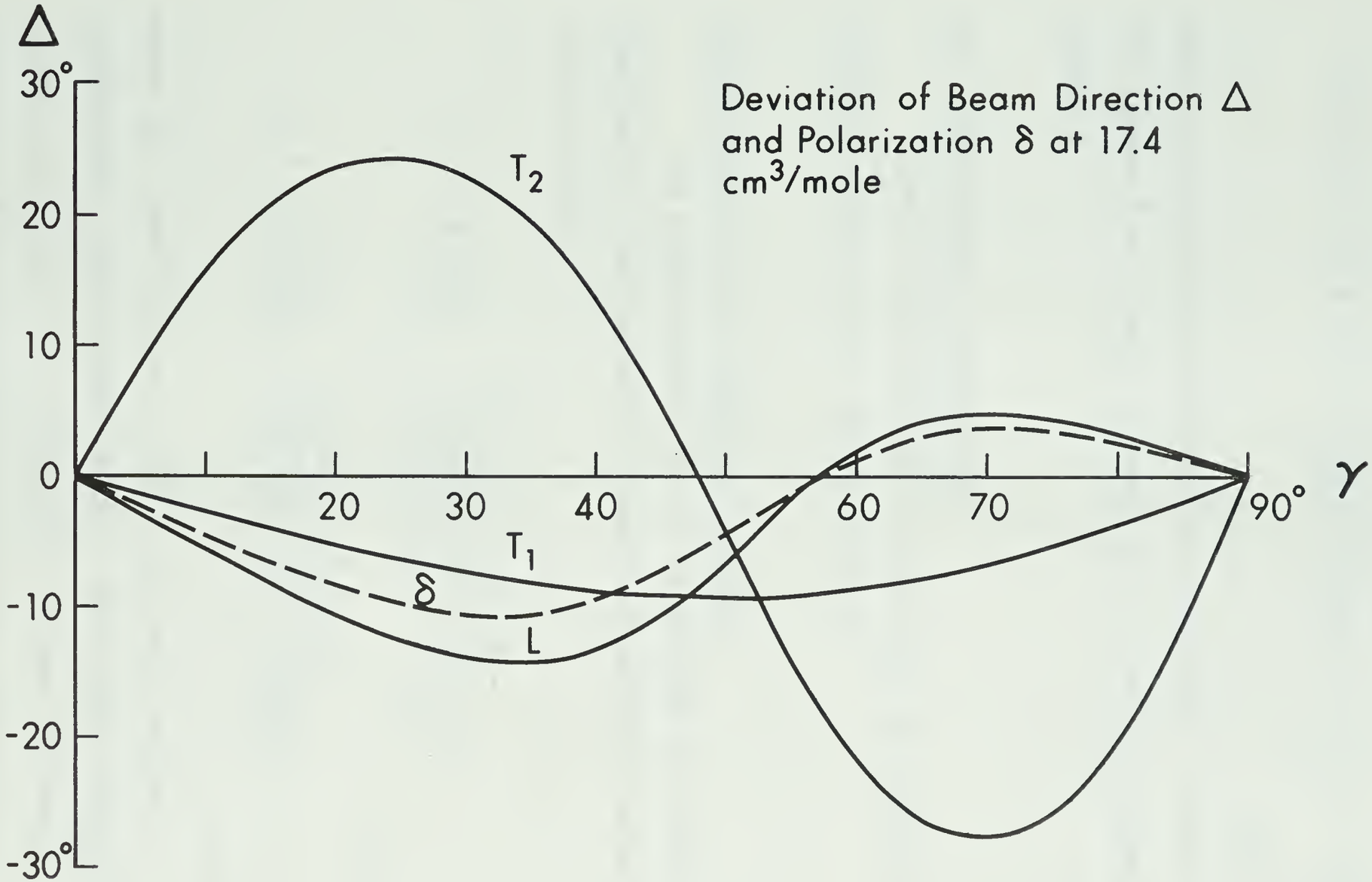

Figure 3 Orientation dependence of the beam deviation (Δ) and polarization (δ) at 17.4 cm^3/mole.

$$\cos \Delta_{T_2,L} = \left[1 + \left(1 - \left(\frac{c_{44}}{\rho v^2} \right) \right)^2 \left(\frac{p_2^4}{\sin^2\gamma} + \frac{p_3^4}{\cos^2\gamma} - 1 \right) \right]^{-\frac{1}{2}} \tag{2.3-19}$$

where p_2, p_3 are the polarization directions. The beam deviations for a molar volume of 17.4 cm^3 are given in figure 3.

2.4 Thermodynamic Quantities

Several thermodynamic quantities of interest are closely related to the sound velocity.

Compressibility and Elastic Constants

The compressibility can be defined at constant temperature (isothermal) or constant entropy (adiabatic) as (Nye (1957)),

$$\kappa_T \equiv -\frac{1}{V}\left(\frac{\partial V}{\partial P}\right)_T = \frac{c_{11}^T + c_{12}^T - 4c_{13}^T + 2c_{33}^T}{(c_{11}^T + c_{12}^T)c_{33}^T - 2(c_{13}^T)^2}, \tag{2.4-1}$$

$$\kappa_S \equiv -\frac{1}{V}\left(\frac{\partial V}{\partial P}\right)_S = \frac{c_{11}^S + c_{12}^S - 4c_{13}^S + 2c_{33}^S}{(c_{11}^S + c_{12}^S)c_{33}^S - 2(c_{13}^S)^2}, \tag{2.4-2}$$

where c_{ij}^T and c_{ij}^S are elastic constants defined isothermally and adiabatically. Using some simple thermodynamic relations, the difference between adiabatic and isothermal elastic constants is easily shown to be

$$(c_{ij}^S - c_{ij}^T)/c_{ij}^T \simeq (C_P - C_V)/C_V \sim T^4, \qquad (2.3\text{-}3)$$

where C_P and C_V are the heat capacities at constant pressure and constant volume. For the case of He^4, where the ratio of the lattice parameters c/a is independent of volume, then as shown by Franck and Wanner (1970),

$$c_{11} + c_{12} = c_{33} + c_{13} \qquad (2.4\text{-}4)$$

so the compressibility becomes

$$\kappa = 3/(c_{33} + 2c_{13}). \qquad (2.4\text{-}5)$$

Debye Temperature

The specific heat of a Debye solid at low temperatures is (Maradudin et al. (1971)),

$$C_V = \frac{12\pi^4}{5} Nk_B \left(\frac{T}{\Theta}\right)^3 \qquad (2.4\text{-}6)$$

Θ is a function of volume only for the ideal Debye solid, but for real solids it is also a slowly varying function of temperature. The Debye temperature at T = 0 is related to the sound velocities (not necessarily at T = 0) by

$$\Theta_0 = \frac{h}{k_B} \left(\frac{3N}{4V}\right)^{1/3} v_D \,, \qquad (2.4\text{-}7)$$

where the Debye velocity is:

$$v_D = \left[\int \left(v_L^{-3} + v_{T_1}^{-3} + v_{T_2}^{-3}\right) \frac{d\Omega}{12\pi}\right]^{-1/3} . \tag{2.4-8}$$

Grüneisen Constant

The Grüneisen constants are in general defined by

$$\gamma_{\underline{k}j} = - \frac{\partial \ell n \omega_{\underline{k}j}}{\partial \ell n V} . \tag{2.4-9}$$

Note that since the dynamical matrix in (2.1-10) is independent of volume, $\gamma_{\underline{k}j}$ will only be non-zero for an anharmonic solid. Now from (2.4-7), (2.4-8) and (2.1-12), if $\gamma_{\underline{k}j}$ is independent of $\underline{k}$ and j, then we have only one Grüneisen constant given by

$$\gamma_o = - \frac{\partial \ell n \Theta_o}{\partial \ell n V} . \tag{2.4-10}$$

If a system can be described by a reduced equation of state,

$$\phi(V) = \phi_o(V) \cdot f[T \cdot \phi(V)], \tag{2.4-11}$$

where usually $\phi(V) = \Theta^{-1}$, then

$$\gamma_o = \gamma = - \frac{\partial \ell n \theta}{\partial \ell n V} = \frac{V}{C_v} \frac{\partial P}{\partial T}\bigg|_v . \tag{2.4-12}$$

Second Sound

The propagation of second sound may be understood on an elementary level by using the method of Ward and Wilks (1952) with the Boltzmann equation of Callaway (1959):

$$\frac{\partial f}{\partial t} + \frac{c}{p}\,\underline{p}\cdot\underline{\nabla} f = \frac{f_o - f}{\tau_u} + \frac{f_\lambda - f}{\tau_N} \,. \qquad (2.4\text{-}13)$$

τ_n and τ_N are the total relaxation times for resistive and momentum-conserving phonon processes. The resistive processes relax the distribution to f_o and the conservative forces relax it to f_λ. Defining the energy density as:

$$E = \int cpf d^3p, \qquad (2.4\text{-}14)$$

it is easily shown that,

$$\frac{\partial^2 E}{\partial t^2} + \frac{1}{\tau_u}\frac{\partial E}{\partial t} - \frac{c^2}{3}\nabla^2 E = 0. \qquad (2.4\text{-}15)$$

Thus second sound is a damped oscillation of the energy density. We assume a plane wave solution,

$$E = E_o + E_1\, e^{i(\omega t - \underline{k}\cdot\underline{r})} \qquad (2.4\text{-}16)$$

Then the real and imaginary parts of the wave number

k are:

$$k_r = \frac{\omega}{c}\left[\frac{3}{2}\left(\sqrt{1+1/\omega^2\tau_u^2}+1\right)\right]^{\frac{1}{2}} \qquad (2.4\text{-}17)$$

and

$$k_i = \frac{\omega}{c}\left[\frac{3}{2}\left(\sqrt{1+1/\omega^2\tau_u^2}-1\right)\right]^{\frac{1}{2}}. \qquad (2.4\text{-}18)$$

If $\omega\tau_u \lesssim 1$, then $k_r/k_i \sim 1$ and we have diffusive propagation. But if $\omega\tau_u >> 1$, then,

$$c_2 = \omega/k_r = c/\sqrt{3} \qquad (2.4\text{-}19)$$

and

$$\alpha_2 = \frac{\sqrt{3}}{2} \cdot \frac{\omega}{c} \cdot \frac{1}{\omega\tau_u}. \qquad (2.4\text{-}20)$$

The second sound velocity has been calculated for several polarizations of phonons in an isotropic material by Sussmann and Thellung (1963) to be:

$$c_2^2 = \frac{1}{3}\left(\sum v_i^{-3}\right)/\left(\sum v_i^{-5}\right). \qquad (2.4\text{-}21)$$

c_2 has also been calculated for the more general anisotropic case by Beck (1975), Banerjee and Pao (1974), Hewko (1973) and Hardy (1970).

The statistical average implied by the relaxation time approximation of equation (2.4-13) must be taken over a time much longer than the total relaxation time.

$$\text{i.e.} \quad \omega(\tau_u^{-1} + \tau_N^{-1})^{-1} << 1. \tag{2.4-22}$$

Now $(\omega\tau_U)^{-1}<<1$, so (2.4-22) is satisfied only if

$$\omega\tau_N<<1. \tag{2.4-23}$$

Thus we have a window for second sound propagation, as originally shown by Guyer and Krumhansl (1964):

$$\omega\tau_N<<1<<\omega\tau_u \ . \tag{2.4-24}$$

2.5 Adiabatic Sound Propagation

In order for sound to propagate adiabatically (in quasi-equilibrium), the heat which flows across one wavelength must be much less than that required to equalize the temperature (Bhatia (1967)).

$$\text{i.e.} \quad Q_1 << Q_2, \tag{2.5-1}$$

$$\text{where} \quad Q_1 = \kappa\Delta T/v \simeq \frac{1}{3}\frac{C_v}{V}.\frac{v_D}{v}.v_D\tau_u\Delta T \tag{2.5-2}$$

$$\text{and} \quad Q_2 = \tfrac{1}{2}\Delta T.\frac{C_P}{V}.\frac{\lambda}{2} \ . \tag{2.5-3}$$

$$\text{Therefore} \quad \omega\tau_u << \frac{3\pi}{2}\left(\frac{C_P}{C_V}\right)\left(\frac{v}{v_D}\right)^2 \sim 1. \tag{2.5-4}$$

Equation (2.5-4) means that sound propagates adiabati-

cally at high temperatures or low frequencies.

From a microscopic viewpoint, a sound wave in an ideal crystal will be attenuated and shifted in velocity for three separate reasons, each operative under a different set of conditions. At low temperatures the sound waves behave like a beam of phonons which is scattered by the thermal phonons. This mechanism will be discussed in section 2.7. At higher temperatures, $\omega\tau_N<1$, a longitudinal wave will create a periodic density variation so that regions of compression are warmer than those of rarefaction. Heat is then conducted irreversibly between these regions either through normal diffusive heat conduction or through second sound propagation, as discussed in section 2.6.

Also at higher temperatures, when $\omega\tau<<1$ (adiabatic region), the phonon gas is strained by the passage of the sound wave. The phonon frequencies will be locally modified through equation (2.4-9) and then will relax towards their equilibrium valve, so that energy is dissipated. Several authors have investigated this mechanism, including Akhieser (1939), Pomeranchuk (1941), Bömmel and Dransfeld (1960), Woodruff and Ehrenreich (1961) and Maris (1967, 1971).

In this temperature range a Boltzmann transport equation approach is valid. Assuming only umklapp processes are important, and that $\gamma_{\underline{k}j}$ is a constant for all

modes, Woodruff and Ehrenreich (1961) find the attenuation is given by,

$$\alpha \simeq \frac{\pi}{3} \frac{\gamma^2 C_V T}{\rho V v^2} \cdot \omega\tau \ . \qquad (2.5\text{-}5)$$

Maris (1971) has calculated the adiabatic velocity v_a in this region to be:

$$v_a - v_o = \frac{1}{2\rho V v}\left\{ \sum_{\underline{k}j} \tilde{\gamma}_s(\underline{k}j)\hbar\omega(\underline{k}j)[n(\underline{k}j) + \tfrac{1}{2}] - C_V T \ x \right.$$
$$\left. x \ (\langle\gamma_s^2(\underline{k}j)\rangle - \langle\gamma_s(\underline{k}j)\rangle^2) \right\} \qquad (2.5\text{-}6)$$

where $n(\underline{k}j)$ is the phonon occupation number,

$$\tilde{\gamma}_s(\underline{k}j) = \gamma_s^2(\underline{k}j) - \frac{\partial\gamma_s(\underline{k}j)}{\partial\varepsilon_{\gamma\delta}} \cdot e_\gamma(\underline{K}J)\cdot\hat{K}_\delta \ , \qquad (2.5\text{-}7)$$

$$\gamma_s(\underline{k}j) = -\frac{1}{\omega(\underline{k}j)} \frac{\partial\omega(\underline{k}j)}{\partial\varepsilon_{\alpha\beta}} \cdot e_\alpha(\underline{K}J)\cdot\hat{K}_\beta \ , \qquad (2.5\text{-}8)$$

and $\langle f(\underline{k}j)\rangle$ is $f(\underline{k}j)$ averaged over the heat capacities of all phonon modes. $\underline{e}(\underline{K}J)$ is the polarization of the sound wave $\underline{K}J$; $\hat{\underline{K}}$ is a unit vector in the $\underline{K}$ direction, and $\varepsilon_{\alpha\beta}$ is the strain tensor. Equation (2.5-8) is similar to (2.4-9). For the case of an isotropic material obeying a reduced equation of state, (2.5-6) reduces to:

$$v_a - v_o = \frac{\gamma}{2\rho V v}\left(\gamma - \frac{d\ell n\gamma}{d\ell nV}\right) U. \qquad (2.5\text{-}9)$$

Including one higher order term in the internal energy U (Maradudin et al.(1971)), (2.5-9) implies:

$$\Delta v/v \sim aT^4 + bT^6. \qquad (2.5\text{-}10)$$

2.6 Sound Propagation at Intermediate Temperatures

At this point the various phonon scattering processes must be examined more closely (see Reissland (1973)). Resistive processes are of several types. Scattering from impurities is usually insignificant in helium because of the high purity obtainable. A discussion of scattering from other lattice imperfections such as dislocations and vacancies will be left to sections 2.8 and 2.9. Phonons in an ideal crystal still experience umklapp scattering:

$$\sum \underline{k}_i = \sum \underline{k}_f + \underline{K} , \qquad (2.6\text{-}1)$$

where $\underline{k}_i$ and $\underline{k}_f$ are initial and final phonon momenta while $\underline{K}$ is a reciprocal lattice vector. Energy is always conserved:

$$\sum \omega_i = \sum \omega_f . \qquad (2.6\text{-}2)$$

For an n-phonon process, at least one phonon must have $|\underline{k}| \geq |\underline{K}/(n-1)|$, so that at low temperatures umklapp processes become unimportant.

If $\underline{K} = 0$ in (2.6-1), then we have normal processes. For three-phonon processes when the frequency of the sound wave $\omega_s << kT/\hbar$, then (2.6-2) becomes

$$\omega' = \omega + \omega_s = \omega + (\nabla_{\underline{k}}\omega)\cdot\underline{\Delta k} \ . \qquad (2.6\text{-}3)$$

Using the group velocity $\underline{v}_g$ and the phase velocity $\underline{v}_p$ defined by (2.1-11) and (2.1-12), $\omega' - \omega$ will have a maximum value of

$$\Delta\omega_{max} = |\underline{v}_g(\underline{k}j)|\cdot|\underline{\Delta k}| \ , \qquad (2.6\text{-}4)$$

and $$\Delta\omega = \omega_s = |\underline{v}_p|\cdot|\underline{k}_s| \ . \qquad (2.6\text{-}5)$$

$$\text{Therefore } |\underline{v}_p||\underline{k}_s| = \underline{v}_g(\underline{k}j)\cdot\underline{\Delta k} \leq |\underline{v}_g(\underline{k}j)|\cdot|\underline{\Delta k}|. \qquad (2.6\text{-}6)$$

Therefore three phonon processes are only possible if for some thermal phonons $\underline{k}j$,

$$|\underline{v}_g(\underline{k}j) \geq |\underline{v}_p|_{sound}, \qquad (2.6\text{-}7)$$

i.e. there must be anomalous dispersion in order that a longitudinal sound wave may interact via three-phonon

processes.

Now by intermediate temperatures I mean:

$$\omega\tau_N<1 \text{ and } \tau_N<\tau_U \ . \qquad (2.6\text{-}8)$$

This region may not exist at sufficiently high frequencies, but it could be extended if anomalous dispersion is present. If (2.6-8) is satisfied, Maris (1971) gives:

$$\alpha = \frac{\omega^2 T\kappa}{2\rho v^5} \langle\gamma(\underline{k}j)\rangle^2 . \frac{1}{1+\omega^2\tau_o^2} \qquad (2.6\text{-}9)$$

$$\text{and} \quad v = v_a + \frac{\omega\kappa T}{2\rho v^3} \langle\gamma(\underline{k}j)\rangle^2 . \frac{\omega\tau_o}{1+\omega^2\tau_o^2} \ , \qquad (2.6\text{-}10)$$

where κ is the thermal conductivity and

$$\tau_o = \frac{\kappa}{CVv^2} \left[\frac{3v^2 \langle v^{-2}(\underline{k}j)\rangle}{\langle \underline{v}(\underline{k}j)\cdot\underline{v}_g(\underline{k}j)/v^2(\underline{k}j)\rangle^2} - 1 \right] \ . \qquad (2.6\text{-}11)$$

Several other authors (Guyer (1966), Niklasson (1970), Banerjee and Pao (1974)) have made calculations in this region.

Both normal heat diffusion and second sound propagation contribute to the attenuation when $\omega\tau_o>>1$. For a simple isotropic material,

$$\tau_o = \frac{2}{3}\left(\frac{v_D}{v}\right)^2 \tau \ , \qquad (2.6\text{-}12)$$

where τ is the relaxation time found from the thermal conductivity and thoroughly discussed by Guyer and Krumhansl (1966) and Hogan et al. (1969). Figure 4 shows the relaxation times τ_N, τ_U and τ in helium at 124.4 bar and for a 1 cm wide specimen. The curves are extrapolated from the data of Hogan et al. (1969) and Lawson et al. (1973) in appendix 2. Although for the frequencies used in this work we are never in the intermediate temperature region, the relaxation times are not definitive since different methods of measurement consistently give different results (Rogers (1972), Berman et al. (1966), Bertman et al. (1966)).

2.7 Sound Propagation in the Low Temperature Limit

In the low temperature limit ($\omega\tau >> 1$) we might expect isothermal sound propagation. However in order to even speak of a sound wave we must have a wavelength much greater than the mean free path:

$$\lambda >> \ell \quad \text{or} \quad \omega\tau << 1. \qquad (2.7\text{-}1)$$

The isothermal region is never reached since normal sound propagation breaks down at the same point that second sound propagation breaks down (equation (2.4-24)).

As the relaxation time becomes very large the phonons no longer interact with the lattice except at

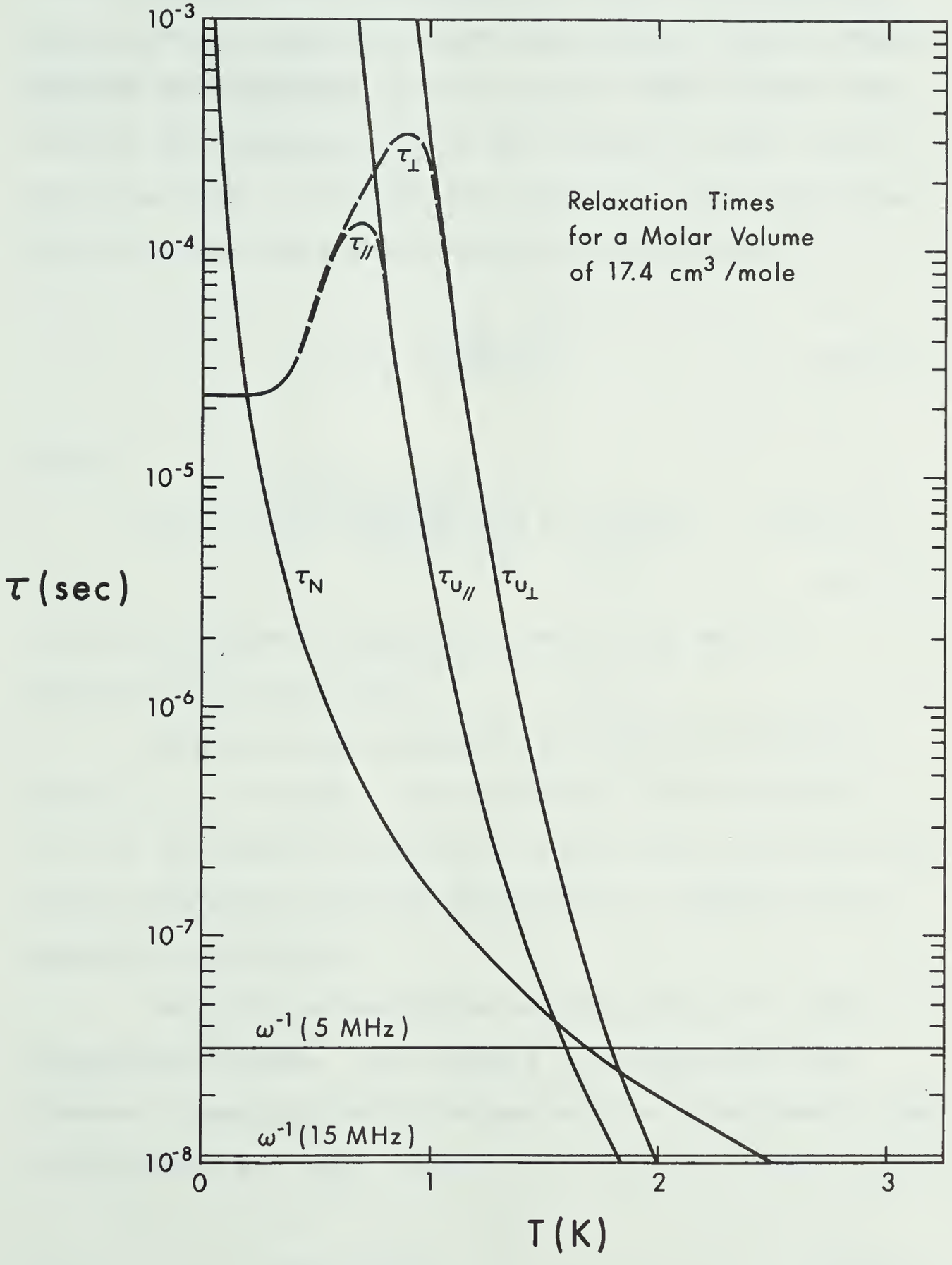
Relaxation Times
for a Molar Volume
of 17.4 cm³ /mole
τ (sec)
T (K)
τ⊥
τ//
τN
τU//
τU⊥
ω⁻¹ (5 MHz)
ω⁻¹ (15 MHz)
10⁻³
10⁻⁴
10⁻⁵
10⁻⁶
10⁻⁷
10⁻⁸
0
1
2
3

Figure 4

boundaries and so they propagate ballistically. The sound wave may then be treated as a beam of low-energy phonons which populate a particular state $N(\underline{K}J)$. These phonons are scattered and the energy levels change only through the anharmonicity of the crystal. Maris (1967, 1971) has done a perturbation calculation and finds that this so-called zero sound velocity is given by

$$v_z = v_a + \frac{\gamma_{eff}^2 C_V T}{2\rho V v} \tag{2.7-2}$$

where

$$\gamma_{eff}^2 = \left\langle \frac{\gamma^2(\underline{k}j)\,\underline{K}\cdot\underline{v}_g(\underline{k}j)}{[\Omega - \underline{K}\cdot\underline{v}_g(\underline{k}_j)]_P} \right\rangle + \langle\gamma^2(\underline{k}j)\rangle - \langle\gamma(\underline{k}j)\rangle^2, \tag{2.7-3}$$

v_a is the adiabatic velocity from (2.5-6) and P signifies principal part.

Therefore there should be a shift in velocity near $\omega\tau \sim 1$. Together the second and third terms of (2.7-3) are positive while the first term is positive for normal dispersion and either positive or negative for anomalous dispersion.

In order to calculate attenuation in the low temperature régime, the effects of scattering from phonons of various polarizations must be considered. The calculations are very lengthy but in general (Maris (1971)),

$$\alpha \sim \Omega\, T^4. \tag{2.7-4}$$

2.8 Dislocations

Because of solid helium's high purity, dislocations and vacancies (section 2.9) are the only lattice defects we need consider.

If dislocations are pinned at nodes (intersections) then they can only slip between pinning points so that under the influence of a low amplitude strain field we have a situation not unlike a vibrating string. This model has been investigated by Granato and Lücke (1956, 1966) who find,

$$\alpha(\omega) = \frac{K}{2\pi v_o} \cdot \frac{\omega^2 d}{[(\omega_o^2-\omega^2)^2 - (\omega d)^2]}, \qquad (2.8\text{-}1)$$

$$\frac{\Delta v(\omega)}{v_o} = -\frac{K}{2\pi} \cdot \frac{\omega_o^2-\omega^2}{[(\omega_o^2-\omega^2)^2 - (\omega d)^2]} \cdot \qquad (2.8\text{-}2)$$

Here $\omega_o = \eta/\ell$, (2.8-3)

$$\eta^2 \simeq 2G/\rho(1-\nu) = 2v_o^2/(1-\nu), \qquad (2.8\text{-}4)$$

and $K = \Lambda\Delta_o\eta^2R^2$ (2.8-5)

where ℓ is the length of the dislocation between pinning points, $G \simeq c_{44}$ is the shear modulus, $\nu \simeq c_{13}/c_{33}$ is Poisson's ratio, $d \alpha T^n$, where $n \sim 5$ (Brailsford (1972)) is a damping factor, Λ is the total length of

dislocations per unit volume, $\Delta_o \simeq 4(1-\nu)/\pi^2$ and R^2 is an orientation factor given by

$$R^2 = \sin\gamma \cos\gamma \cos\phi \ . \qquad (2.8\text{-}6)$$

ϕ is the angle between the slip plane and slip direction.

Not all dislocation loops are of the same length ℓ so some distribution must be used such as that proposed by Koehler (1952):

$$N(\ell)\, d\ell = \frac{\Lambda}{L^2} e^{-\ell/L}\, d\ell \ . \qquad (2.8\text{-}7)$$

Then
$$\alpha = \frac{\Lambda}{L^2} \int_o^\infty \ell\alpha(\omega)\, e^{-\ell/L}\, d\ell \qquad (2.8\text{-}8)$$

and
$$\frac{\Delta v}{v_o} = \frac{\Lambda}{L^2} \int_o^\infty \ell\, \frac{\Delta v(\omega)}{v_o}\, e^{-\ell/L}\, d\ell. \qquad (2.8\text{-}9)$$

Wanner et al. (1976) have approximated equation (2.8-9) by realizing that there are only small contributions to $\Delta v/v$ from very long loops ($\ell >> L$) and very short loops ($\ell << \ell_c$) where,

$$\ell_c = \eta/\omega = [2G/\rho(1-\nu)\omega^2]^{\frac{1}{2}} \ . \qquad (2.8\text{-}10)$$

As well, loops just slightly larger and slightly smaller than ℓ_c effectively cancel one another. Therefore only

two short ranges of ℓ, one larger and one smaller than ℓ_c, have much effect and we may write:

$$\frac{\Delta v}{v_o} = \frac{4 v_o^2 R^2}{\pi^3} \left[\frac{\Lambda_2}{\omega^2+d^2} - \frac{\Lambda_1 (k^2-1)}{(k^2-1)^2 \omega^2 + d^2} \right] . \qquad (2.8\text{-}11)$$

In (2.8-10) $\Lambda_2 > \Lambda_1$ and k is an additional parameter fixed by the dislocation length distribution:

$$k = \ell_c / \langle \ell_1 \rangle = \frac{\ell_c}{\Lambda_1} \int_0^{\ell_c} N(\ell)\, d\ell \ . \qquad (2.8\text{-}12)$$

For an exponential distribution,

$$k = \frac{\ell_c}{L} \frac{\Lambda}{\Lambda_1} \left(1 - e^{-\ell_c/L}\right) , \qquad (2.8\text{-}13)$$

$$\Lambda_2 = \Lambda (1+\ell_c/L)\ e^{-\ell_c/L} \qquad (2.8\text{-}14)$$

and $$\Lambda_1 = \Lambda - \Lambda_2 \ . \qquad (2.8\text{-}15)$$

2.9 Vacancies and Superfluidity in Solid Helium

A recent review of vacancies in solid helium may be found in Glyde (1976). As originally shown by Hetherington (1968) vacancies in solid helium are non-localized as a consequence of the very large atomic motions. There is then a band of vacancy energies with its mean value

being the usual local vacancy formation energy ε_o. The total tunnelling rate to all other sites may then be estimated through the uncertainty principle to be,

$$t \simeq \frac{1}{2\pi} \left(\frac{2\Delta\varepsilon}{\hbar}\right) , \qquad (2.9\text{-}1)$$

where $\Delta\varepsilon$ is one half of the bandwidth. Hetherington calculated $\Delta\varepsilon \sim 6K$ and $t \sim 3\times10^{11}\,sec^{-1}$ in He^3. Values for He^4 are similar (Miyoshi et al. (1970)).

In He^3, the non-localized vacancies will have a very short mean free path $\sim a$, since the uncorrelated spins do not provide a periodic background (Glyde (1976)). However in He^4, the rapidly tunnelling vacancies can take on wave-like properties (Andreev and Lifshitz (1969), Guyer et al. (1971)), but only when they can travel several lattice sites during one phonon period,

$$\text{i.e.} \quad T < ht/k = 2\Delta\varepsilon/k . \qquad (2.9\text{-}2)$$

Andreev and Lifshitz (1969) have estimated that vacancies will propagate as waves when the diffusion coefficient is greater for non-localized vacancies than for localized ones,

$$\text{i.e.} \quad T < \Theta\,(\Delta\varepsilon/\Theta)^{1/9} . \qquad (2.9\text{-}3)$$

Also the repulsive interaction energy between vacancies must be less than the bandwidth so

$$T < \varepsilon_o / \ell n \ (mc^2/\Delta\varepsilon) \ , \qquad (2.9\text{-}4)$$

where m is the atomic mass and c is the sound velocity. Then for nearest neighbours the energy spectrum is

$$\varepsilon(q) = \varepsilon_o + 2\pi\hbar zt \cos q a/2 \ , \qquad (2.9\text{-}5)$$

where zt again is the bandwidth. The calculated bandwidth is quite insensitive to volume (Guyer et al. (1971)).

The existence of the vacancy wave energy band and of bound vacancy states (Andreev (1975)) will modify the phonon spectrum near the band edges and at $\varepsilon_o \pm 4\Delta\varepsilon$ and $\varepsilon_o \pm 2\Delta\varepsilon$ (Kondratenko (1976)). However it would be fortuitous if these energies occurred near the sound wave frequency.

We might expect that the large zero point motion in solid helium would result in the presence of a finite number of vacancies even at $T = 0$, so that we may have a Bose condensate and a superfluid solid (Andreev and Lifshitz (1969), Chester (1970)). Then there will be four sound propagation branches with the three normal modes having spectra:

$$\omega(\underline{k}) = \omega_o(\underline{k}) + \frac{\omega_o(\underline{k})}{2\rho} \quad (\rho_3^s \cos^2\gamma' + \rho_1^s \sin^2\gamma') \tag{2.9-6}$$

for a hexagonal crystal. γ' is the angle between the c-axis and the direction of polarization $(\gamma - \delta)$, while ρ_i^s is the superfluid density in direction i:

$$\rho_i^s = \rho - [\partial^2\varepsilon/\partial p_i^2]^{-1} . \tag{2.9-7}$$

Estimates of ρ_s/ρ range all the way from 10^{-6} (Guyer (1971)) to 0.2 (Saslow (1976)).

The existence of zero point defects may not be necessary (Leggett (1970)) for superfluidity in the solid, although it would enhance the effect. Saslow (1977) has done an extensive microscopic and hydrodynamic treatment of the problem from this viewpoint. He shows that a superfluid velocity cannot be developed from a Galilean transformation on a periodic material. Therefore it would be extremely difficult to detect true superfluid flow. However there will still be a small effect on the sound velocity:

$$v^2 = v_o^2 \, [1 - \bar{\delta} \, v_4^2/(v_o^2 - v_4^2)] \tag{2.9-8}$$

where v_4 is the fourth sound velocity given by

$$v_4^2 = \rho^s \, (\partial\mu/\partial\rho)_{S,\varepsilon} \tag{2.9-9}$$

and $\bar{\delta} = 1 - \rho^{-1} S(\partial\rho/\partial S)_{\mu,\varepsilon} + \rho^{-1} (\partial\rho/\partial\varepsilon_{11})_{S,\mu}$.

(2.9-10)

μ is the chemical potential, ε is the strain and S is the entropy.

CHAPTER 3

EXPERIMENT

3.1 Cryogenic Systems

The two major experimental requirements for the study of solid helium are a refrigeration system and a pressure handling system.

3.1-1 Cryostat

The low temperature end of the cryostat is shown in figure 5. The pressure cell was bolted onto a graphite and copper support column which was attached to the He^4 pot. The weight of the pressure cell did not allow it to be supported by the delicate dilution refrigerator. Copper rings at several stages provided convenient locations for thermal anchoring.

Cooling to about 1 K was obtained by circulating gas through the dilution refrigerator while pumping on the He^4 pot. Under normal operating conditions the He^4 would last for several days without a refill. In order to reach lower temperatures the gas mixture of approximately 0.2 moles He^3 and 0.5 moles He^4 was condensed through the still. Then the still was pumped slowly until the temperature of about 0.5 K was reached. At this point circulation was started, the still heater turned on to about 1 mW and the dilution refrigerator commenced

FIGURE 5

CRYOSTAT

1. Needle valve
2. Pressure line
3. Allen-Bradley carbon thermometers (10 Ω, 0.1W)
4. Thermal contacts
5. He^4 pot
6. Still heater (200 Ω)
7. Still (S.H.E. minifridge)
8. Copper rings
9. Mixing chamber
10. Speer carbon thermometers (220 Ω, 0.5W)
11. Pressure line heater (100 Ω)
12. Vacuum pumping line
13. He^4 pumping line
14. He^3 pumping line
15. He^3 return line
16. Flow-limiting capillary
17. Continuous heat exchanger
18. Calibrated germanium thermometer (S.H.E. Corp.)
19. BeCu pressure cell
20. Heater (100 Ω) for crystal growth
21. rf feedthrough
22. Vacuum can

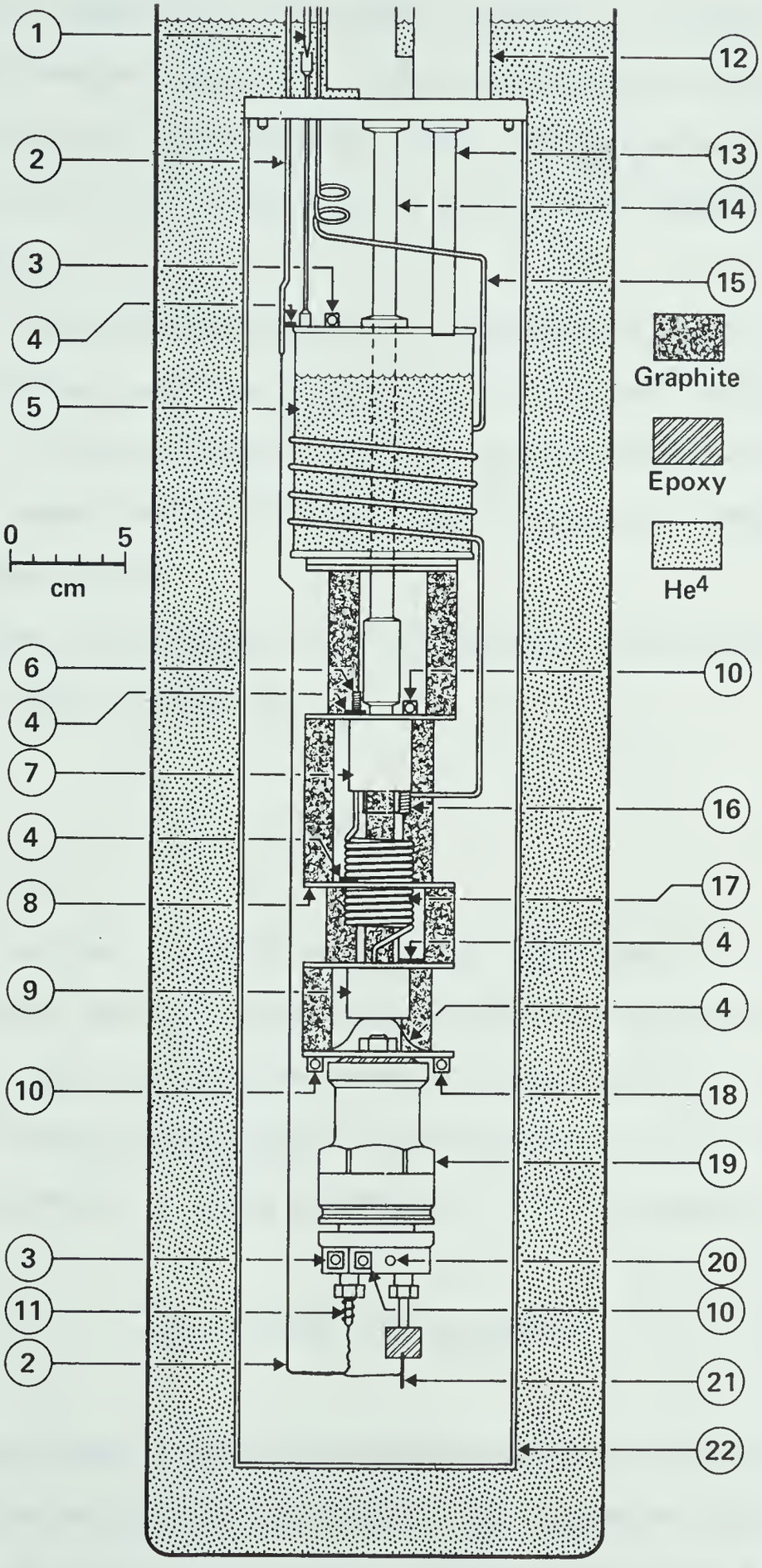
1
2
3
4
5
6
4
7
4
8
9
10
3
11
2
12
13
14
15
Graphite
Epoxy
He4
10
16
17
4
4
18
19
20
10
21
22
0
5
cm

operation. When the temperature reached a stable minimum the still heater power was reduced to 0.25 mW and recondensation of He^3 was stopped. The refrigerator then continued in a one-shot mode to the lowest temperatures attainable.

Without the presence of the pressure cell, its support column and the pressure line the refrigerator reached a minimum temperature of approximately 40 mK. With the experiment in place, 240 mK was the lowest possible temperature.

The cooling power of a dilution refrigerator is given by Betts (1968) as

$$\dot{Q} \simeq 10\dot{n}_3 R T_D^2 \ , \qquad (3.1\text{-}1)$$

where $\dot{n}_3$ is the circulation rate in moles/sec, R is the gas constant and T_D is the temperature of the mixing chamber. The circulation rate was measured with a flowmeter of the type described by Almond et al (1972) to be 6×10^{-5} moles/sec. Then equation (3.1-1) becomes

$$\dot{Q} = 5 \times 10^4 \ T_D^2 \ \text{erg/sec.} \qquad (3.1\text{-}2)$$

Most of the heat input was determined to be flowing through the solidified helium in the pressure line. From Hogan et al. (1969) the thermal conductivity for $T \leq 1$ K

and in a tube of inner diameter d is given by

$$\kappa = \frac{1}{3} C_v v_D \alpha d/V , \qquad (3.1\text{-}3)$$

where α is a numerical constant slightly larger than 1. Then for a line of length L anchored at the He^4 pot of temperature T_o, the heat flow is

$$\dot{Q} \simeq 4.3\text{x}10^7 d^3 (T_o^4 - T_D^4)/L \text{ erg/sec.} \qquad (3.1\text{-}4)$$

Equating (3.1-2) and (3.1-4), we find:

$$T_D^2 = 8.6\text{x}10^2 d^3 T_o^4/L . \qquad (3.1\text{-}5)$$

For $L = 40$ cm, $d = 0.03$ cm and $T_o = 1.2$ K, then $T_D \simeq 80$ mK. With all other heat losses included, the experiment should still cool to at least 100 mK. The cause of this large discrepancy was only found after the present data had been recorded. Through a miscalculation the thermal anchor at the He^4 had far too small a conductivity (approximately $40 \cdot \Delta T$ erg/sec). This is negligible compared to the heat input of 2000 erg/sec calculated from (3.1-2) with $T_D \sim 0.2$ K.

The illustration of the pumping systems in figure 6 is self-explanatory. I should only add that the rather large volume (2 litres) of the first liquid nitrogen trap

FIGURE 6

PUMPING SYSTEMS

1. He^3-He^4 gas mixture storage
2. Molecular sieve (Linde 13X)
3. Flowmeter
4. Dilution refrigerator (S.H.E. minifridge)
5. Booster pump (NRC 123)
6. Sealed rotary pump for He^3 circulation
7. He^3 supply
8. He^4 supply
9. Diffusion pump
10. Rotary pump for cleaning system
11. He^4 exchange gas storage
12. Diffusion pump
13. Rotary pump for vacuum can
14. Booster pump (NRC 123)
15. Rotary pump for He^4 pot
16. Thermocouple gauges (NRC 531)
17. Cold cathode gauges (Balzers HV5)

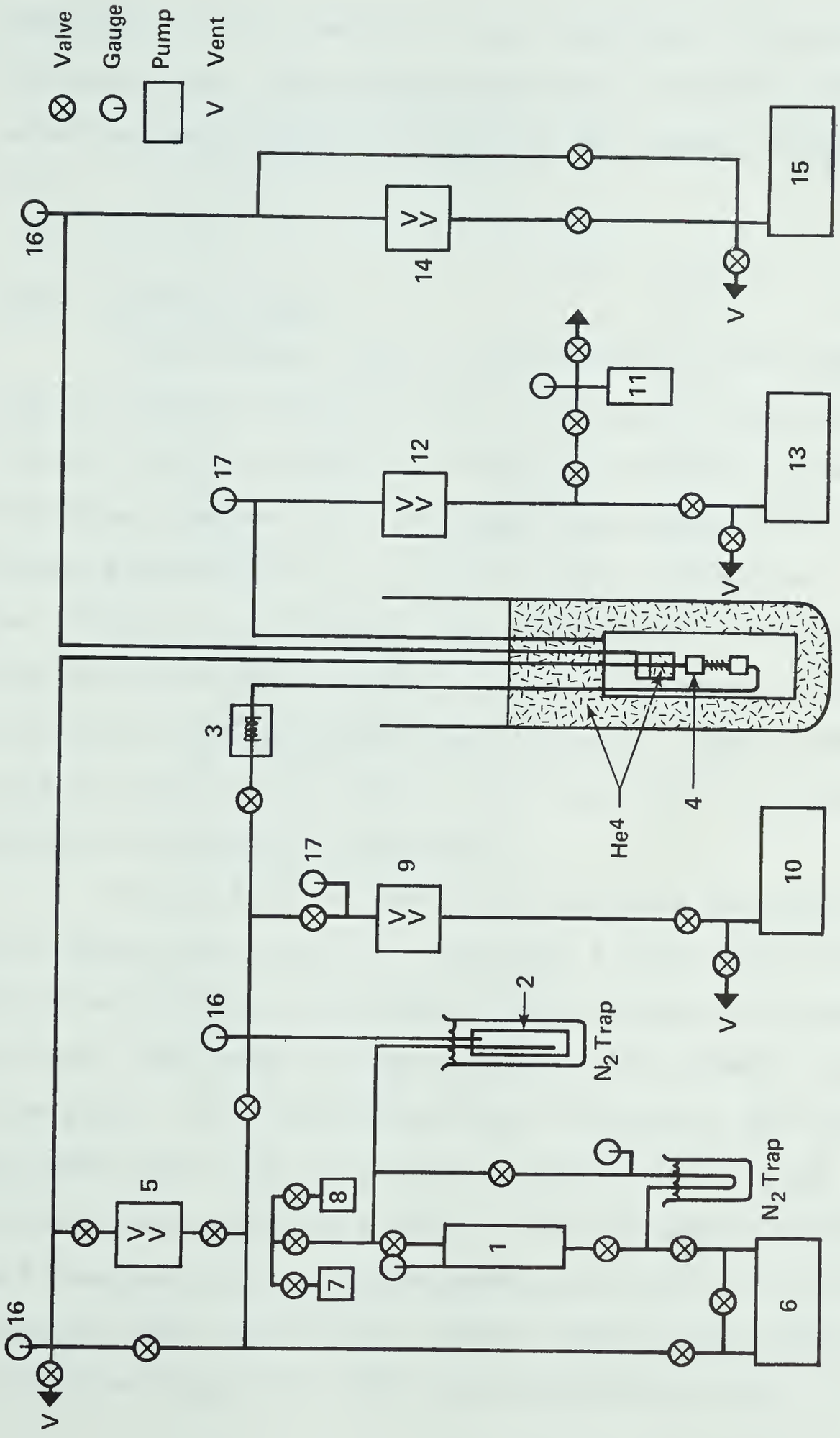
Valve
Gauge
Pump
V Vent
16
17
14
15
12
11
13
3
17
9
10
16
2
N_2 Trap
He4
4
5
8
7
1
N_2 Trap
6
16
V

accounted for the quantity of gas required in the circulation system. The volume of the trap containing the molecular sieve was 250 mℓ, and of the storage volume, 90 ℓ.

3.1-2 Pressure Cell

The pressure cell or bomb (figure 7) was constructed of hardened beryllium copper to hold pressures of 300 bar and to maintain the helium at constant volume. The inner diameter is 28 mm while the distance from the ½-inch transducer to the mirror can be varied from 7 to 10 mm. With this arrangement even signals with the maximum beam deviation (see section 2.3) can be observed without any losses through hitting the side wall. Such a situation is essential in order to make quantitative measurements of ultrasonic attenuation.

The plate from which the transducer was suspended was tightly held between a ledge and a split ring circlip by 12 set screws. Six screws, three pushing and three pulling, were used to hang the transducer assembly from this plate. The reflecting mirror was made of BeCu and polished flat to ¼ wavelength of sodium light. After its threads were coated with Stycast 2850 GT epoxy (Emerson and Cummings Inc.) it was screwed into place. The entire cell was then bolted onto a copper plate on the support structure (figure 5), with the transducer end down. The

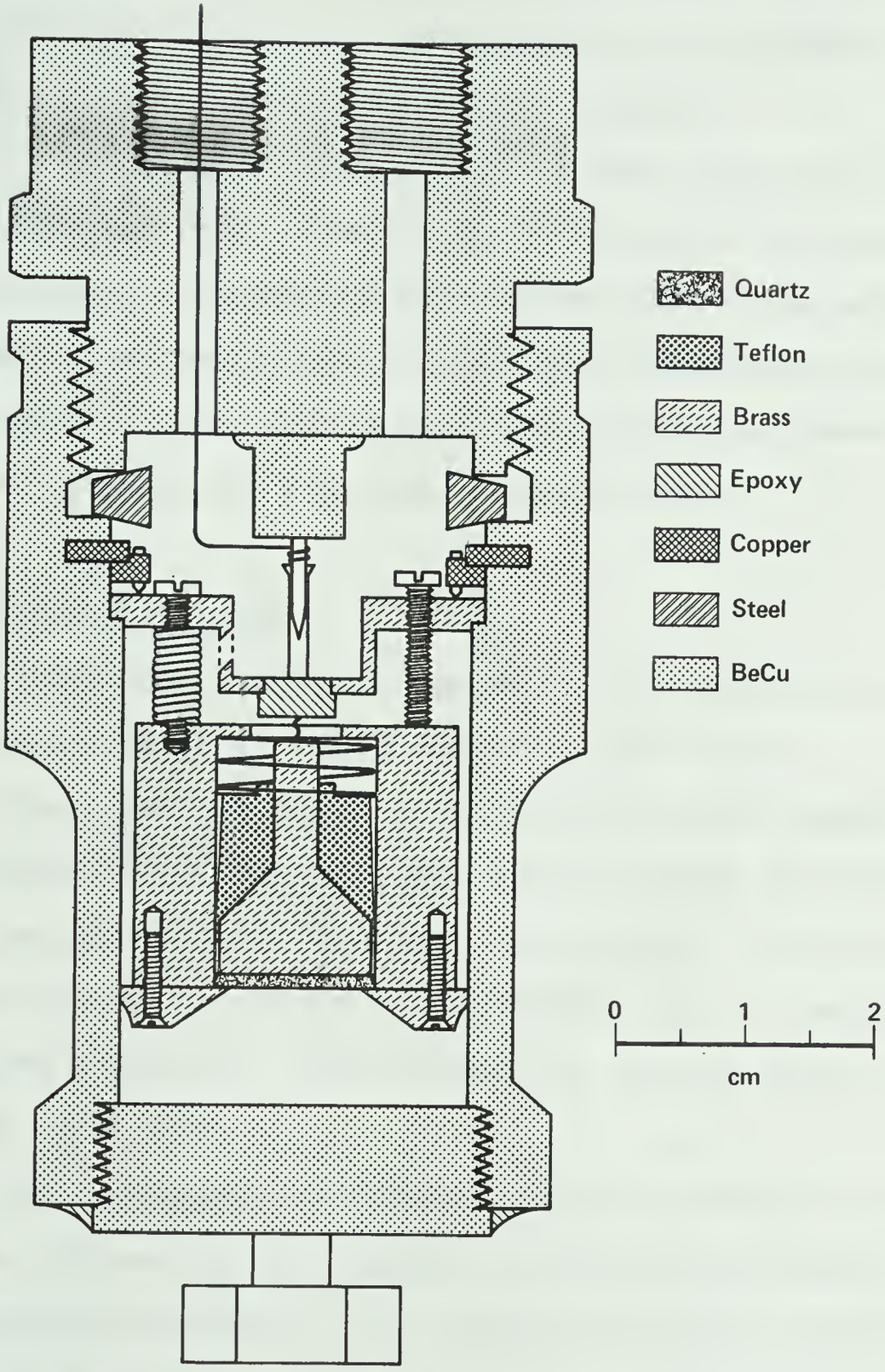

Figure 7 High pressure cell and ultrasonic assembly.

pressure line and rf miniature coaxial cable (Lake Shore Cryotronics Type A) were entered into the bomb through separate high pressure feedthroughs.

The pressure capillary was a CuNi tube of 0.3 mm i.d. and 0.5 mm o.d. leading as far as the helium bath and from there a large tube was led out of the cryostat to an external ballast volume (about 2×10^4 times the volume of the bomb). The helium used in the pressure system was purified by passing it through liquid helium.

3.1-3 Crystal Growth

Using the following procedure, high quality crystals were obtained for about half of the attempts.

The bomb was first warmed up to several degrees above the melting point and then slowly cooled by circulating gas through the dilution refrigerator. The pressure line was heated by passing 3 ma through the 80 Ω manganin wire wound around it. This heater had several extra turns near the bomb end.

The progress of the solidification process in the bomb was followed by monitoring the ultrasonic signal. As solidification commenced, the echoes visible in the liquid disappeared entirely. As the liquid-solid interface reached the transducer, the echo train for the solid appeared. At this point the gas circulation rate was raised to increase the cooling rate. A few crystals were

annealed in a temperature gradient for twenty or thirty minutes at this time by turning on the temperature-controlled heater on the warm end of the bomb. Any crystals with fewer than 100 visible echoes after this procedure were discarded. With the bomb heater then switched off, the current through the pressure line heater was increased to about 10 ma and solidification continued. This large current was necessary to keep the pressure line open at all times in order that solidification might occur at constant pressure. Superior crystals have previously been grown by this method (Franck and Hewko (1973)). In a few cases where crystals were accidentaly grown at constant volume, the ultrasonic echoes almost entirely disappeared. Once the temperature of the bomb began to fall rapidly, solidification was assumed to be completed. All heaters were then switched off and gas circulation was stopped. The entire process lasted 6-8 hours.

We have no direct evidence for the quality of the crystals, but there are two reasons for supposing that we had generally high quality specimens. The large number of clean echoes visible (as many as 175 for crystal A8-d) imply a small number of crystal defects which, if present, would adversely affect the attenuation. Some very low angle grain boundaries could be present but these are of little importance in ultrasonics as long as they are not too numerous. As well, the range of absolute velocities

observed (including discarded crystals) was 735-840 m/sec; this spans almost the entire range of velocities expected (see figure 2).

3.2 Thermometry

The principal secondary thermometers were constructed from 220 Ω, 0.5 Speer carbon resistors (Black et al. (1964), Oda et al. (1974)), whose resistance was measured by an S.H.E. model ARB automatic resistance bridge. Power dissipation was typically 10^{-11} - 10^{-12} watts. The thermometers were prepared by grinding the outer coatings from the resistors and covering them with thinned GE varnish (#7031) which was baked on at 90°C. The resistors were inserted and varnished into machined copper blocks which were screwed to the copper support plate, to the bomb and to the still. The 42 AWG manganin wire leads were thermally anchored at the mixing chamber, the heat exchangers, the still and the He^4 pot.

The thermometers were calibrated in two ways. Initially a CMN paramagnetic thermometer was constructed (Abel et al. (1964), Fisher (1972)) and the susceptibility measured with a Hartshorn-type mutual inductance bridge (Maxwell (1965)). The CMN salt pill was calibrated against the vapour pressure of He^4 at temperatures above 1 K. As there were some problems reading the bridge this method was not entirely satisfactory so the thermometers

were later compared to an S.H.E. germanium resistance thermometer calibrated from 30 mK to 5 K and measured on the ARB bridge. This thermometer was held in a machined copper block with Corning silicone vacuum grease. This later calibration raises the temperatures recorded with the data in this work by about 40 mK.

3.3 Ultrasonics

3.3-1 Transducer Assembly

The ultrasonic etalon, as supplied by Valpey-Fisher, was a ½-inch diameter quartz transducer with a fundamental frequency of 5 MHz. It was overtone polished to provide good excitation of higher harmonics, and coated on both sides with a thin film of AuCr alloy. As can be seen in figure 7, the front of the transducer was held at the rim by a brass flange 3 mm thick and 25 mm in diameter with a 10 mm diameter hole in the centre. Six radial grooves were scored on the back of the flange to prevent an unwanted pressure build-up. The flange and the bottom end of the main body of the transducer assembly were polished flat to 2 fringes of sodium light. Six screws held the flange to the body. Backing the transducer was a brass piston polished to 2 fringes of sodium light and inserted into a teflon sleeve. The piston was bevelled at the top to dampen reflections in the brass while the

teflon sleeve had a 2° bevel so that it would be self-levelling. With the teflon sleeve in place the piston had the rf lead wire attached to it and then was spring-loaded into the large brass cylinder (25 mm diameter) which formed the main body of the assembly.

Optically polished surfaces and the choice of a spring of the proper size and force constant were found to be crucial for the attainment of a good ultrasonic signal.

The assembly was mounted within the bomb by three pairs of push-pull screws as described in section 3.1-2.

3.3-2 Electronics

Figure 8 is a block diagram of the electronics. The technique employed was a modified pulse-echo-overlap method as described by May (1958), Chung et al. (1969), Papadakis (1964, 1967) and Van Nest et al. (1969). The heart of the system is a highly stable (to better than 1 part in 10^7 per day) frequency synthesizer, model 5100 by Rockland Instruments. It operates at a frequency ν in the neighbourhood of 50 kHz such that

$$1/\nu = 2D/v \ , \qquad (3.3\text{-}1)$$

where v is the sound velocity and D is the distance from transducer to mirror. This signal is divided by a

BLOCK DIAGRAM OF ULTRASONICS

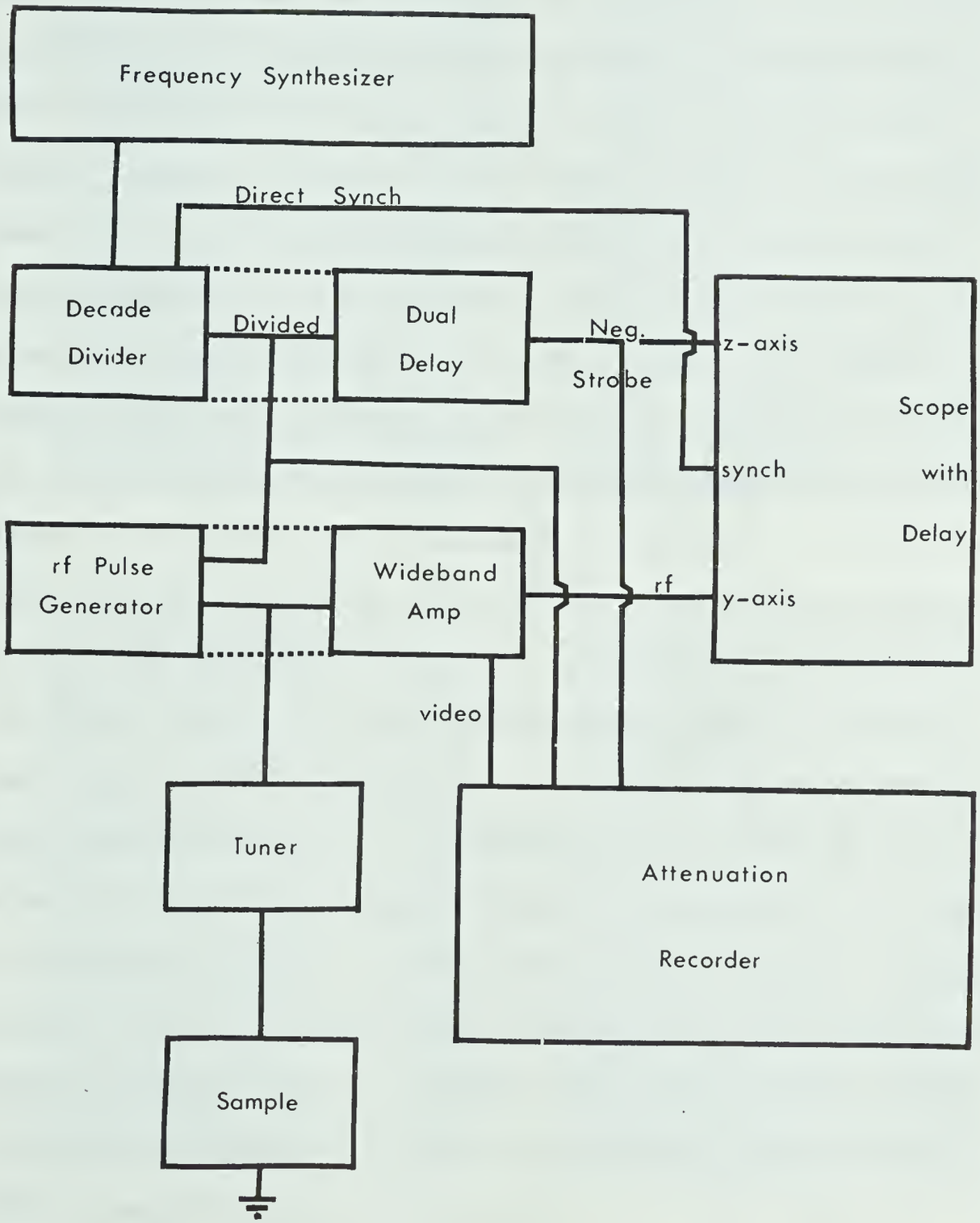

Figure 8

factor of 100 or 1000 in a MATEC 121 decade divider - dual delay generator and is used to trigger the rf pulse generator-wide band amplifier (MATEC 6600 with plug-in 760). The rf pulse is sent by 50 Ω coaxial cable through a system of two passive tuning networks, one supplied by MATEC (model 60) and the second a twin-tee stub tuner network (Wanner (1970)). The pulse is sent to the transducer and the returning echoes again pass through the tuning networks to be amplified by the model 6600. The resulting signal is applied to the y-axis of a Hewlett-Packard 182C oscilloscope with plug-ins 1808A and 1825A. The oscilloscope is triggered with the undivided pulse-shaped signal from the frequency synthesizer. If one uses the continuous delay on the oscilloscope trigger circuit, any part of the pulse train may be observed. Because of the image retention of the oscilloscope screen and the human eye, the rf contents of all echoes may be observed simultaneously and will all appear to be lined up if equation (3.3-1) is satisfied (as in figure 9(b)). Then the velocity is $2D\nu$. If the velocity or trigger frequency changes then the echoes shift relative to one another as seen in figure 9(c,d). As well, the oscilloscope may be internally triggered in order to view the entire echo train (figure 9(a)).

When the signal-to-noise ratio became small, a double negative strobe was applied to the z-axis of the

Figure 9 - Ultrasonic Echo Train and Echo Overlap (in Liquid Helium)

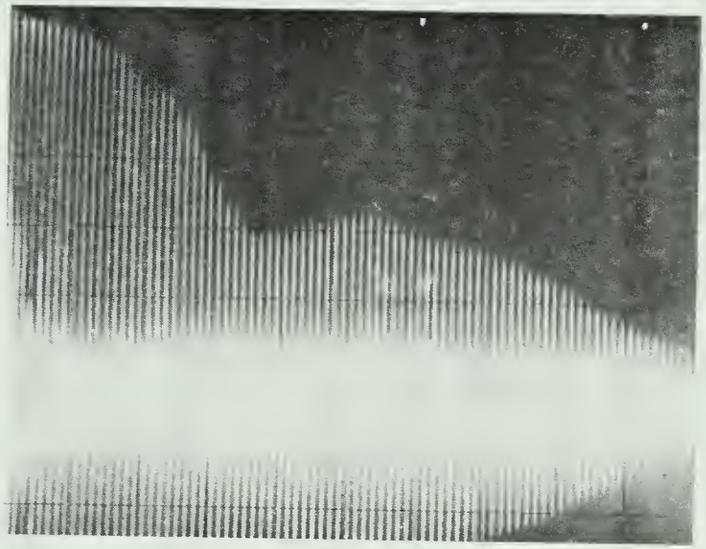

(a) Echo Train

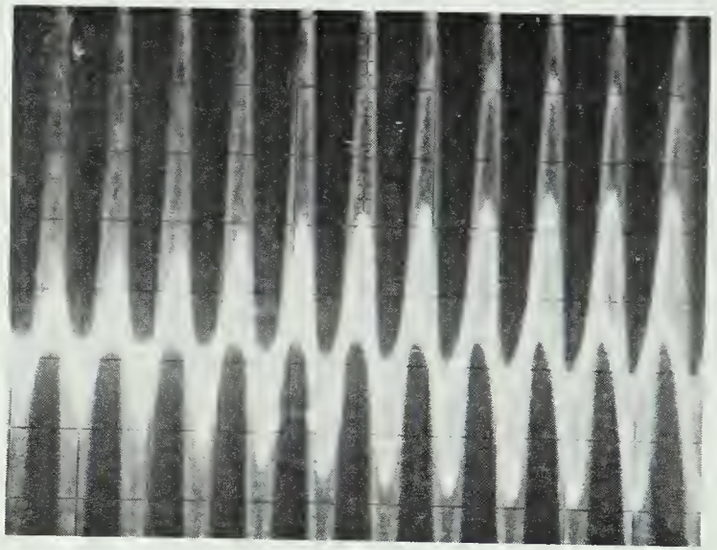

(b) Overlap - 41057 Hz

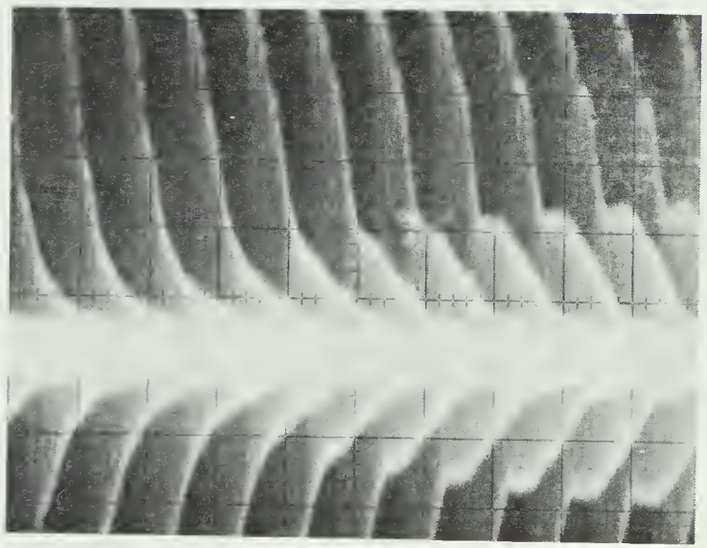

(c) 41067 Hz

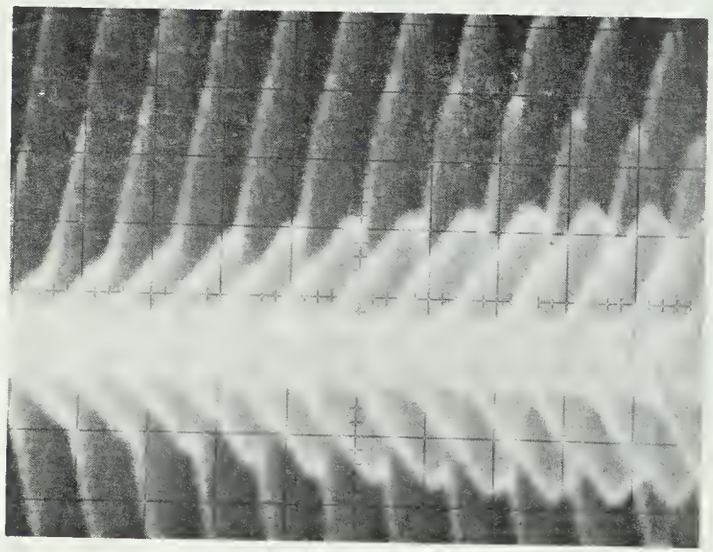

(d) 41047 Hz

oscilloscope. The two strobe pulses were delayed by the dual delay generator so that they were synchronous with any two selected echoes. Then only those two echoes remained visible on the oscilloscope screen while other echoes and most of the noise were deleted.

Some attempt was made to measure attenuation with a MATEC 2470A attenuation recorder. It automatically measures the decrement between two pre-selected echoes and continuously copies it onto a chart recorder. The presence of the highly non-exponential echo envelope (see section 3.3-4) limited the usefulness of this method. Instead the attenuation was determined by photographing the echo train with a Hewlett-Packard 197A oscilloscope camera and manually measuring the decrement.

The initial pulse had an amplitude of 200 to 400 Vpp and a width of approximately 4 μs. The repetition rate was $\nu/100$ at higher temperatures and $\nu/1000$ at lower temperatures. There was no discernible power dependence of the velocity upon changing either the pulse height or repetition rate.

Very careful tuning of both passive networks was necessary in order to obtain the best signal and partially compensate for the very large acoustic mismatch (over 100) between quartz and solid helium.

3.3-3 Method

Initially the cell was filled with methanol and the resulting ultrasonic echoes were observed. The degree of non-parallelism between the transducer and reflector was monitored by watching the echo envelope (section 3.3-4). The push-pull screws were then adjusted and tightened to lock the transducer in place, parallel to the mirror.

Measurements were taken first in liquid helium while the cell was maintained in equilibrium with the helium bath through the medium of He^4 exchange gas in the vacuum can. From the known velocity v_L in the liquid (Vignos and Fairbank (1966) as corrected by Wanner (1970) and Abraham et al.(1970)), the transducer to reflector distance D was determined from $D = v_L/2\nu$. It was assumed that D changed little upon freezing so that the absolute velocity could then be determined in the solid. Thenceforth only changes in velocity, or changes in ν, needed to be recorded.

The true condition for overlap is given by McSkimin and Andreatch (1962) as,

$$\frac{1}{\nu} = \frac{2pD}{v} + \frac{n}{f} \quad . \qquad (3.3\text{-}2)$$

Here p is the number of round trips between trigger pulses (usually $p = 1$), f is the rf frequency and $n = 0$

when succeeding echoes are correctly superposed. The oscilloscope can be triggered with $n \neq 0$ so that each echo is displaced by n rf periods relative to the previous echo. The rf oscillations will still appear aligned and for long pulses or short echo trains the effect will not be obvious. However from (3.3-2) it can be seen that if f is varied, the overlap condition will not be fulfilled if $n \neq 0$. McSkimin's method then is to vary f for several overlaps in order to find the one independent of f. In practice this choice was always confirmed by comparing $1/\nu$ with the average time between echoes along the entire pulse train. McSkimin's criterion was applied at each different rf frequency.

Once the absolute velocity was determined, the temperature was slowly lowered and ν was adjusted regularly in order to keep the echoes in alignment and to follow the same rf oscillations over the entire temperature range. Measurements for any one rf frequency were performed over a period of two days, often repetitively over certain temperature ranges. Some crystals were cycled with respect to temperature and frequency with excellent reproducibility.

3.3-4 Errors in Measurement

The uncertainty in the measurement of D, and therefore in the absolute velocity, is 0.1%, based on the

reproducibility of the measurements. The largest errors in the determination of the orientation arise from the extrapolation of the elastic constants to 17.4 cm^3 (appendix 1). This is estimated to be about 2%, since the extrapolation to 16 cm^3 (Reese et al.(1971)) is correct to better than 5 %. The error in orientation is very much a function of the velocity, because of the wide variation in $dv/d\gamma$ (figure 2). For $42° \leq \gamma \leq 90°$, the velocity is double-valued. In these cases a most likely orientation is chosen by observing the interference pattern. A pattern similar to that seen in the liquid was considered to arise from an orientation with a small beam deviation (figure 3). For orientations with a large Δ, the beam will sample a different part of the reflector and so the interference pattern will change. The measuring error in $\Delta v/v$ varies inversely with the number of echoes observed. In practice the error for 100 echoes is about 2×10^{-6} and for 2 echoes (as measured at low temperatures) about 5×10^{-5}. The limiting factors are the jitter in the trigger pulses and various small effects which are dependent upon echo number.

The finite pulse length causes variations in transit time for different parts of the pulse (Merkulov and Tret'yakov (1975)) so that there was an observed velocity change of about $2\text{-}3 \times 10^{-5}$ across the pulse. This error is effectively eliminated by always following the

same rf oscillations near the centre of the pulse at all temperatures.

Also exerting a small influence on the sound propagation is diffraction of the beam. This effect has been investigated by a number of authors (Seki et al (1956), Khimunin (1975), Papadakis (1966, 1972)). Papadakis (1966) has made calculations for anisotropic materials so his results are of the greatest interest to the present work. Diffraction of the beam results in a wave front which is no longer planar, and varying with distance travelled, so that there is a phase shift in the detected signal. As well the wave will interfere with itself at the transducer, causing an apparent change in attenuation. This last effect is negligible when compared with other problems involved in measuring the attenuation in solid helium. In general the phase shift is a complicated function of wavelength λ, transducer diameter a and distance travelled z, but the phase shift is approximately linear in $S = z\lambda/a^2$ for $S \lesssim 0.5$ (at 5 MHz, $S \simeq 0.023\ n$, where n is the number of round trips). The proportionality constant varies with the anisotropy, but is always smaller in solid helium (where the anisotropy parameter $b = v_3$ of Waterman (1959) is 0.25 along the c-axis and $0.12 \cos^2\psi$ in the basal plane, ψ being the azimuthal angle) than in isotropic liquid helium ($b = 0$). The largest influence of diffraction in the present work

is on the measurements of dispersion. The changes in $\Delta v/v$ in the liquid should be about -4×10^{-5} between 5 and 15 and about -6×10^{-6} between 15 and 25 MHz. The effect in the solid will always be less and rarely more than half of that in the liquid.

The greatest geometrical effect, especially with respect to attenuation measurements, arises from a lack of parallelism between the transducer and the reflector. This problem has been investigated in a rather simple way by Truell et al. (1969) and Abraham et al. (1969). The present calculations are much more detailed.

Rigorously we begin with an initial velocity distribution on the transducer Im f_o $(x,y;t)$. Then the Fourier transform is:

$$F_o\ (r,\theta;\omega) = \int_{-\infty}^{\infty} e^{-i\omega t} f_o(r,\theta;t)\,dt. \qquad (3.3\text{-}3)$$

The phase delay of the $n^{\underline{th}}$ echo for attenuation α and velocity c is:

$$\phi_n(r,\theta;\omega) = (\omega/c - i\alpha) \times (\text{distance travelled}). \qquad (3.3\text{-}4)$$

Then the Fourier transform for the $n^{\underline{th}}$ echo is:

$$F_n(r,\theta;\omega) = F_o(r,\theta;\omega)\ e^{-i\phi_n(r,\theta;\omega)}. \qquad (3.3\text{-}5)$$

Finally, the received signal for the $n^{\underline{th}}$ echo will be:

$$\text{Im } f_n(t) = \frac{1}{2\pi} \int_{-\infty}^{\infty} d\omega e^{i\omega t} \frac{4}{\pi a^2} \int_0^{a/2} r dr \int_0^{2\pi} d\theta F_n(r,\theta;\omega), \tag{3.3-6}$$

where a is the diameter of the transducer.

Generally, for reasonably long pulses, the centre of the pulse may be treated as monochromatic so that the preceding method is only required when considering the ends of the pulse. Then we may write, for a fundamental frequency Ω,

$$f_n(t) = \frac{4}{\pi a^2} \int_0^{a/2} r dr \int_0^{2\pi} d\theta e^{-i\phi_n(r,\theta;\Omega)} f_o(r,\theta;t). \tag{3.3-7}$$

In the simplest case,

$$f_o(r,\theta;t) = \begin{cases} e^{i\Omega t}, & 0 \leq t \leq T \\ 0, & \text{otherwise.} \end{cases} \tag{3.3-8}$$

If the reflector is tilted relative to the transducer, as in figure 10(a), then:

$$\phi_n(r,\theta;\omega) = \omega(t_n + 2t'_n \frac{r}{a} \cos\theta) - i(\nu_n + 2\nu'_n \frac{r}{a} \cos\theta), \tag{3.3-9}$$

where $t_n = 2nD/c$ $\qquad$ $\nu_n = 2n\alpha D$

$t'_n = nd/c$ $\qquad$ $\nu'_n = n\alpha d.$

Transducer - Reflector Arrangements

(a) Tilted Reflector

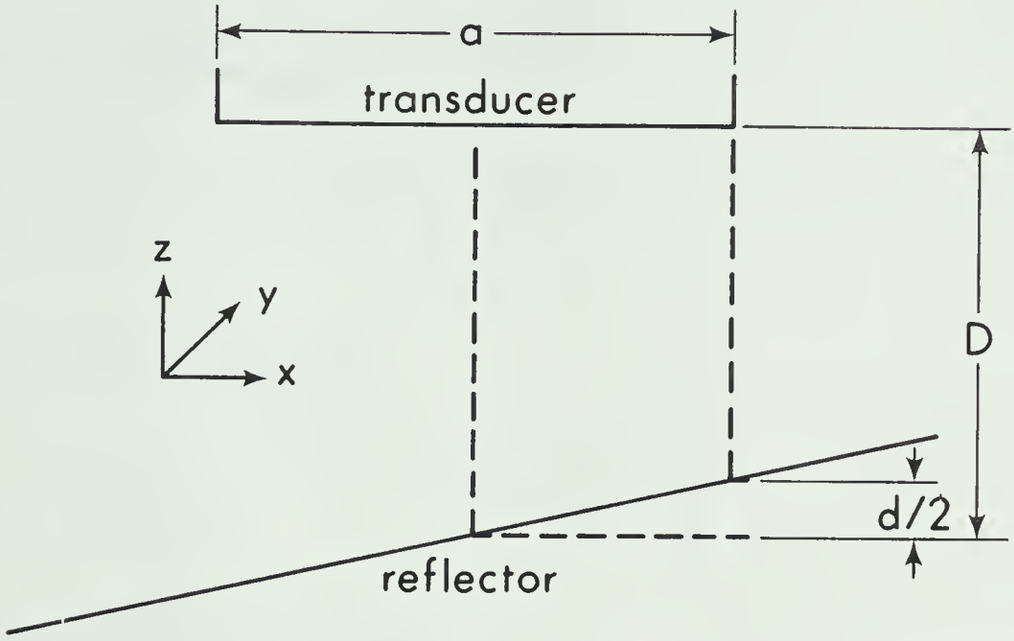

(b) Curved Reflector

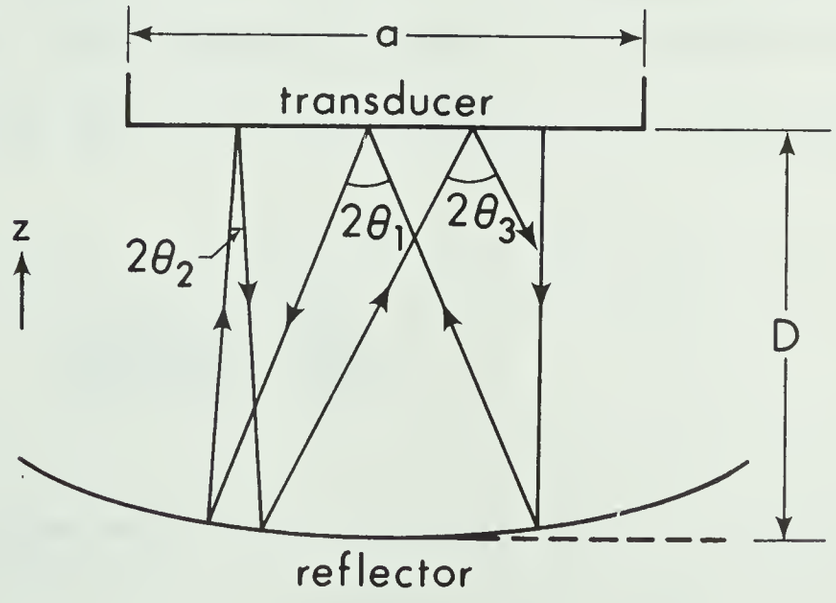

Figure 10 Transducer-reflector configurations

Then equation (3.3-7) may be integrated to give

$$\text{Im } f_n(t) = e^{-\nu_n} \cdot \frac{2|J_1(\Omega_o t_n')|}{|\Omega_o t_n'|} \sin[\Omega(t-t_n) + \delta_1 + \eta_n^{(1)}]. \tag{3.3-10}$$

Here $\delta_1 = \arctan \omega_o/\Omega \simeq \omega_o/\Omega$

$$\omega_o = \alpha c$$

$$\eta_n(1) = \arg J_1(\Omega_o t_n')$$

$$\Omega_o = \Omega - i\omega_o,$$

and J_n is the Bessel function of order n. Then the rf wave is modulated by an amplitude $2e^{-\nu_n}|J_1(\Omega_o t_n')|/|\Omega_o t_n'|$ and phase-shifted by $\delta_1 + \eta_n^{(1)}$. The maxima and minima of this envelope may be calculated exactly, but since the effects are only important when α is small, we may simply write that to first order in ω_o/Ω, the maxima occur at

$$\frac{J_1(\Omega t_n')}{J_o(\Omega t_n')} = \frac{\Omega t_n'}{\nu_n + 2}, \tag{3.3-11}$$

and the minima at

$$J_1(\Omega t_n') = 0. \tag{3.3-12}$$

If $\nu_n << 2$, then we have

$$n_{max} = \frac{c}{\Omega d} (0, 5.14, 8.42, 11.62, 14.8, \ldots),$$

$$n_{min} = \frac{c}{\Omega d} (3.83, 7.02, 10.17, 13.32, \ldots) . \qquad (3.3\text{-}13)$$

Then for any two selected echoes n_1 and n_2, the true attenuation α is given in terms of the "measured" attenuation α' as,

$$\alpha = \alpha' + \frac{\ell n[J_1(t'_{n_2})/J_1(t'_{n_1})] + \ell n(n_1/n_2)}{2D(n_2-n_1)} . \qquad (3.3\text{-}14)$$

To first order in ω_o/Ω,

$$\tan \eta_n^{(1)} = (\omega_o/\Omega)[1 - \Omega t'_n J_o(\Omega t'_n)/J_1(\Omega t'_n)] . \qquad (3.3\text{-}15)$$

Then for two echoes n_1 and n_2, the measured velocity is larger than the actual velocity by

$$\frac{\Delta c}{c} = \frac{c}{2\Omega D} \frac{\omega_o}{\Omega} \left[\Omega t'_{n_1} \frac{J_o\ \Omega t'_{n_1}}{J_1\ \Omega t'_{n_1}} - \Omega t'_{n_2} \frac{J_o\ \Omega t'_{n_2}}{J_1\ \Omega t'_{n_2}} \right] . \qquad (3.3\text{-}16)$$

The transducer does not necessarily vibrate in a piston-like manner as in equation (3.3-8) (Papadakis (1971)), especially if clamped at the edge. A simple case to treat mathematically is:

$$f_o(r;t) = \begin{cases} (1-4r^2/a^2)\ e^{i\Omega t}, & 0<t<T \\ 0, & \text{otherwise.} \end{cases} \qquad (3.3\text{-}17)$$

Then $\text{Im}\ f_n(t) = e^{-\nu_n} \cdot \dfrac{4|J_2(\Omega_o t'_n)|}{|\Omega_o t'_n|^2} \sin\left[\Omega(t-t_n)+\delta_2+\eta_n^{(2)}\right]$,

(3.3-18)

where $\delta_2 = \arctan\left[2\Omega\omega_o/(\Omega^2+\omega_o^2)\right] \simeq 2\omega_o/\Omega$

and $\eta_n^{(2)} = \arg J_2(\Omega_o t'_n)$.

Then the maxima occur at

$$J_2(\Omega t'_n)/J_1(\Omega t'_n) = \Omega t'_n/(\nu_n+4), \qquad (3.3\text{-}19)$$

and the minima at

$$J_2(\Omega t'_n) = 0. \qquad (3.3\text{-}20)$$

$$n_{min} = \frac{\Omega}{cd}\ [5.14,\ 8.42,\ 11.62,\ 14.80,\ \ldots] \qquad (3.3\text{-}21)$$

and $n_{max} = \dfrac{\Omega}{cd}\ [0,\ 6.38,\ 9.76,\ 13.02,\ 16.22,\ \ldots]$.

Also, $\alpha = \alpha' + \dfrac{\ell n[J_2(\Omega t'_{n_2})/J_1(\Omega t'_{n_1})]+2\ \ell n(n_1/n_2)}{2D(n_2-n_1)}$,

(3.3-22)

$$\text{and} \quad \frac{\Delta c}{c} = \frac{c}{2\Omega D} \cdot \frac{\omega_o}{\Omega} \left[\Omega t'_n \frac{J_1(\Omega t'_{n_1})}{J_2(\Omega t'_{n_1})} - \Omega t'_{n_2} \frac{J_1(\Omega t'_{n_1})}{J_2(\Omega t'_{n_2})} \right] . \tag{3.3-23}$$

Equation (3.3-17) is not necessarily an accurate description of the true physical situation, but (3.3-18) suggests that qualitatively any deviation from a piston-like velocity distribution will result in an even larger apparent attenuation than that given by (3.3-10).

The velocity corrections δ_1 and δ_2 are negligible when measuring dispersion since $\omega_o << \Omega$. The error in velocity between successive echoes (equation (3.3-16) or (3.3-23)) is less than 5×10^{-6} for $\alpha \simeq 0.1$ cm^{-1} and for low n.

Instead of being tilted, the reflector may be curved as in figure 10(b) where the curvature of the reflector is given by

$$z = \frac{\beta}{2} r^2 . \tag{3.3-24}$$

Then the angle of reflection Θ_n with the normal to the transducer for the n^{th} echo can be shown to obey the recursion relation

$$\Theta_n = 2(1-2\beta D)\Theta_{n-1} - \Theta_{n-2}, \tag{3.3-25}$$

with $\Theta_o = 0$

and $\Theta_1 = 2\beta(r^2+r_o^2+2rr_o\cos\theta)^{\frac{1}{2}}$,

where r_o arises from the beam deviation (section 2.3):

$$r_o = D \tan \Delta. \tag{3.3-26}$$

Let $$\Theta_n^2 = \Theta_1^2 \, U_n^2 \, (1-2\beta D)/4\beta D(1-\beta D). \tag{3.3-27}$$

Then $$U_n = 2(1-2\beta D)\, U_{n-1} - U_{n-2} , \tag{3.3-28}$$

where $U_o = 0$

$$U_1 = [1-(1-2\beta D)^2]^{\frac{1}{2}} .$$

Equation (3.3-28) defines the Chebyshev polynomials of the second kind. Then the phase shift for the n^{th} reflection is

$$\phi_n(r,\theta;\omega) = \frac{\omega}{c}\left[2nD + \left(\frac{r^2+r_o^2+2rr_o\cos\theta}{4D(1-\beta D)}\right) \right. \quad x$$

$$\left. x \sum_{m=1}^{n} [U_m(1-2\beta D) - U_{m-1}(1-2\beta D)]^2\right] - i\nu_n , \tag{3.3-29}$$

where we ignore the slight variation in attenuation from differences in reflector to transducer distance. Then

using (3.3-8) and (3.3-29) in (3.3-7),

$$f_n(t) = \frac{8e}{a^2}^{-\nu_n} e^{i\Omega(t-t_n)} \int_0^{a/2} dr.r \exp\left\{-i \frac{\Omega}{c} \frac{r^2+r_o^2}{4D(1-\beta D)} \right. \times$$

$$\left. \times \sum_{m=1}^{n} (U_m - U_{m-1})^2 \right\} J_o \left[\frac{\Omega}{c} \cdot \frac{2rr_o}{4D(1-D)} \sum_{m=1}^{n} (U_m - U_{m-1})^2 \right] . \quad (3.3\text{-}30)$$

If we define

$$\zeta_n = \frac{\Omega}{2cD} \sum_{m=1}^{n} [U_m(1-2\beta D) - U_{m-1}(1-2\beta D)]^2 , \quad (3.3\text{-}31)$$

and use a series representation for J_o, then it is easy to show (Hansen (1975)), that $f_n(t)$ becomes:

$$\text{Im } f_n(t) = \frac{8e^{-\nu_n}}{a^2\zeta_n} \left| P\left(\frac{i\zeta_n a^2}{4} \middle| 2, i\zeta_n r_o^2\right) \right| \sin [\Omega(t-t_n) + \eta_n^{(3)}] \quad (3.3\text{-}32)$$

where P is the non-central chi-square probability function (Abramowitz et al. (1964)) and

$$\eta_n^{(3)} = \frac{\pi}{2} - \arg P\left(\frac{i\zeta_n a^2}{4} \middle| 2, i\zeta_n r_o^2\right) . \quad (3.3\text{-}33)$$

P is given by

$$P(i\zeta_n a^2/4|2,i\zeta_n r_o^2) = 1-e^{-i\zeta_n(r_o^2/2 + a^2/8)} \; x$$

$$\sum_{k=o}^{\infty} \sum_{j=o}^{k} \frac{(i\zeta_n r^2/2)^k (i\zeta_n a^2/8)^j}{k!j!} . \qquad (3.3\text{-}34)$$

P is difficult to evaluate, but for $r_o << a/2$,

$$P \simeq 1-e^{-i\zeta_n a^2/8} \; [1 - \zeta_n^2 r_o^2 a^2/16]. \qquad (3.3\text{-}35)$$

Therefore,

$$|P| \simeq 2|\sin \zeta_n \, a^2/16| \; [1 - \frac{\zeta_n r_o^2}{4} \cdot \frac{\zeta_n a^2}{8}]. \qquad (3.3\text{-}36)$$

Then the maxima of $|P|/\zeta_n$ occur at:

$$\tan\zeta_n a^2/16 = (\zeta_n a^2/16) \; [1 - \zeta_n^2 r_o^2 a^2/16], \qquad (3.3\text{-}37)$$

or

$$\zeta_n = (16/a^2)(1-16r_o^2/a^2)(0, \; 4.49, \; 7.73, \; 10.90, \; 14.07, \; \ldots). \qquad (3.3\text{-}38)$$

Now $$\zeta_n = \frac{\Omega}{2cD} \sum_{m=1}^{n} [U_m - U_{m-1}]^2$$

$$= \frac{\beta\Omega}{c} [n + U_{2n} \; (1-\beta D)/2U_1^2(1-\beta D)]$$

$$\simeq \frac{\Omega}{c}\left[n\beta + \frac{1}{4D}\sin 2n\sqrt{2\beta D}\right] . \qquad (3.3\text{-}39)$$

Therefore to find β, solve:

$$\sin 2n\sqrt{2\beta D} = 4\beta D\left[-n + \frac{16c}{\beta\Omega a^2}(1-16r_o^2/a^2)(0,\ 4.49,\ 7.73,\ \ldots)\right], \qquad (3.3\text{-}40)$$

where n refers to a maximal echo.

The minima in $|P|/\zeta_n$ occur when $\zeta_n a^2/16 = m\pi$, or

$$\sin 2n\sqrt{2\beta D} = 4\beta D\left[-n + \frac{16c}{\beta\Omega a^2}(3.14,\ 6.28,\ 9.42,\ 12.57,\ \ldots)\right].$$

Finally, using equation (3.3-36),

$$\eta_n^{(3)} = \frac{\pi}{2} - \arctan\left\{\left[\cot(\zeta_n a^2/16)\right]\left[1+\frac{(\zeta_n r_8 a/4)^2\cos\zeta_n a^2/8}{1-\cos\zeta_n a^2/8}\right]^{-1}\right\}. \qquad (3.3\text{-}42)$$

CHAPTER 4

RESULTS

4.1 Velocity of Sound

4.1-1 High Temperature Region

All crystals were measured at a volume of 17.4 ± 0.05 cm^3/mole. The largest error in the determination of the absolute velocity arises from any changes in the transducer to reflector distance D. This error was estimated from measurements of D on successive crystals to be 0.1%. The accuracy of the velocity for purposes of orientation determination is estimated to be better than 2%.

Curves of velocity v (divided by an arbitrary v_o) versus temperature are shown for ten crystals in figures 11 to 20. For the first four samples, measurements were only taken at 5 MHz, while all three frequencies of 5, 15 and 25 MHz were used for the last six.

The curves are least-squares fits of equation (2.5-10) to the data points in the high temperature region only. Equation (2.5-10) was obeyed very well in all cases with the constants having the values listed in table 1 and illustrated in figure 21.

As is apparent from figure 21, the scatter in the values of a and b is too large to allow a meaningful

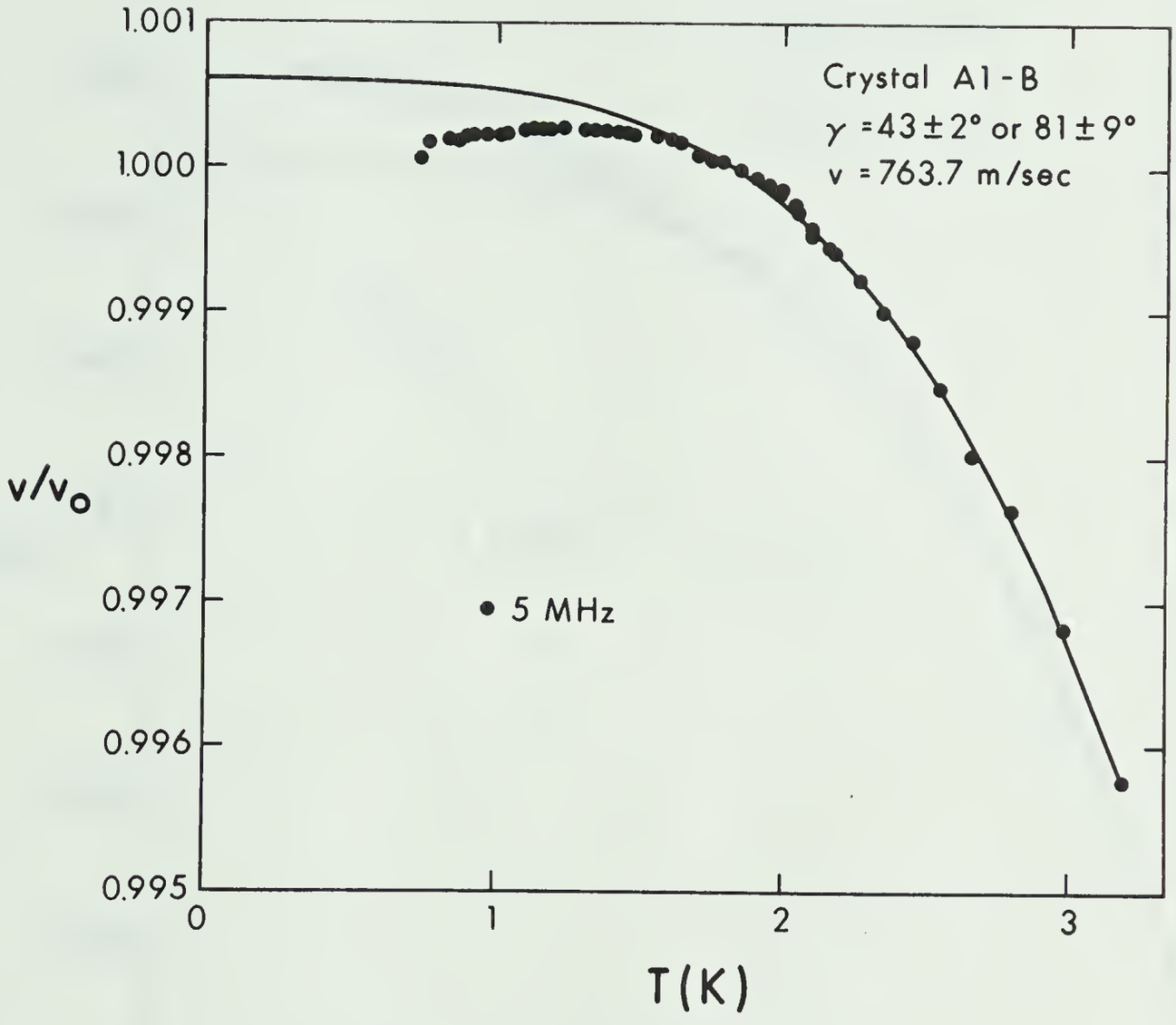

Figure 11 Reduced sound velocity as a function of temperature.

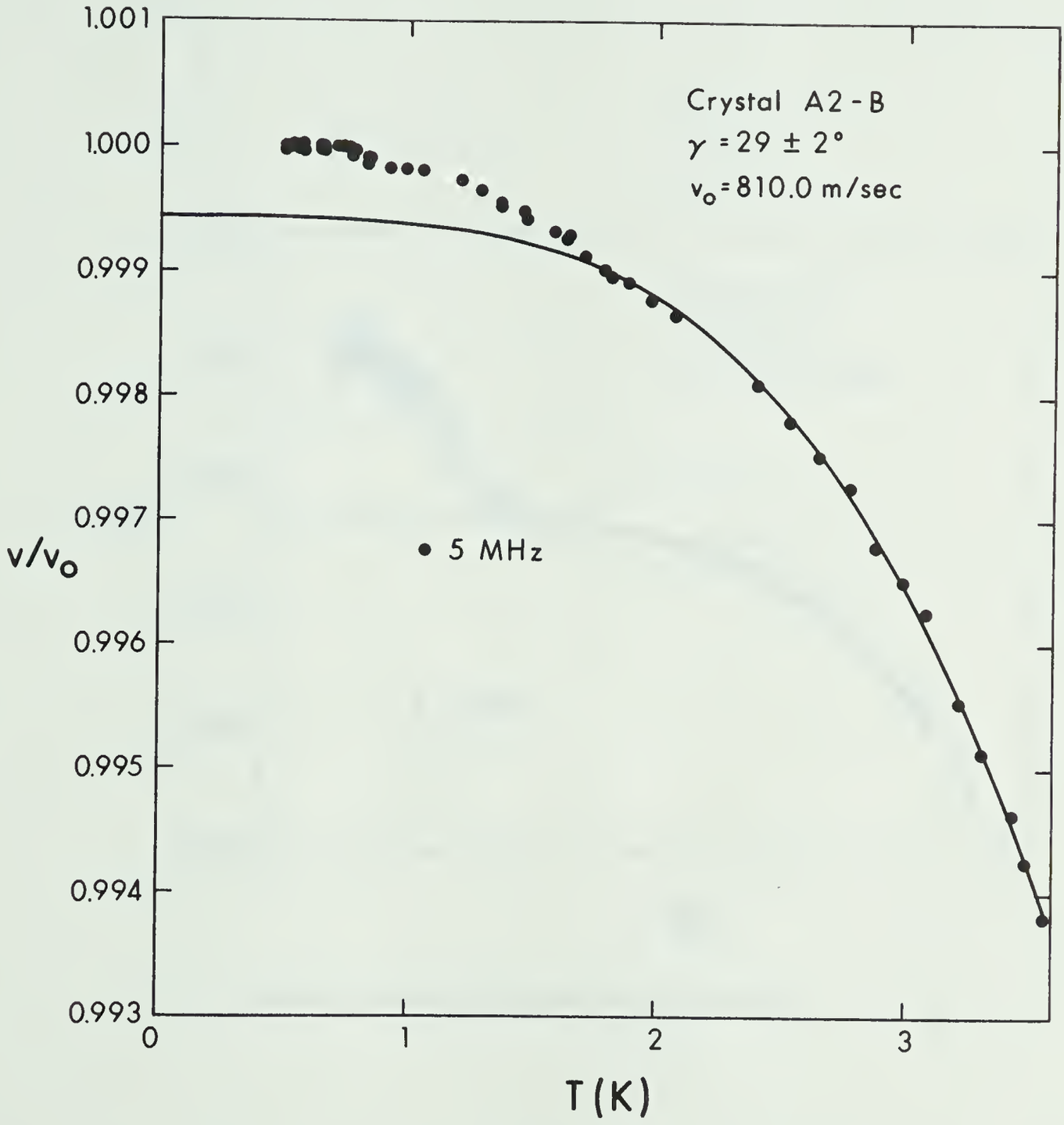

Figure 12 Reduced sound velocity as a function of temperature.

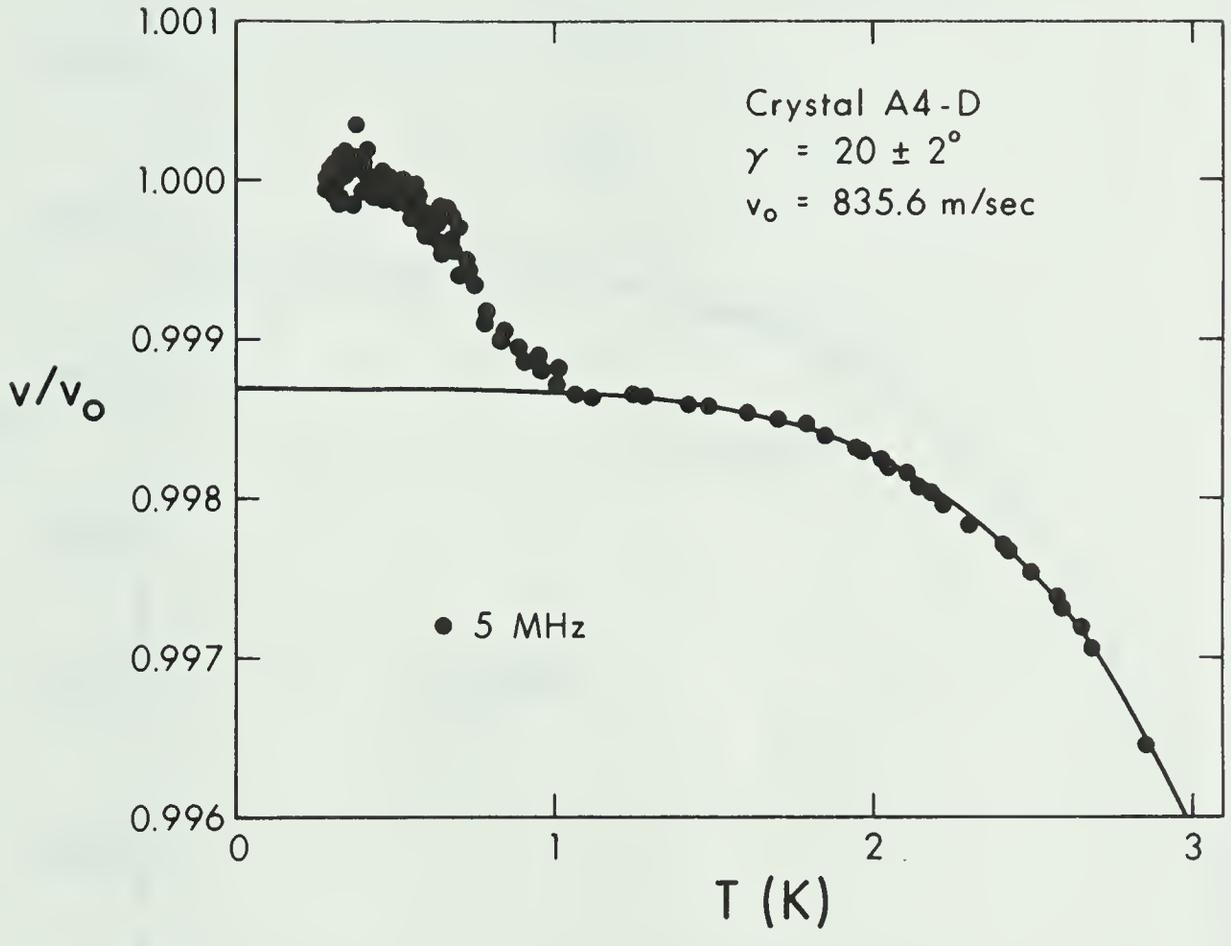

Figure 13 Reduced sound velocity as a function of temperature.

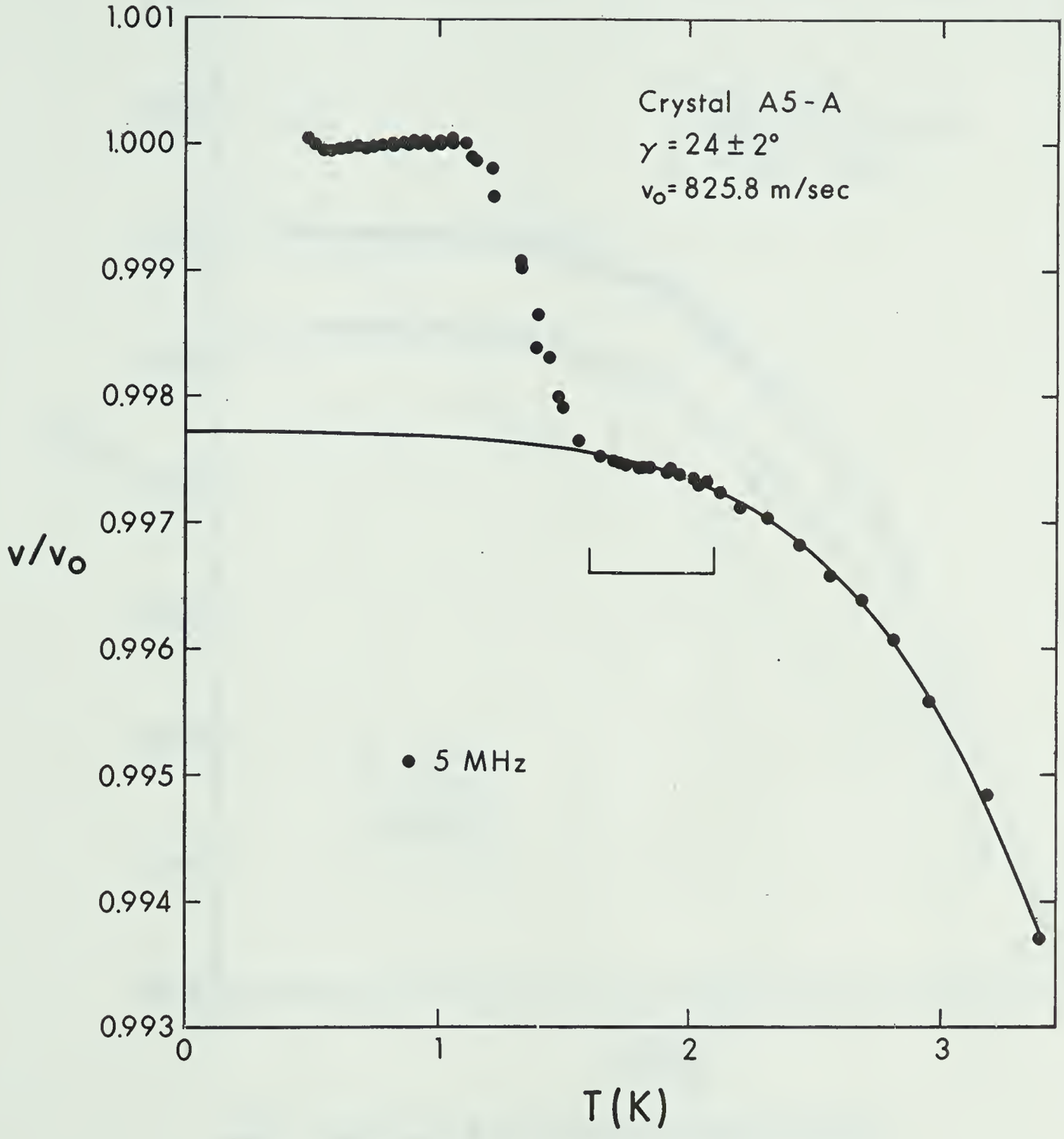

Figure 14 Reduced sound velocity as a function of temperature.

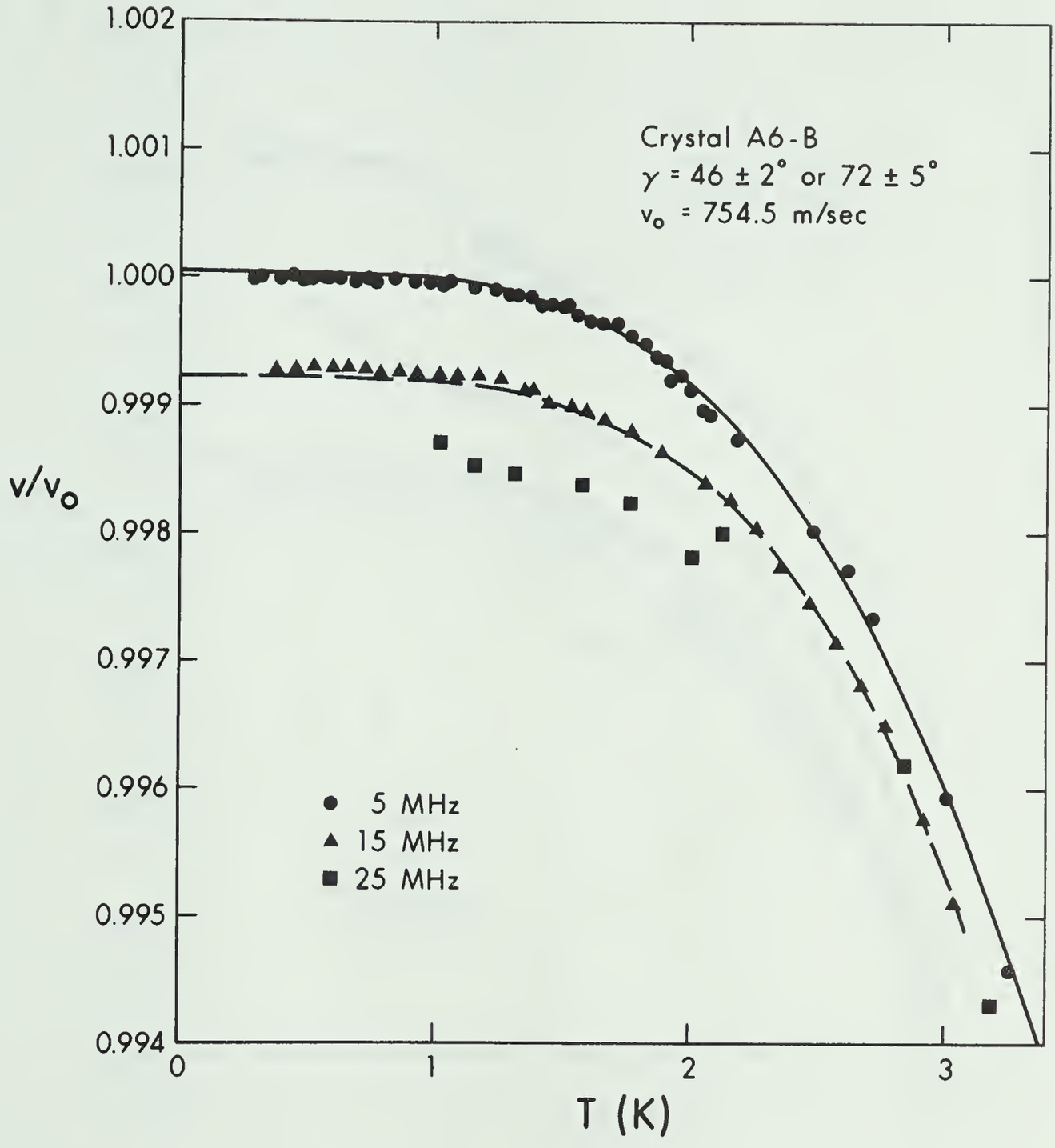

Figure 15 Reduced sound velocity as a function of temperature and frequency.

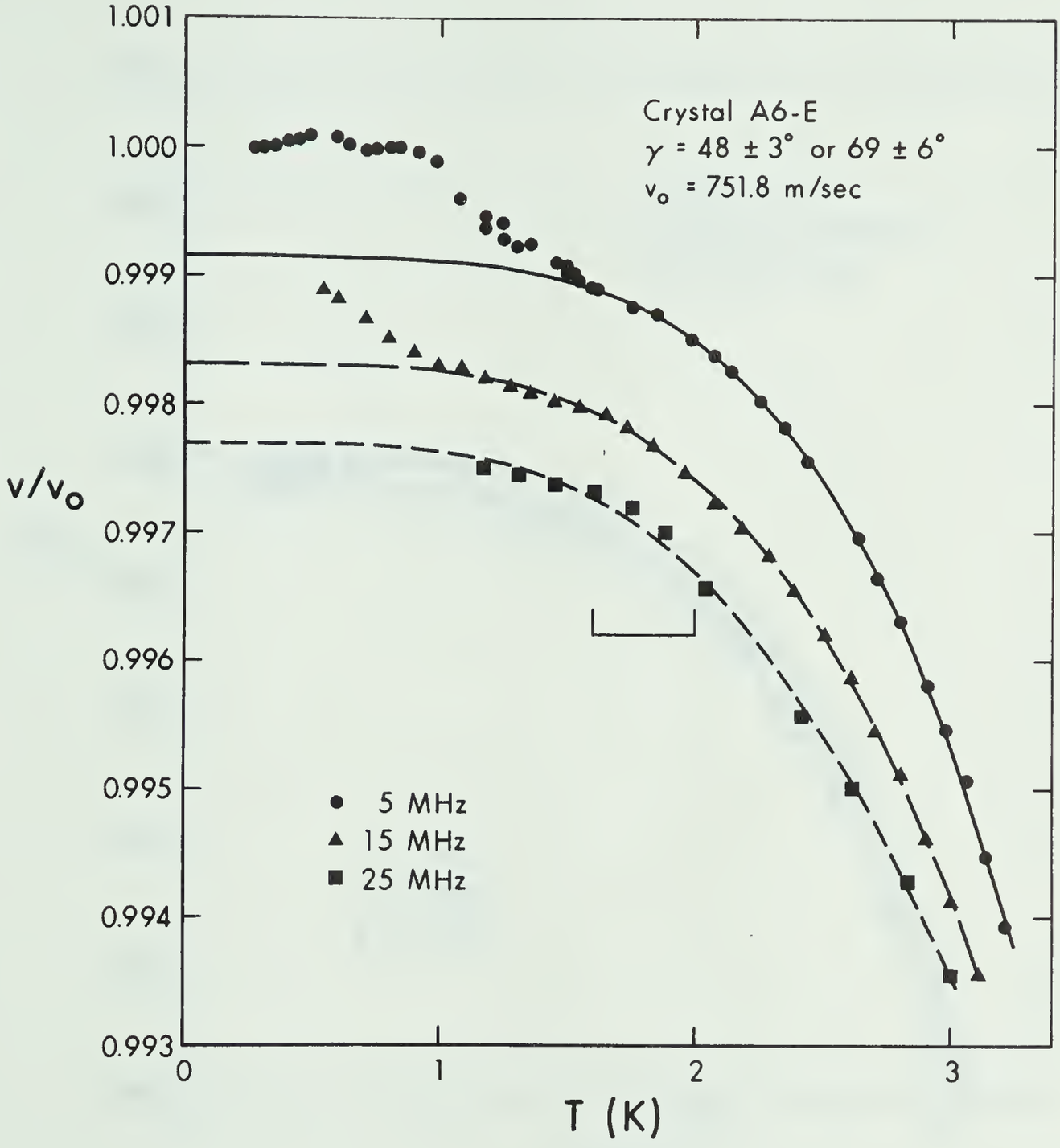

Figure 16 Reduced sound velocity as a function of temperature and frequency.

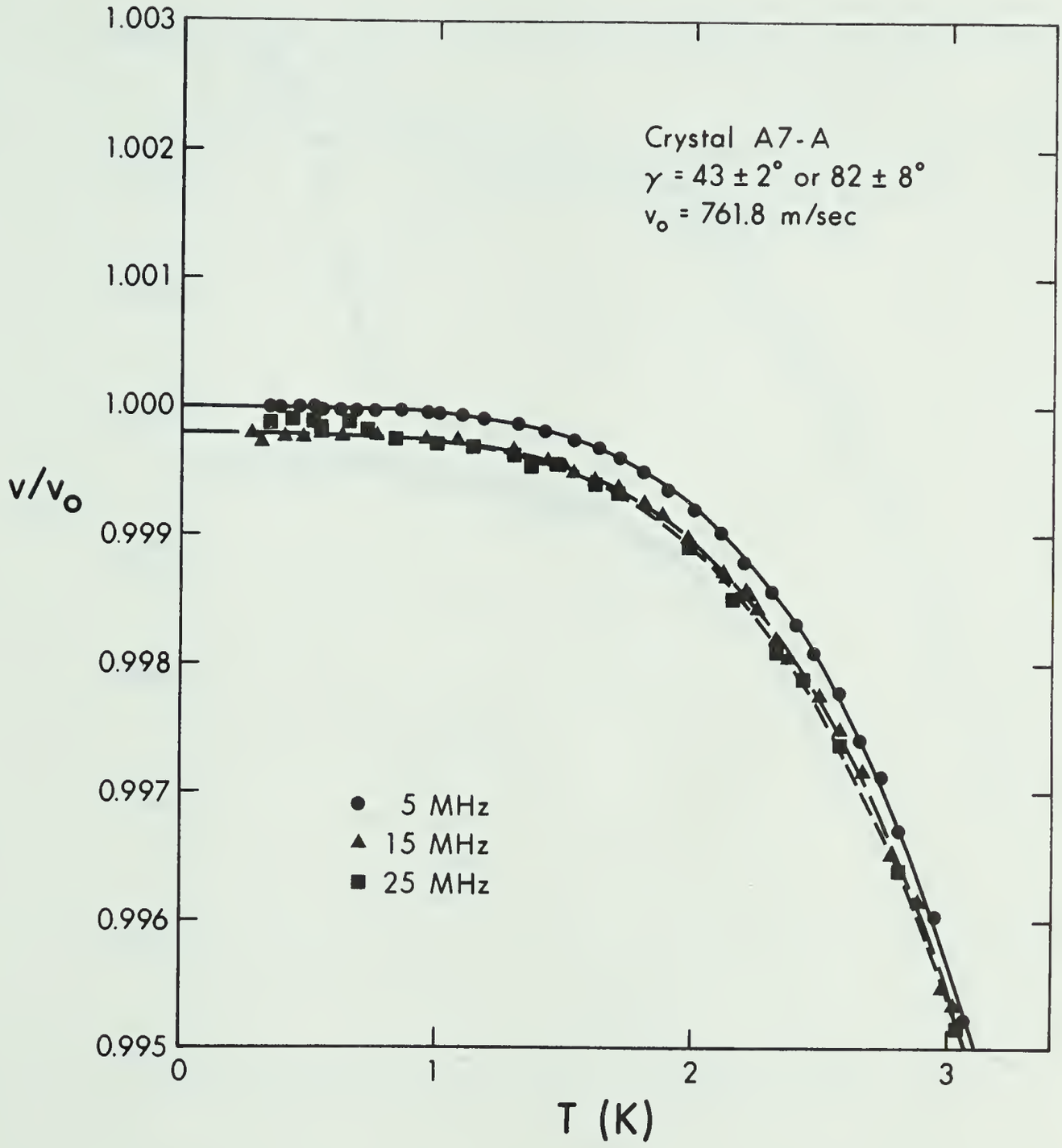

Figure 17 Reduced sound velocity as a function of temperature and frequency.

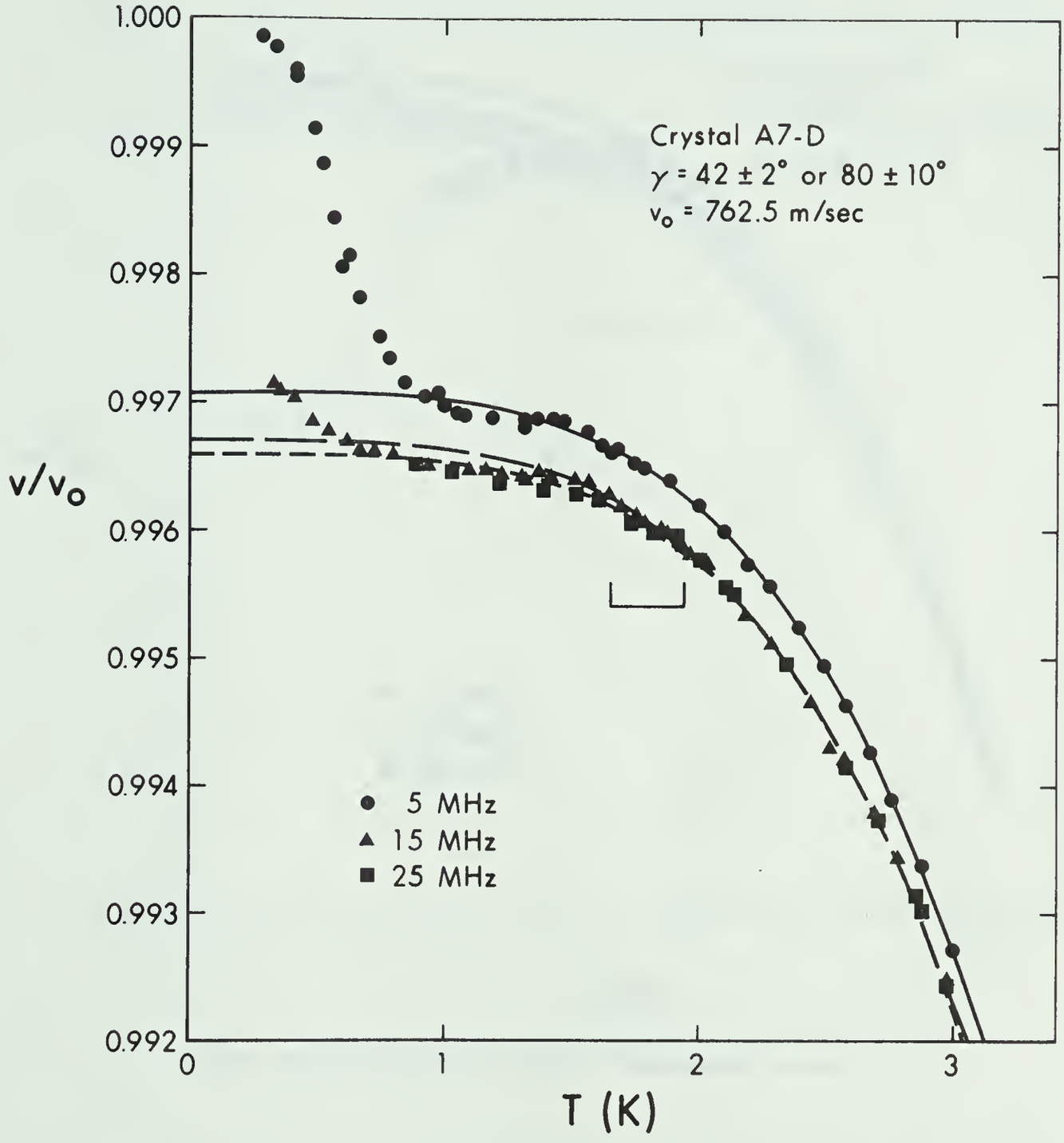

Figure 18 Reduced sound velocity as a function of temperature and frequency.

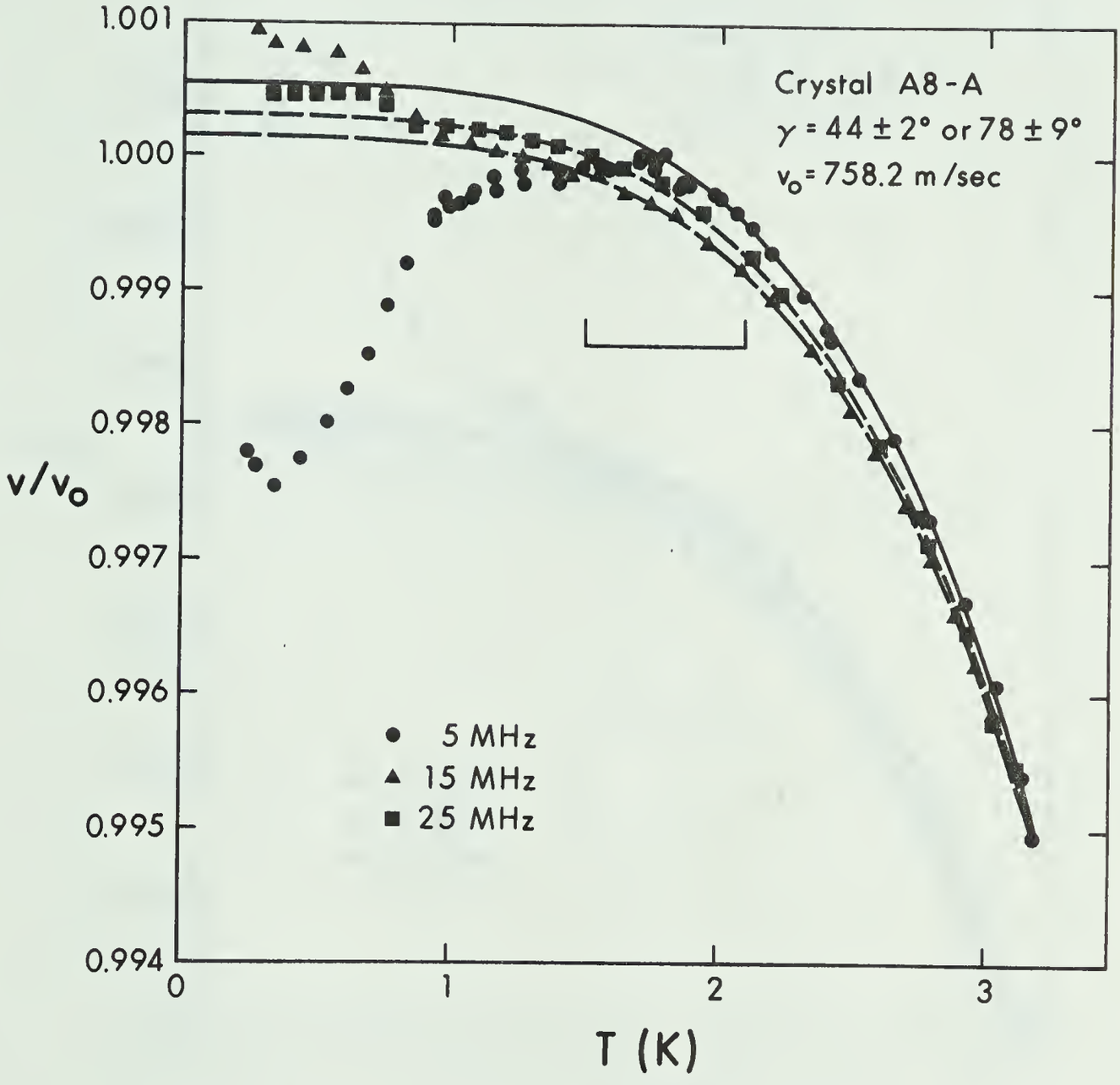

Figure 19 Reduced sound velocity as a function of temperature and frequency.

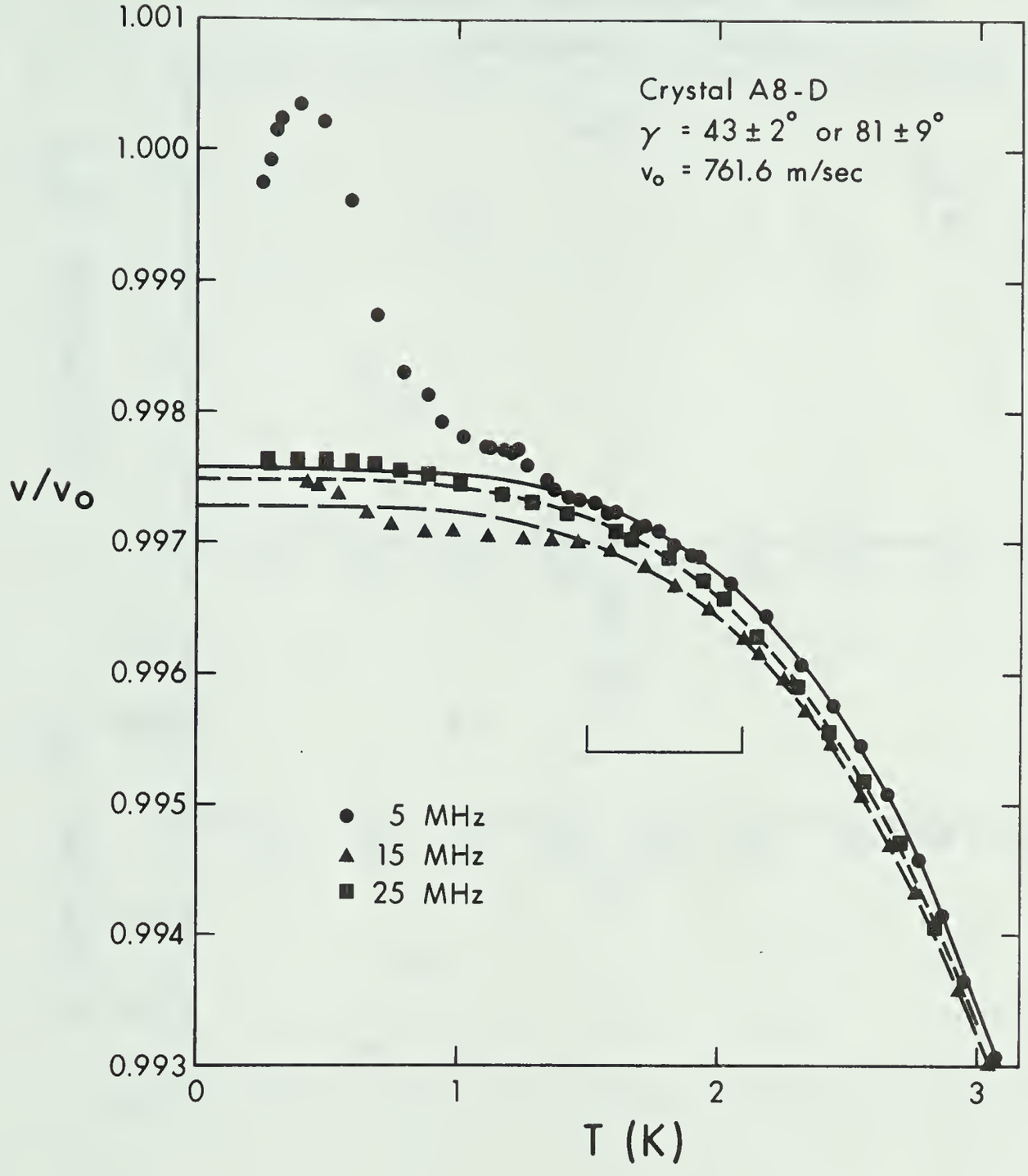

Figure 20 Reduced sound velocity as a function of temperature and frequency.

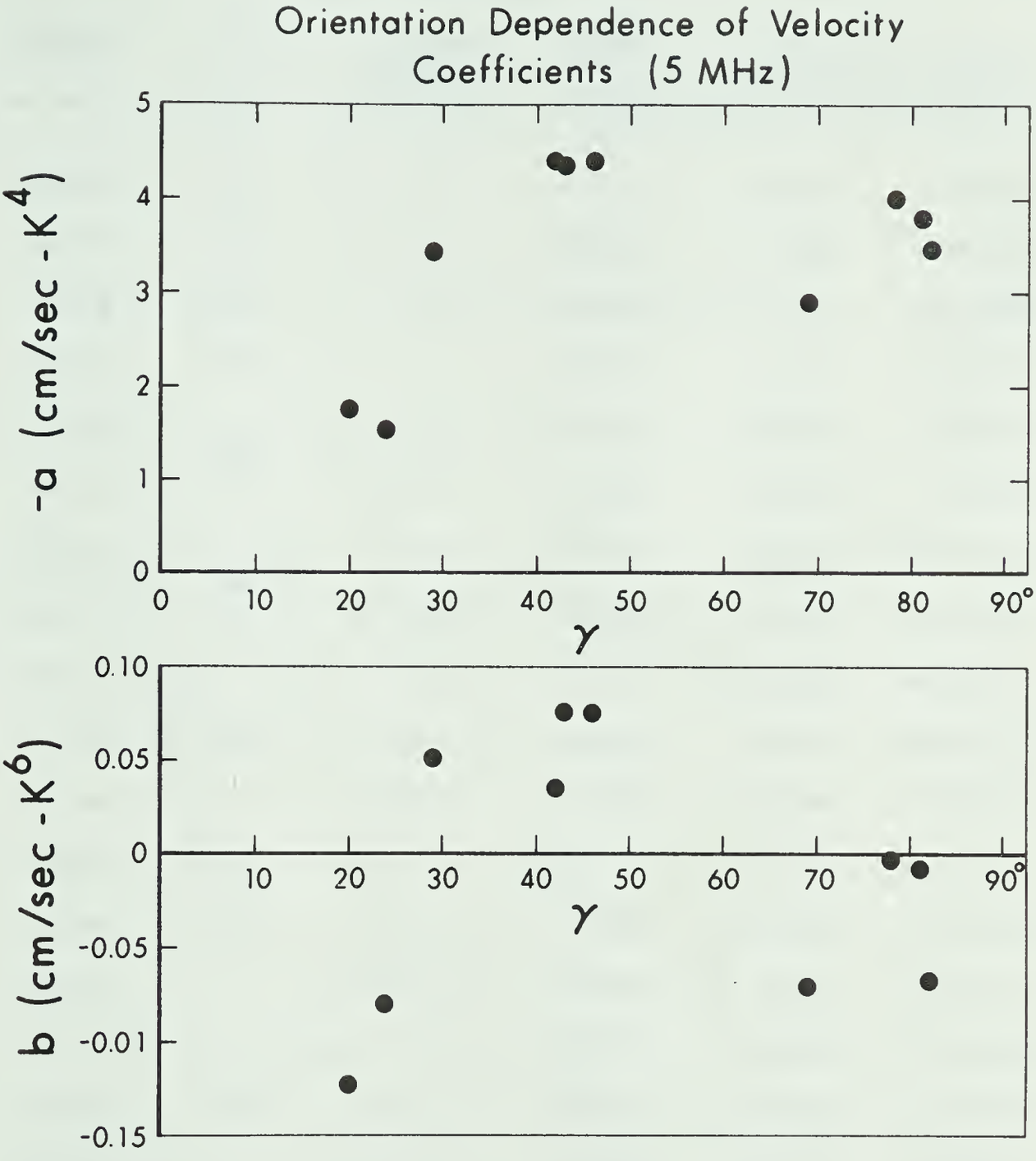

Figure 21 Orientation dependence of adiabatic sound velocity coefficients in equation (2.5-10).

TABLE 1

Crystal	γ(°)	rf Freq. (MHz)	v_a(T=0 (cm/s)	a (cm/s-K^4)	b (cm/s-K^6)
A1-b	43	5	76416	-4.35	0.076
A2-b	29	5	80951	-3.45	0.052
A4-d	20	5	83447	-1.74	-0.123
A5-a	24	5	82392	-1.53	-0.082
A6-b	46	5	75450	-4.39	0.076
A6-c		15	75396	-3.76	0.013
A6-e	69	5	75112	-2.91	-0.071
A6-f		15	75048	-4.42	0.062
A7-a	82	5	76176	-3.48	-0.067
A7-b		15	76160	-3.93	-0.017
A7-c		25	76160	-4.54	0.046
A7-d	42	5	76027	-4.41	0.035
A7-e		15	75998	-4.76	0.072
A7-f		25	75990	-4.02	-0.003
A8-a	78	5	75856	-4.00	-0.003
A8-b		15	75827	-4.13	0.032
A8-c		25	75839	-4.19	0.028
A8-d	81	5	75970	-3.79	-0.006
A8-e		15	75948	-4.27	0.048
A8-f		25	75963	-4.57	0.071

calculation of the temperature dependence of the elastic constants. However both a and b clearly reach maximum values at intermediate angles with minima at $\gamma = 0°$ and 90°. Very approximately it can be estimated that,

$$\Delta c_{33}/c_{33} \simeq - (3\pm1)\times10^{-5}T^4 - (3\pm1)\times10^{-6}T^6 \qquad (4.1\text{-}1)$$

and $$\Delta c_{11}/c_{11} \simeq - (8\pm2)\times10^{-5}T^4 - (2\pm1)\times10^{-6}T^6 \ . \qquad (4.1\text{-}2)$$

$\Delta c_{44}/c_{44}$ will have a very large T^6 term, as already found in bcc He^3 (Wanner et al.(1973)). Table 1 also shows a fairly consistent trend to larger T^4 contributions and towards more positive-going T^6 terms at higher frequencies.

A very large dispersion of -2×10^{-4} to -8×10^{-4} (as extrapolated to T = 0) between 5 and 15 MHz, and somewhat less between 15 and 25 MHz, is observed over the entire measured temperature range below melting. There is a slight tendency for the dispersion to become smaller at higher temperatures. In most crystals the dispersion is normal, but because it is some five orders of magnitude larger than expected from a simple sine curve, the dispersion must necessarily become anomalous at some higher frequency. In fact two crystals, A8-a and A8-d (figures 19 and 20), do show positive dispersion at 25 MHz. To ensure that the observed frequency dependence was not

an instrumental effect, measurements were also taken in the liquid at 4.1 K, where the dispersion was found to be -6×10^{-5} between 5 and 15 MHz and -1×10^{-5} between 15 and 25 MHz. These results agree well with the expected effects of beam diffraction (section 3.3).

The dispersion has no discernible dependence upon orientation.

4.1-2 Low Temperature Region

Although the dispersion continues to the lowest temperatures, in most crystals it changes dramatically as the temperature is reduced because of an anomaly in the sound velocity which begins at some temperature between 1 and 1.8 K (at 5 MHz) and continues to the lowest measured temperature. The anomaly has been observed previously (Franck and Hewko (1973), Wanner and Mueller (1974), Wanner et al.(1976)). Within the anomalous region the deviation from the extrapolated adiabatic velocity is as much as $\Delta v/v = 3 \times 10^{-3}$. The anomaly can be either positive-going (the most common situation), or negative, as seen in the two samples A1-b and A8-a (figures 11 and 19). Perhaps most striking of all are crystals A6-b and A7-a (figures 15 and 17) which show no signs of any anomaly at all.

Neither the magnitudes nor the onset temperatures of the anomalies exhibit any dependence upon orientation.

Many crystals show a small negative-going anomaly in the temperature range just above the onset temperature. In most cases the velocity reaches a constant value after experiencing a very rapid change. Crystals A8-a and A8-d show a velocity beginning to return towards the adiabatic value at the lowest temperature. These are the same two samples in which anomalous dispersion was observed at 25MHz.

The anomalies exhibit a marked frequency dependence. At 15 MHz they become smaller and move to temperatures some 15 to 35% lower, and at 25 MHz are smaller again and at the same or a slightly lower temperature. The small high temperature anomaly becomes larger at higher frequencies, especially in crystal A8-d.

4.2 Attenuation of Sound

4.2-1 The Echo Envelope

In order to obtain a reliable value for the attenuation when it is small, the effects of interference must be included as outlined in section 3.3-4. Figures 22-23 show the echo train as photographed on the oscilloscope screen for liquid helium at 4.1 K and for seven crystals near melting.

Two difficulties arise. If the reflector is tilted then the beam will wander further in the -x

Figure 22 - Echo Trains at 5 MHz

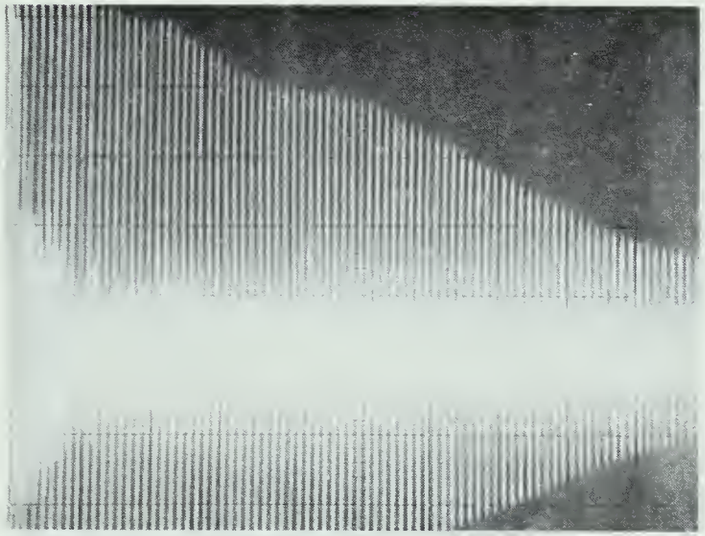

(a) Liquid 4.1 K

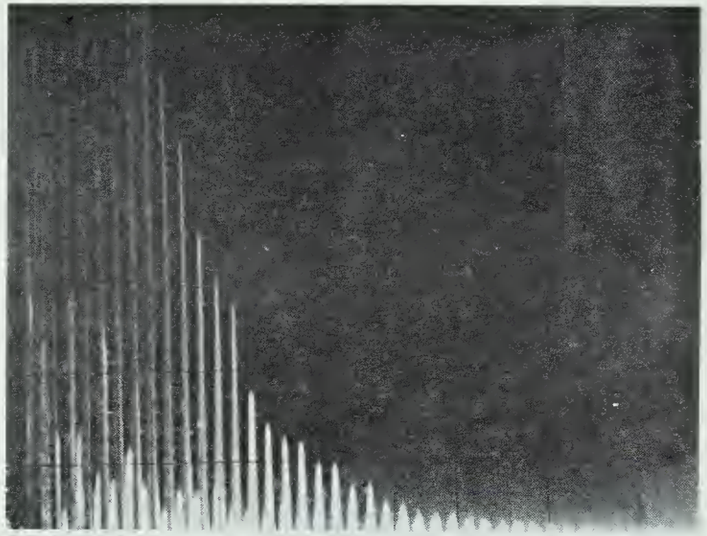

(b) Crystal A5-a 3.31 K

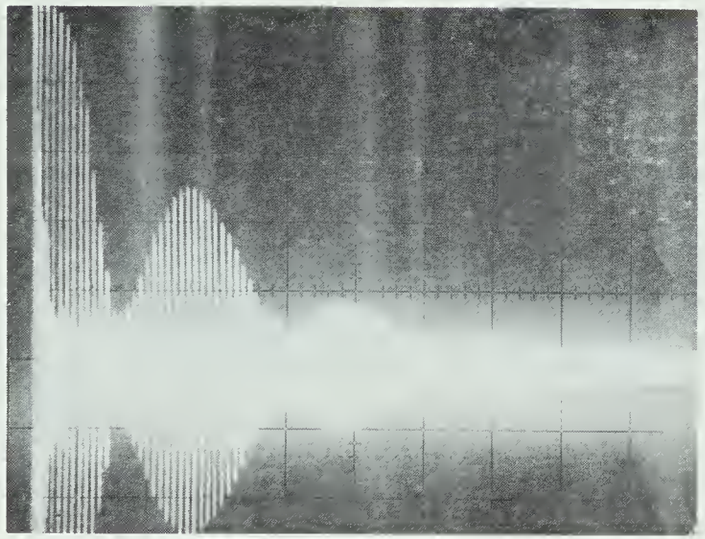

(c) Crystal A6-b 2.80 K

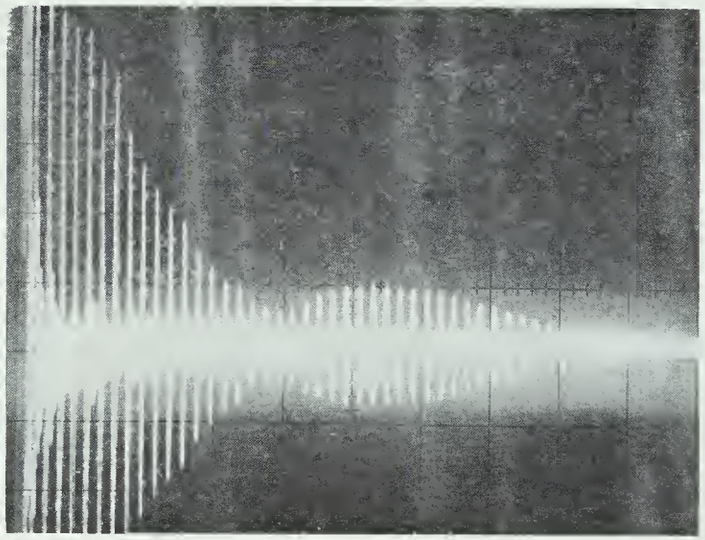

(d) Crystal A6-e 3.18K

Figure 23 - Echo Trains at 5 MHz

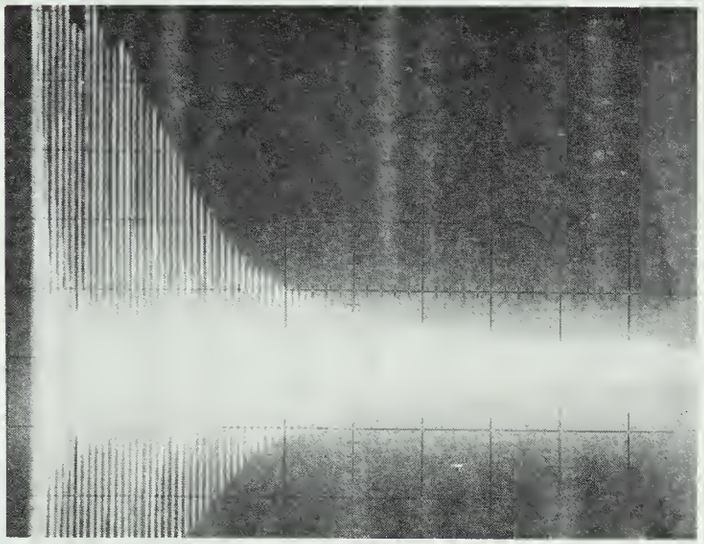

(a) A7-a 3.31 K

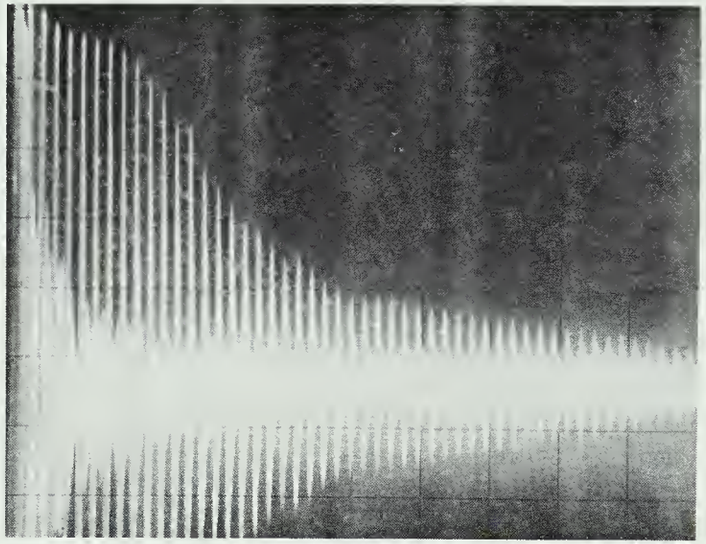

(b) A7-d 3.00 K

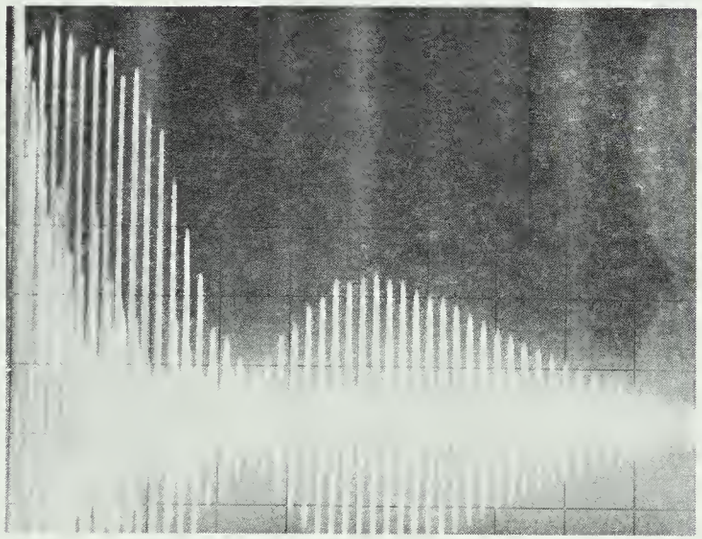

(c) A8-a 3.19 K

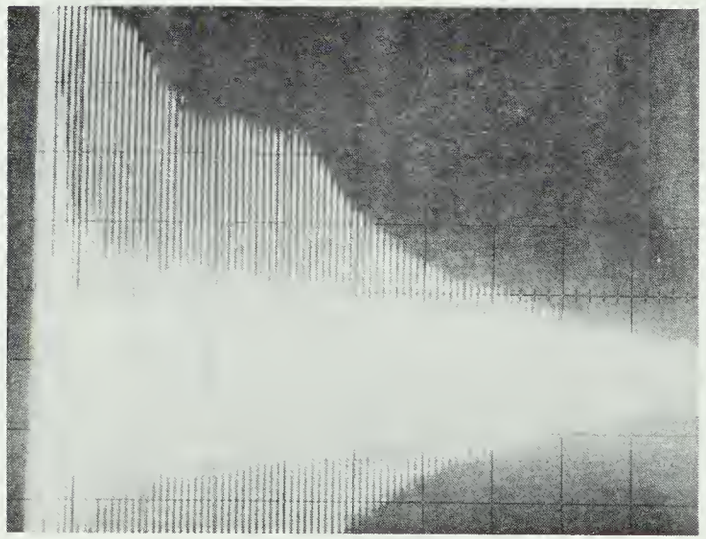

(d) A8-d 3.37 K

direction (as in figure 10(a)) with each reflection until it will finally disappear for

$$n \simeq a/(2Dd)^{\frac{1}{2}} . \qquad (4.2\text{-}1)$$

At 5 MHz this will occur at

$$n \simeq 7\, n_{max}^{\frac{1}{2}} \qquad (4.2\text{-}2)$$

where n_{max} is the echo number of the first maximum. Typically then the signal should disappear for $n \sim 40$, but it obviously does not. This difficulty is avoided if the reflector is shaped as in figure 10(b). Secondly, for a tilted reflector, the interval from n = 0 to the first minimum should be approximately twice as long as from the first minimum to the first maximum. Such a feature is not always observed, as for crystal A6-b in figure 22. Again, the curved reflector is less restrictive and can fit the observed envelope reasonably well over the first two maxima. The attenuation, then, is analyzed using equations (3.3-32) to (3.3-42).

β in equation (3.3-24) ranged from 5×10^{-5} to 10^{-4} cm^{-1}, corresponding to a radius of curvature of 10^4 to 2×10^4 cm. This compares with a radius of $\sim 10^4$ cm expected from the elastic modulus of beryllium copper. It is interesting to note that the attenuation near the

melting point, about 0.01 cm^{-1}, is only 4% of the values of around 0.25 cm^{-1} that one would obtain by looking only at the echoes previous to the first minimum, as was done by Hiki and Tsuruoka (1976).

4.2-2 Attenuation Results

Figures 24-25 show the echo train at low temperatures for six crystals, as well as the 15 MHz and 25 MHz signals for crystals A8-d near melting. Attenuation as a function of temperature and frequency is illustrated in figures 26-31.

For most crystals the attenuation follows a consistent pattern. At higher temperatures it rises gradually with decreasing temperature and then more quickly as the onset of the velocity anomaly is approached. It continues to rise to the lowest temperatures measured. There is a suggestion of an attenuation peak in some crystals at low temperatures, especially at 15 MHz, but the large measurement uncertainties preclude any definite conclusion. The attenuation increases by as much as 100 times between melting and 0.3 K. Most interesting are the two crystals A6-b and A7-a. The absence of an anomaly in these is dramatically confirmed by the attenuation, which increases only slightly to the lowest accessible temperatures. At 5 MHz most crystals which show 100 or so echoes at melting have only 2-4 remaining at 0.3 K.

Figure 24 - Attenuation of Echo Trains at 5 MHz

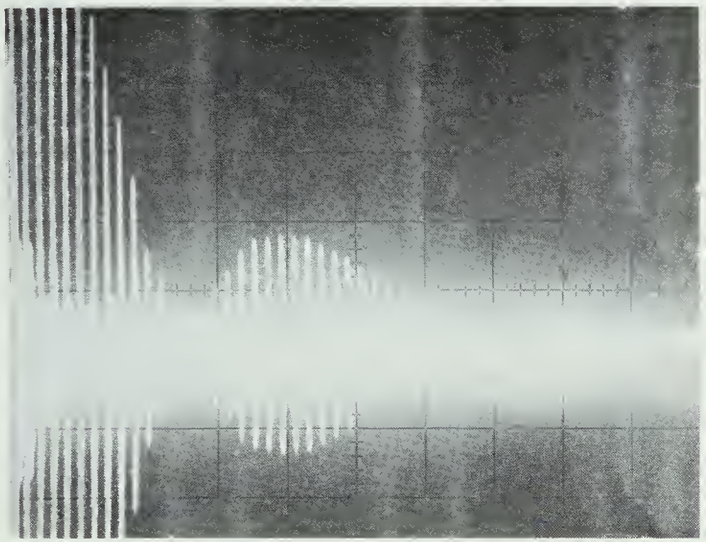

(a) A6-b 0.35 K

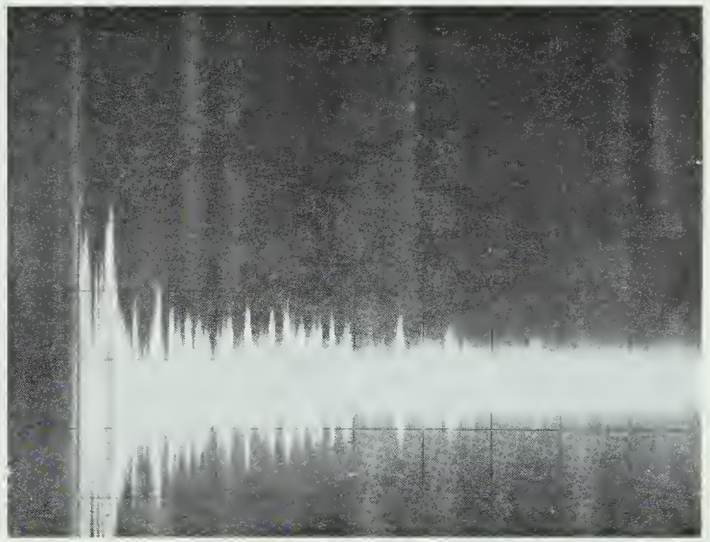

(b) A6-e 0.27 K

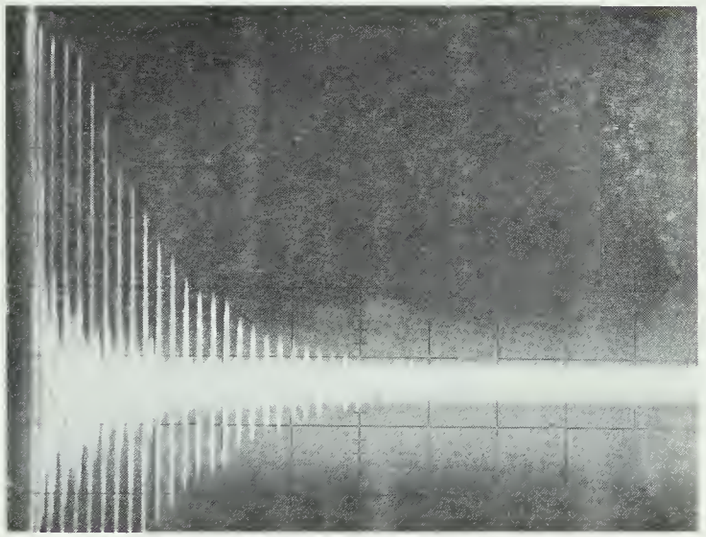

(c) A7-a 0.35 K

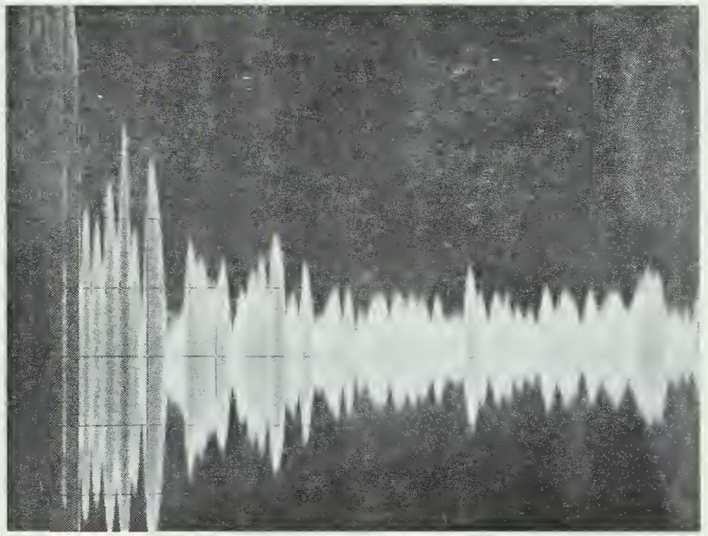

(d) A7-d 0.44 K

Figure 25 - Attenuation at 5 MHz and Echo Trains at 15 MHz (A8.e) and 25 MHz (A8.f)

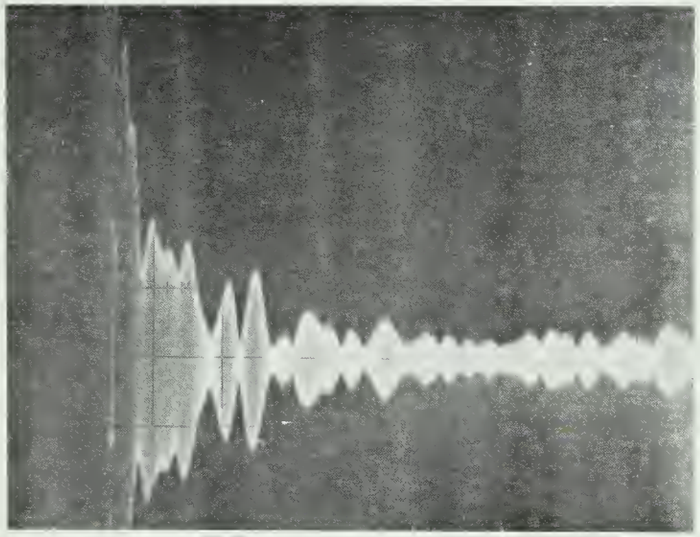

(a) A8-a 0.26K

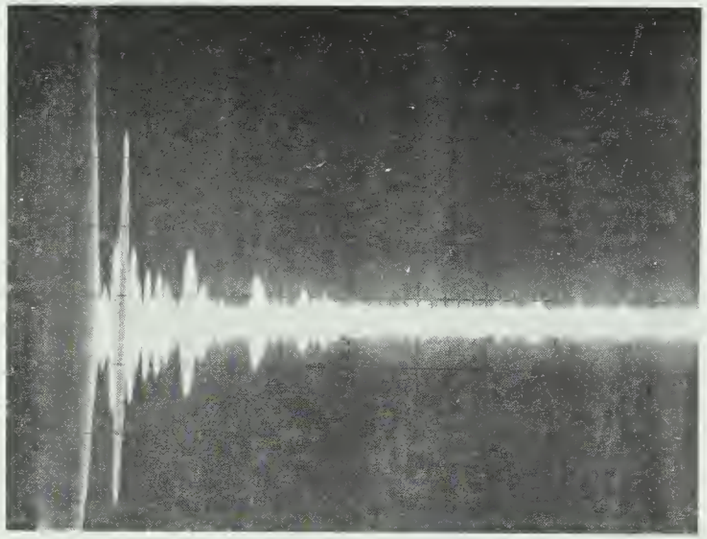

(b) A8-d 0.25K

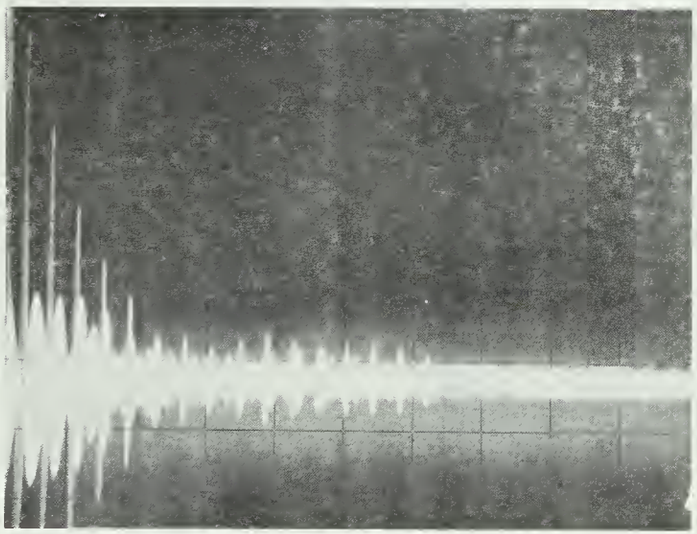

(c) A8-e 3.16K

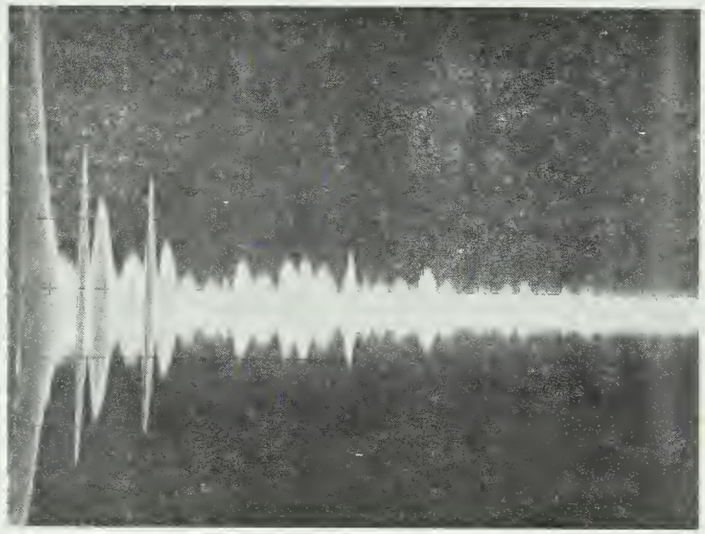

(d) A8-f 2.95 K

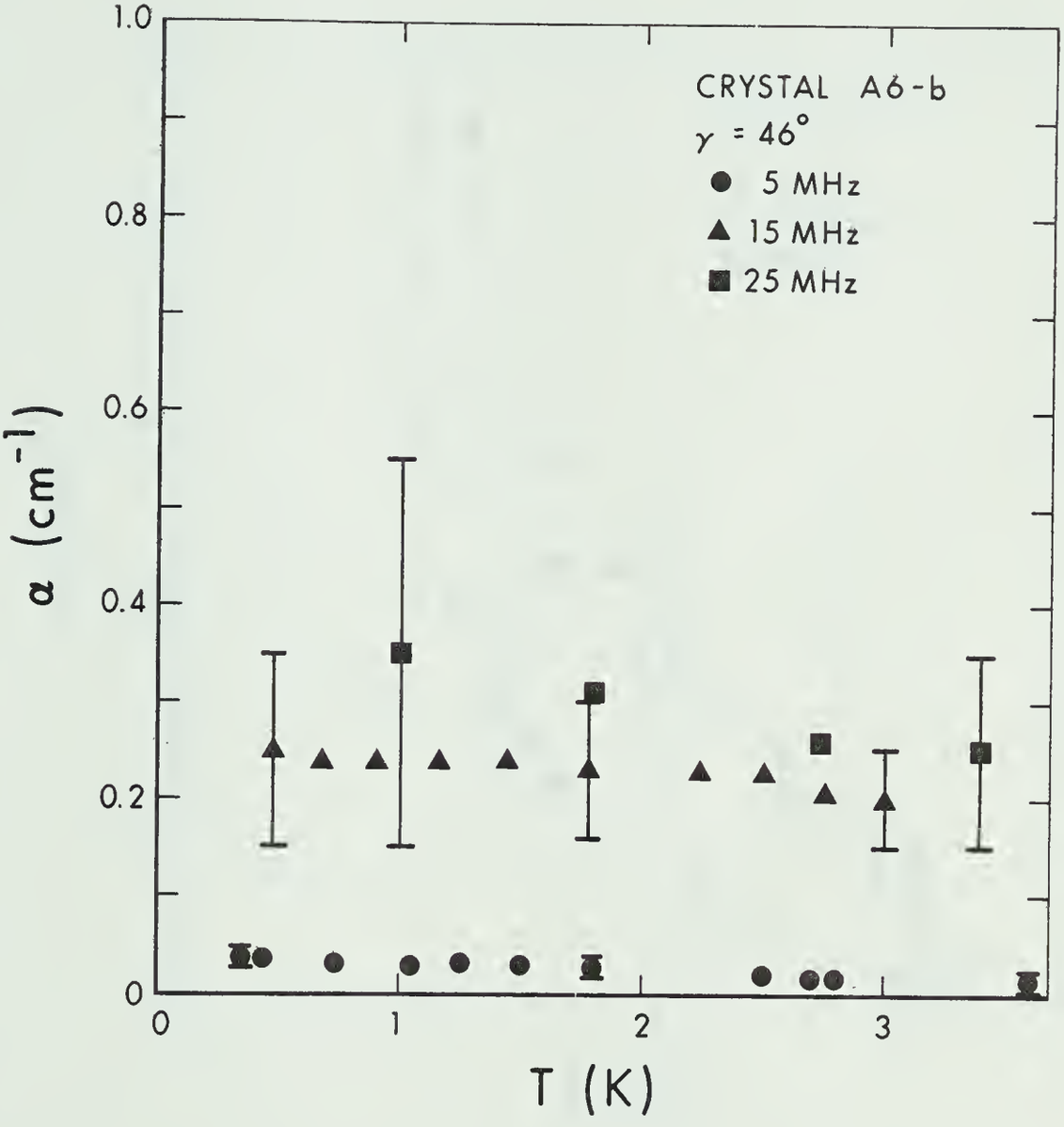

Figure 26 Attenuation as a function of temperature and frequency.

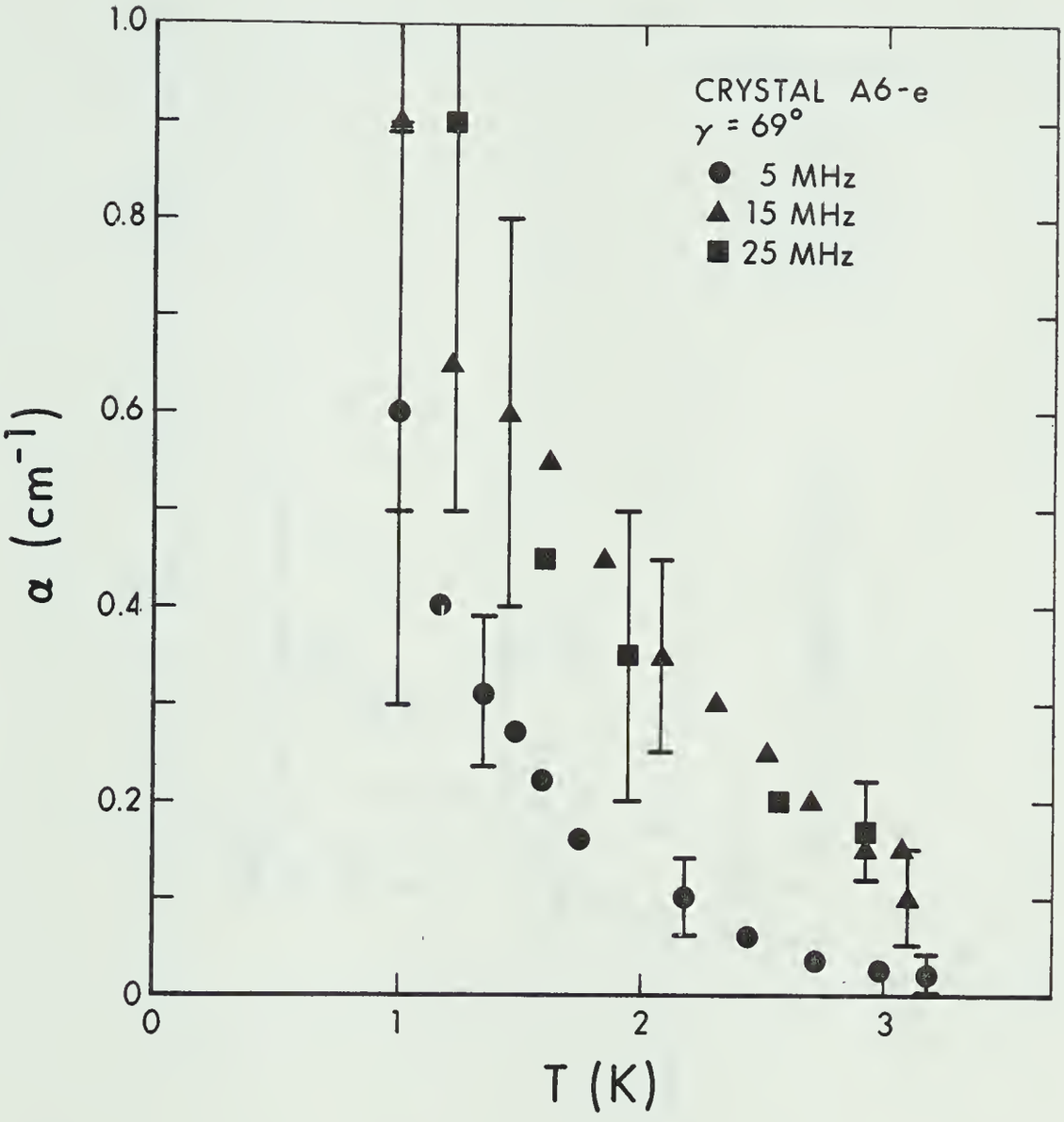

Figure 27 Attenuation as a function of temperature and frequency.

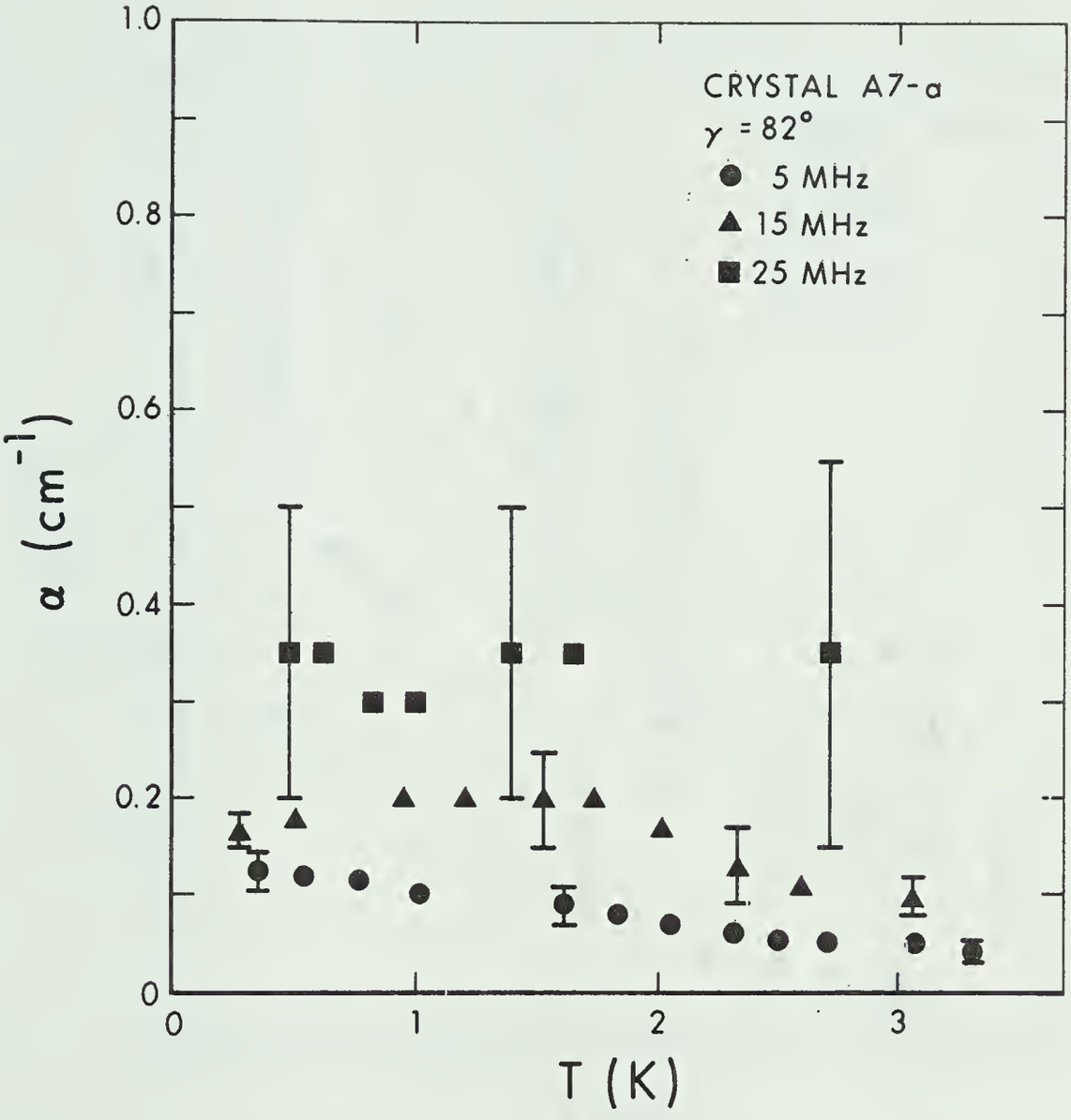

Figure 28 Attenuation as a function of temperature and frequency.

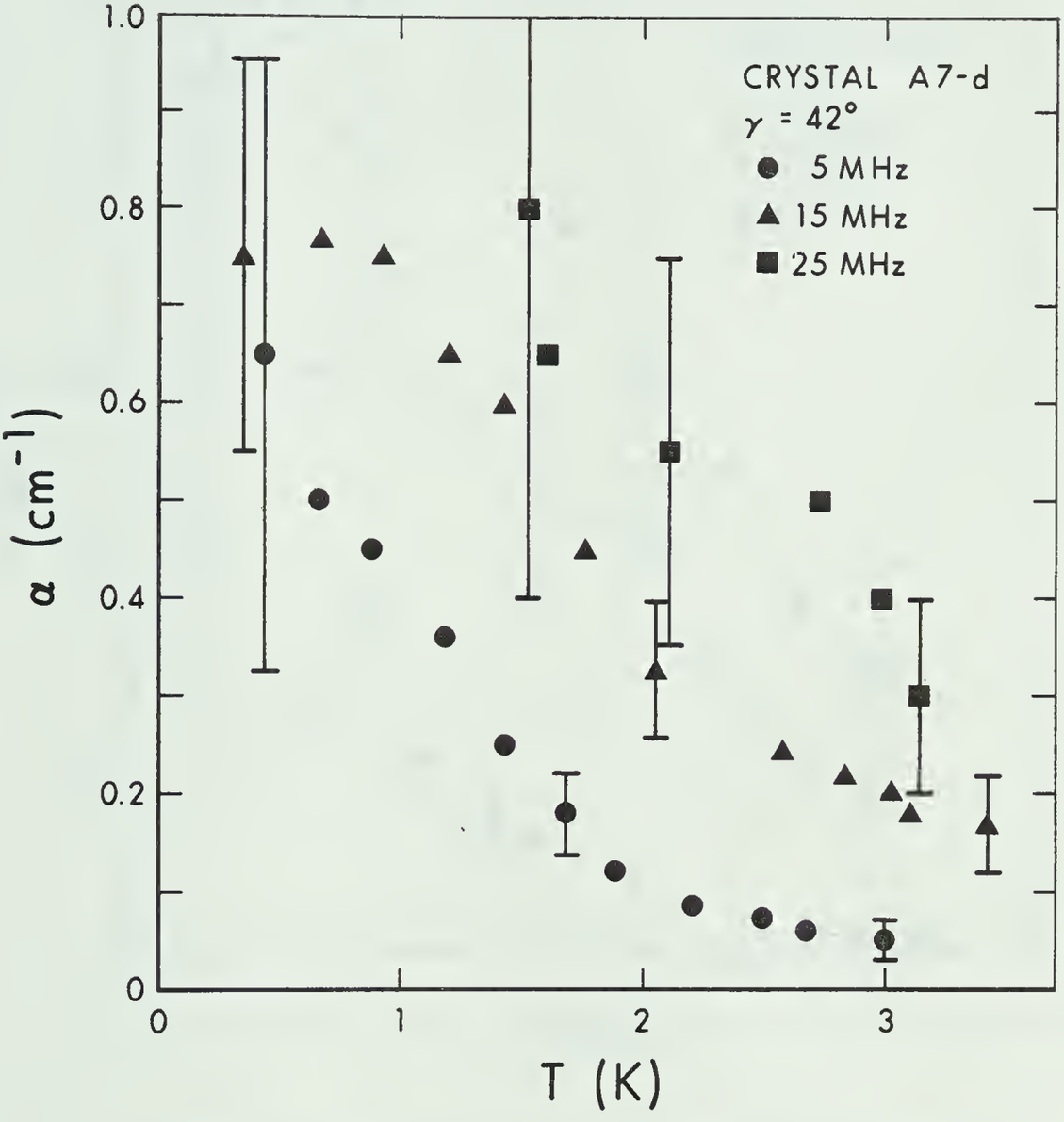

Figure 29 Attenuation as a function of temperature and frequency.

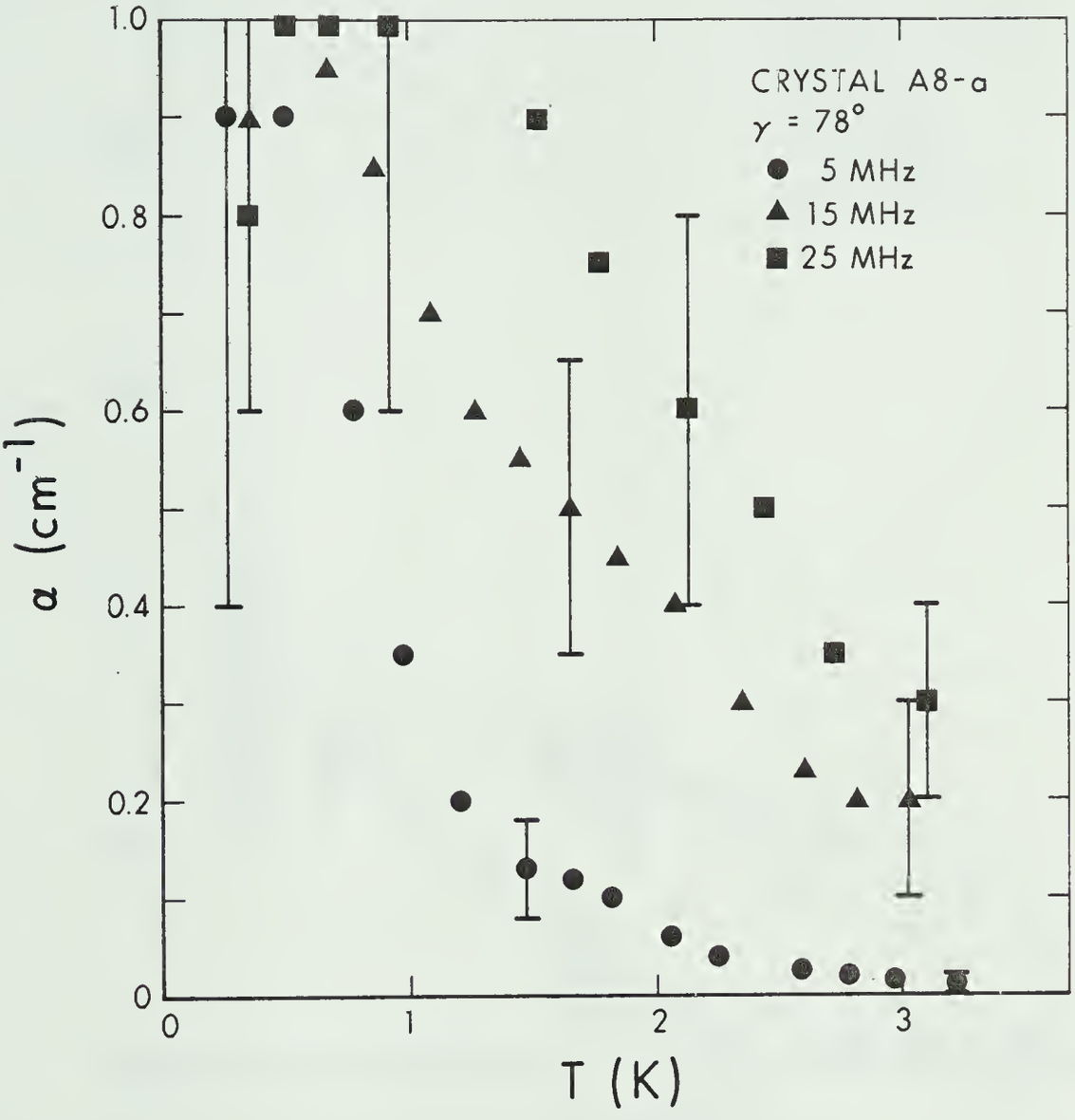

Figure 30 Attenuation as a function of temperature and frequency.

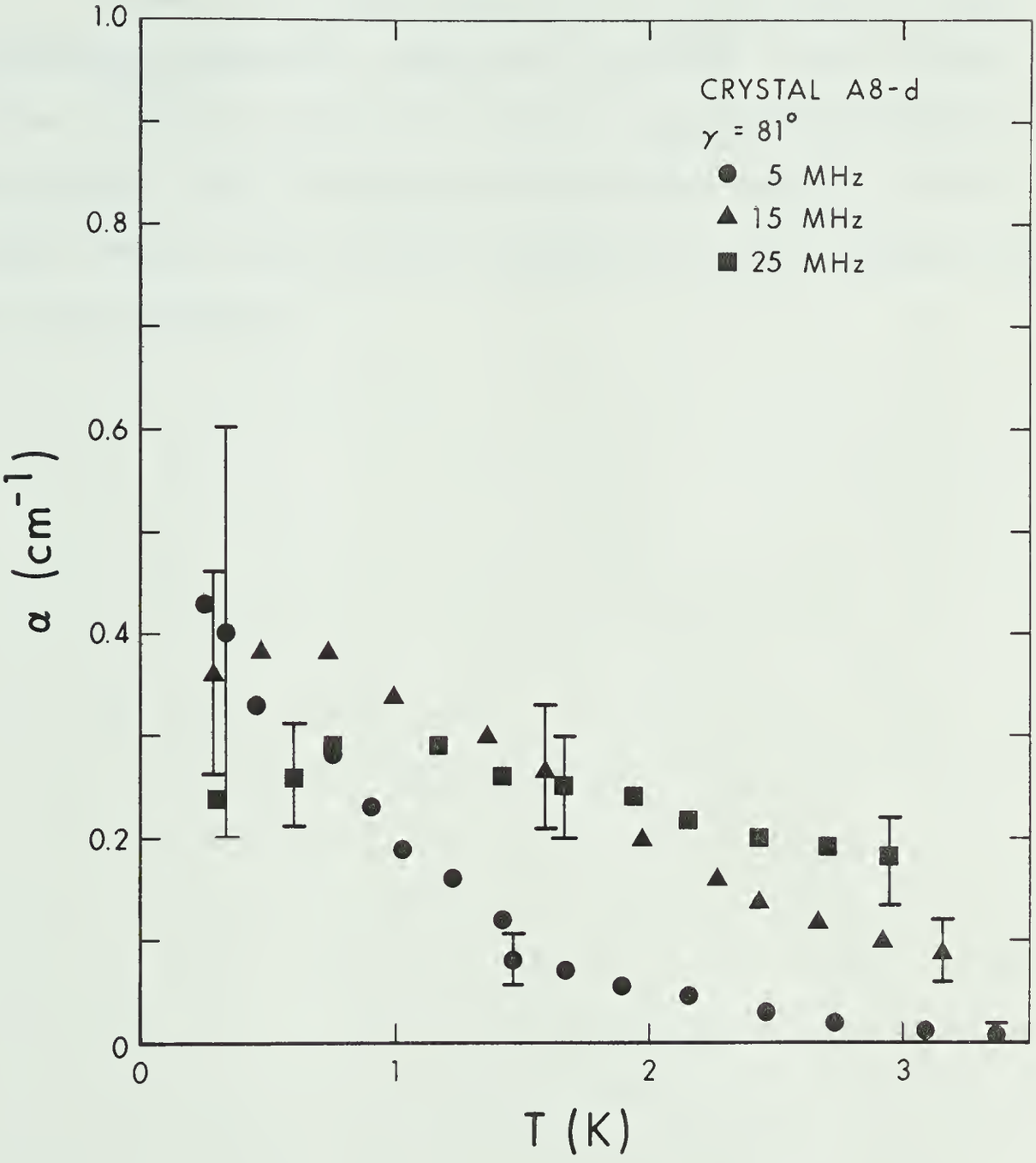

Figure 31 Attenuation as a function of temperature and frequency.

These two exceptions still show 40-60 visible echoes at that temperature.

There is a consistent rise in attenuation with increasing frequency, especially between 5 and 15 MHz, where α is as much as 20 times larger at the higher frequency. The 25 MHz results generally show a still higher value, although the uncertainties are rather large at this frequency.

CHAPTER 5

DISCUSSION OF RESULTS

5.1 Dispersion

For a simple linear chain model one would only expect a velocity change of $\Delta v/v \sim 10^{-9}$ between 5 and 15 MHz. The observed effect is five orders of magnitude larger and so cannot continue very long before some anomalous dispersion sets in at higher frequencies. In fact two crystals, A8-a and A8-d, do already show such anomalous dispersion between 15 and 25 MHz. We cannot predict the extent of the positive dispersion, particularly if it ranges all the way up to thermal energies (in this experiment $kT/\hbar\omega \sim 10^3$). If this were so then $\Omega\tau<1$ to much lower temperatures than expected from thermal measurements, since three phonon scattering processes would be allowed (section 2.6). In liquid helium such an effect has been described by Benin (1976), Wehner (1974) and Maris (1973). They calculate that the existence of both small-angle three phonon scattering and wide-angle scattering formed from many back-to-back small-angle collisions result in a region of second sound propagation existing well into the $\omega\tau>1$ régime. The transition to ballistic propagation also becomes more complicated. There is evidence of wide-angle scattering in solid helium, as discussed by Rogers (1972).

It is uncertain from the data if the large dispersion is in some way linked to the velocity anomaly. On the one hand, the crystals which exhibit no anomaly still have a large dispersion, but on the other hand it may be significant that the two crystals which show the velocity anomaly beginning to disappear at low temperatures also exhibit positive dispersion at 25 MHz.

5.2 The Adiabatic Region

Equation (2.5-10) is a very good representation of the adiabatic behaviour of the sound velocity. Unfortunately (2.5-9) does not work at all. Ahlers (1970) obtained the Grüneisen constant from specific heat as:

$$\gamma = 1.02 + 0.083\ V. \qquad (5.2\text{-}1)$$

Then $$[\gamma - d\ell n\ \gamma / d\ell n\ V]_{V = 17.4} = 1.81\ , \qquad (5.2\text{-}2)$$

so that (2.6-10) predicts a velocity increasing with rising temperature. Obviously then the use of an averaged Grüneisen constant may be valid for thermal measurements, but it breaks down completely when the sound velocity is considered; then equation (2.5-6) must be used. Unfortunately almost nothing is known about the Grüneisen constants for individual modes.

Because the constants a and b are frequency

and orientation dependent, the assumption of a reduced equation of state which led to (2.6-10) is invalid. This conclusion has been reached previously by Jarvis et al (1968).

5.3 The Velocity Anomaly

From figure 4 we see that $\omega\tau_u \sim 1$ for 5 MHz sound in the temperature range $1.5<T<1.8$ K. This corresponds roughly to the onset temperatures of the velocity anomaly in various crystals. However figure 4 predicts that the anomaly should begin at a 10% higher temperature for 15 MHz sound; the opposite behaviour is observed. The large τ_N does not permit any region $\omega\tau_N<1<\omega\tau_U$, although it may be that $\omega\tau_N<1$ down to 1.2 K (Rogers (1972), Bertman et al. (1966), Franck and Hewko (1973)). Still there would be at best be only a very narrow second sound window and none at all for higher frequencies, unless there is some interaction with the "driftless" type of second sound which, according to Hardy (1970), can propagate at low temperatures. In any case the effect predicted by equation (2.6-10) is only about $\Delta v/v \sim 10^{-4}$ at 1.2 K and decreases as T^4.

The transition to zero sound is more complicated. In equation (2.7-3), assume an isotropic material with a unique γ .

$$\text{Then } \left(\frac{\gamma_{eff}}{\gamma}\right)^2 = \left\langle \frac{\underline{K}\cdot\underline{v}_g(\underline{k}j)}{\Omega-\underline{K}\cdot\underline{v}_g(\underline{k}j)} \right\rangle_P . \qquad (5.3\text{-}1)$$

If the dispersion is given by

$$\omega = ck\,[1-\delta(k)],\ \delta(k)<<1, \qquad (5.3\text{-}2)$$

then (5.3-1) becomes,

$$\left(\frac{\gamma_{eff}}{\gamma}\right)^2 = \left\langle \frac{[1-\delta(k)+\delta(K)-k\delta'(k)+K\delta'(K)]\cos\theta}{1-[1-\delta(k)+\delta(K)-k\delta'(k)+K\delta'(K)]\cos\theta} \right\rangle_P . \qquad (5.3\text{-}3)$$

Now using a Debye model with $x = \beta\hbar\omega$, $X = \beta\hbar\Omega$, and after performing the angular integration,

$$\left(\frac{\gamma_{eff}}{\gamma}\right)^2 = -\frac{15}{8\pi^4}\cdot P\int_0^{x_D} \left[\ell n\tfrac{1}{2}\left|\delta(x/\beta\hbar c)-\delta(X/\beta\hbar c) + x\delta'(x/\beta\hbar c)/\beta\hbar c - X\delta'(X/\beta\hbar c)/\beta\hbar c\right| + 2\right] \frac{e^x x^4 dx}{(e^x-1)^2} . \qquad (5.3\text{-}4)$$

We can approximate (5.3-4) by assuming an approximately constant value for the logarithmic factor (the x = 1 value) for $x > \alpha^{-1}$ where α is an arbitrary constant such that:

$$(\beta\hbar\Omega)^{-1} >> \alpha > 1. \qquad (5.3\text{-}5)$$

Then:

$$\left(\frac{\gamma_{eff}}{\gamma}\right)^2 \simeq -\frac{15}{8\pi^4} P \int_0^{\alpha^{-1}} [\ell n\tfrac{1}{2}|\delta(x/\beta\hbar c) - \delta(X/\beta\hbar c) +$$

$$+ x\delta'(x/\beta\hbar c)/\beta\hbar c - X\delta'(X/\beta\hbar c)/\beta\hbar c| + 2]\, x^2\, dx$$

$$- 1 - \tfrac{1}{2}\ell n\tfrac{1}{2}[\delta(1/\beta\hbar c) - \delta(X/\beta\hbar c) + \delta'(1/\beta\hbar c)/\beta\hbar c$$

$$- X\delta'(X/\beta\hbar c)/\beta\hbar c]. \qquad (5.3\text{-}6)$$

If we choose simple normal dispersion,

$$\delta(k) = Ak^2 , \qquad (5.3\text{-}7)$$

then,

$$\left(\frac{\gamma_{eff}}{\gamma}\right)^2 \simeq -1 - \tfrac{1}{2}\ell n \frac{3A}{2(\beta\hbar c)^2} . \qquad (5.3\text{-}8)$$

From (5.3-8), $(\gamma_{eff}/\gamma)^2 \sim 2.5$ for T = 1 K and $A = 2\times10^{-16}$. This value is too small to produce the observed anomaly, even above 1 K, and the T^4 temperature dependence would make it negligible below 0.5 K.

A reduction in the normal relaxation time could affect the zero sound régime as well as the second sound region, but again the anomaly should shift to a higher temperature for a higher frequency.

The Granato-Lücke dislocation theory (equation

2.8-11) can be made to fit the data well in almost all cases. However this is not surprising when one considers that there are five parameters (Λ_1, Λ_2, k and g and n in $d = gT^n$) that can be varied. In fact there are only four independent parameters if (2.8-13) is used. But for an exponential distribution, $k \geq 2$, contrary to what Wanner et al. (1976) find in at least one case.

When (2.8-11) was fitted to the data, n varied between 2.7 and 5, while g was of the order of 10^{-7} dyne-sec/cm^2. This value is three orders of magnitude larger than expected from Brailsford (1971) where g is given as,

$$g = \frac{\xi(5)\beta}{\pi\rho b^2}\left(\frac{Nk}{V}\right)^2 \cdot \frac{R(0)}{\Theta^6} , \qquad (5.3\text{-}9)$$

where ξ is the Riemann zeta function, β is a numerical constant $\simeq 1.2\times10^4$, b is the Burgers vector and R(0) is given in terms of the dislocation contribution to the thermal resistance W_D as:

$$R(0) = W_D T^2/\Lambda\big|_{T=0} . \qquad (5.3\text{-}10)$$

Since dislocations generally lie in the basal plane of hexagonal crystals, especially when the ratio of lattice parameters c/a is the ideal spherical atom value, (Hirth and Lothe (1968)), then we let b = a. From Klemens (1958),

$$W_D \simeq \frac{h^2 v_D \gamma^2}{423k^3} \cdot \Lambda b^2 \cdot \qquad (5.3\text{-}11)$$

The $g \sim 8\times10^{-11}$ dyne-sec/cm^2.

Λ was of the order of 10^4 cm^{-2}, an order of magnitude smaller than Wanner et al,(1976) found. For the two crystals A6-b and A7-a only an upper bound for Λ of 10^2 cm^{-2} can be used. We can estimate the dislocation density from the mosaic spread (Hirsch (1956)) seen in neutron scattering experiments (Minkiewicz et al.(1973)). The lower bound for this estimate would be 2×10^5 cm^{-2}, but this figure is a gross underestimation because it assumes that all dislocations bend in the same direction. An upper bound, calculated by assuming a random distribution, should be much closer to the actual value; this procedure gives $\Lambda \sim 2\times10^9$ cm^{-2}. I conclude that Λ is in the range 10^7-10^8 cm^{-2}. The small unphysical Λ needed for a fit to the data compensates for the unphysically large g required.

Although almost any set of data could be fitted well on its own, the 5 MHz constants did not give a good fit at 15 MHz or 25 MHz for the same sample. The magnitude of the observed anomaly did not decrease as fast as the approximately ω^{-2} variation predicted by the theory. More significant was the temperature of the anomaly, represented by the onset temperature or the temperature

T_M of maximum slope $d(\Delta v)/dT$. From (2.8-13), T_M for any one crystal is given quite accurately by

$$T_M^{\,n}/\omega = \text{constant}. \qquad (5.3\text{-}12)$$

Equation (5.3-12) predicts that the anomaly should occur at a temperature 20 to 50% higher at 15 MHz than at 5 MHz, but in all cases the anomaly shifts to a temperature 15 to 35% lower. This argument rules as decisively against the dislocation theory as against any relaxation time theory discussed previously in this section. In fact any resonance type of theory will run afoul of this same objection - the unusual frequency dependence of the anomaly.

Finally it should be noted that although (2.8-11) allows for a negative- or positive-going anomaly, the negative-going interval must occur at a higher temperature, so that once $d(\Delta v)/dT<0$, it cannot be positive again at a lower temperature. This predicted behaviour is contradicted by crystal A8-d.

Saslow (1977) has estimated a velocity change of $\Delta v/v \approx 10^{-4}$ from equation (2.9-8). Equation (2.9-10) can be written:

$$\bar{\delta} = 1 + S\cdot\frac{T}{\bar{V}}\left(\frac{\partial V}{\partial T}\right)_{\mu,\varepsilon}\cdot\frac{1}{\bar{T}}\left(\frac{\partial T}{\partial S}\right)_{\mu,\varepsilon} - \frac{1}{\bar{V}}\left(\frac{\partial V}{\partial \varepsilon_{11}}\right)_{S,\mu} \qquad (5.3\text{-}13)$$

$$\simeq \left[1 - \frac{1}{V}\left(\frac{\partial V}{\partial \varepsilon_{11}}\right)_{S,\mu}\right] + \frac{\alpha T}{3} , \qquad (5.3\text{-}14)$$

where α is the thermal expansion coefficient. For a perfect crystal the bracketted term in (5.3-14) is zero. If Schottky vacancies with energy of formation ϕ are present in a concentration of

$$n/N = e^{-\phi/kT} , \qquad (5.3\text{-}15)$$

from Miyoshi et al.(1970) and Reich (1963),

$$\phi \propto V^{-6} \qquad (5.3\text{-}16)$$

approximately so that

$$\frac{dV}{V} \simeq \left(1 + \frac{6\phi}{kT}\cdot\frac{n}{N}\right) d\varepsilon_{11} . \qquad (5.3\text{-}17)$$

Using (5.3-17) in (5.3-14), we find finally:

$$\bar{\delta} \simeq \frac{\alpha T}{3} + \frac{6\phi}{kT} e^{-\phi/kT} . \qquad (5.3\text{-}18)$$

From Jarivs et al.(1968), α is approximately $6\times10^{-5}\ T^3\ K^{-1}$ at 17.4 cm^3/mole. ϕ is 50 $\pm$10K, so that:

$$\bar{\delta} \simeq 2\times10^{-5}\ T^4 + \frac{300}{T}\cdot e^{-50/T} . \qquad (5.3\text{-}19)$$

At 2K, $\bar{\delta} = 3\times10^{-4}$ and at 1 K is 2×10^{-5}. The large volume dependence of ϕ more or less rules out vacancies as making a significant contribution to the crystal properties at this density. As with zero sound, the T^4 temperature dependence of the effect should obliterate it below 1 K. Also $c_4^2/c_1^2 < 1$, so that the effect is really rather small (and negative), although the fact that c_4^2 rises with decreasing temperature could moderate the T^4 dependence in (5.3-19).

In general the velocity anomaly and other observed effects follow no discernible pattern from crystal to crystal. There does not appear to be any dependence upon orientation. Although the crystals were grown all in the same manner, one is led to examine defect mechanisms since defect types and concentrations can vary. The range of dislocation densities found from the Granato-Lüche theory appears too low. In equilibrium the vacancy concentration is much too low. One cannot however rule out other non-equilibrium defects such as clusters of vacancies or stacking faults. Unfortunately almost nothing is known about these structures in solid helium.

5.4 Attenuation

From equation (2.5-5), the attenuation in the adiabatic region will be

$$\alpha \lesssim 4\times10^{-8}\ T\ e^{16.6/T}\ cm^{-1}, \qquad (5.4\text{-}1)$$

or 2×10^{-5} cm^{-1} at 3.5 K and 7×10^{-4} cm^{-1} at 1.8 K. It would of course be impossible to measure such small attenuations. The difficulty of matching impedances to obtain a good signal for the higher harmonics must almost certainly have contributed to the measured attenuation increasing faster than linearly with frequency.

In a hypothetical second sound region, the attenuation from equation (2.6-9) and figure 4 would be:

$$\alpha \simeq 8\times10^{-5}\ T^4/\tau\ . \qquad (5.4\text{-}2)$$

At T = 1 K, α then would be 0.25 cm^{-1} or more, which is near the measured values. However this attenuation should drop with decreasing temperature as far as the Poiseuille flow maximum. The attenuation is not frequency dependent.

Generally all theories fail because of the continuation of the high attenuation over such a large temperature range. For the dislocation theory also (from (2.8-1)), when $d<\omega$,

$$\alpha \propto d \propto T^n\ , \qquad (5.4\text{-}3)$$

so that the attenuation should be falling rapidly by the time the plateau in the velocity is reached. This situation does not occur. One expects that there will eventually be an attenuation peak and $\alpha \to 0$ as $T \to 0$, but this behaviour has not yet been observed.

CHAPTER 6

CONCLUSIONS

There is a very large frequency dispersion at all temperatures in pure single crystals of hcp solid He^4. The dispersion is usually normal, but both direct and indirect evidence exists for anomalous dispersion at or above 25 MHz. The longitudinal sound velocity rises with decreasing temperature until an anomaly sets in between 1 and 1.8 K. The velocity changes very rapidly with temperature over a range of 0.5 - 1 K and then levels off to a constant value with $(v/v_{adiabatic}) - 1 \sim 1\text{-}3 \times 10^{-3}$. Two crystals show a deviation from this plateau below about 0.3 K. In most samples the anomaly is positive, but two crystals show a negative anomaly while two others exhibit no anomalous behaviour at all. The anomaly becomes smaller and moves to lower temperatures as the frequency is increased.

The attenuation is very small in solid helium near melting, generally 0.01 cm^{-1} or less. Very careful consideration must be given to the echo envelope when measuring these low attenuations. The attenuation rises as the temperature is reduced, slowly at first and then more quickly as the velocity anomaly is reached. The attenuation continues to rise to at least 0.25 K or lower.

There is no theory at present which can explain

the behaviour of the velocity and attenuation in the anomalous region. All theories fail completely on two counts: the anomaly moves to lower temperatures as the frequency is increased; the attenuation continues to be very large down to 0.25 K.

Future work should proceed in three directions: to lower frequencies, to lower temperatures and to an investigation of transverse sound propagation. Most useful of all would be a similar experiment done on very pure He^3, in both the hcp phase (to see if isotopic effects are important) and the bcc phase (to observe the significance of the crystal structure).

BIBLIOGRAPHY

Abel, W.R., Anderson, A.C., Wheatley, J.C., Rev. Sci. Instrum. 35, 444 (1964).

Abraham, B.M., Eckstein, Y., Ketterson, J.B., Vignos, J., Cryogenics 9, 274 (1969).

Abraham, B.M., Eckstein, Y., Ketterson, J.B., Kuchnir, M., Roach, P.R., Phys. Rev. A1, 250 (1970).

Abramowitz, M., Stegun, I.A., Handbook of Mathematical Functions, N.B.S. Applied Mathematics Series No. 55 (1964).

Ahlers, G., Phys. Rev. A2, 1505 (1970).

Akhieser, A., J. Phys. (USSR) 1, 277 (1939).

Almond, D.P., Lea, M.J., Pickett, G.R., Cryogenics 12, 469 (1972).

Andreev, A.F., Sov. Phys. JETP 41, 1170 (1975).

Andreev, A.F., Lifshitz, I.M., Sov. Phys. JETP 29, 1107 (1969).

Banerjee, D.K. and Pao, Y.-H., J. Acoust. Soc. Amer. 56, 1444 (1974).

Beck, H., Dynamical Properties of Solids, G.K. Horton, A.A. Maradudin eds., Vol. 2, p. 205, North Holland, Amsterdam (1975).

Benin, D., Phys. Rev. B13, 1105 (1976).

Berman, R., Bounds, C.L., Rogers, S.J., Proc. Roy. Soc. A289, 66 (1966).

Bertman, B., Fairbank, H.A., White, C.W., Crooks, M.J., Phys. Rev. 142, 74 (1966).

Betts, D.S., Contemp. Phys. 9, 97 (1968).

Bhatia, A.B., Ultrasonic Absorption, Clarendon Press, Oxford (1967).

Black, W.C. Jr., Roach, W.R., Wheatley, J.C., Rev. Sci. Instrum. 35, 587 (1964).

Bömmel, H.E., Dransfeld, K., Phys. Rev. 117, 1245 (1960).

Born, M., Huang, K., Dynamical Theory of Crystal Lattices, Clarendon Press, Oxford (1954).

Brailsford, A.D., J. Appl. Phys. 43, 1380 (1972).

Calder, I.D., Franck, J.P., to be published in Phys. Rev. B, June 1 (1977).

Callaway, J., Phys. Rev. 113, 1046 (1959).

Chester, G.V., Phys. Rev. A2, 256 (1970).

Chung, D.H., Silversmith, D.J., Chick, B.B., Rev. Sci. Instrum. 40, 718 (1969).

Crepeau, R.H., Heybey, O., Lee, D.M., Strauss, S.A., Phys. Rev. A3, 1162 (1971).

DeWette, F.W., Nijboer, B.R.A., Phys. Lett. 18, 19 (1965).

DeWette, F.W., Nosanow, L.H., Werthamer, N.R., Phys. Rev. 162, 824 (1967).

Fisher, R.A., Rev. Sci. Instrum. 43, 386 (1972).

Franck, J.P., Hewko, R.A.D., Phys. Rev. Lett. 31, 1291 (1973).

Franck, J.P., Wanner, R., Phys. Rev. Lett. 25, 345 (1970).

Fredkin, D.R., Werthamer, N.R., Phys. Rev. 167, 607 (1965).

Glyde, H.R., Rare Gas Solids, M.L. Klein, J.A. Venables eds., Vol. I, p. 382, Academic Press, N.Y. (1976).

Gold, L., Phys. Rev. 77, 390 (1950).

Granato, A.V., Lücke, K., J. Appl. Phys. 27, 583 (1956).

Granato, A.V., Lücke, K., Physical Acoustics, W.P. Mason ed., Vol. IV A, p. 225, Academic Press, N.Y. (1966).

Greywall, D.S., Phys. Rev. A3, 2106 (1971).

Guyer, R.A., Phys. Rev. 148, 789 (1966).

Guyer, R.A., Solid State Physics 23, 413 (1969).

Guyer, R.A., Phys. Rev. Lett. 26, 174 (1971).

Guyer, R.A., Krumhansl, J.A., Phys. Rev. 133, A1411 (1964).

Guyer, R.A., Krumhansl, J.A., Phys. Rev. 148, 778 (1966).

Guyer, R.A., Richardson, R.C., Zane, L.I., Rev. Mod. Phys. 43, 532 (1971).

Hansen, E.R., A Table of Series and Products, Prentice-Hall, Englewood Cliffs, N.J. (1975).

Hardy, R.J., Phys. Rev. B2, 1193 (1970).

Hetherington, J.H., Phys. Rev. 176, 231 (1968).

Hetherington, J.H., Mullin, W.J., Nosanow, L.H., Phys. Rev. 154, 175 (1967).

Hewko, R.A.D., Ph.D. Thesis, University of Alberta, Edmonton (1973, unpublished).

Hiki, Y., Tsuruoka, F., Phys. Lett. 56A, 484 (1976).

Hirsch, P.B., Prog. in Metal Phys. 6, 236 (1956).

Hirth, J.P., Lothe, J., Theory of Dislocations, McGraw-Hill, N.Y. (1968).

Hogan, E.M., Guyer, R.A., Fairbank, H.A., Phys. Rev. 185, 356 (1969).

Jarvis, J.F., Ramm, D., Meyer, H., Phys. Rev. 170, 320 (1968).

Jastrow, R., Phys. Rev. 98, 1479 (1955).

Keller, W., Helium 3 and Helium 4, Plenum Press, N.Y. (1969).

Khimunin, A.S., Acustica 32, 192 (1975).

Klemens, P.G., Solid State Physics 7, 1 (1958).

Koehler, J.S., Imperfections in Nearly Perfect Crystals, W. Schockley et al., eds., p. 197, Wiley, N.Y. (1952).

Koehler, T.R., Phys. Rev. Lett. 18, 654 (1967).

Koehler, T.R., Phys. Rev. 165, 942 (1968).

Koehler, T.R., Dynamical Properties of Solids, G.K. Horton, A.A. Maradudin, eds., Vol. 2, p. 1, North-Holland, Amsterdam (1975).

Koehler, T.R. and Werthamer, N.R., Phys. Rev. A5, 2230 (1972).

Kondratenko, P.S., Zh. Eksp. Teor. Fiz. 70, 1826 (1976).

Lawson, D.T., Fairbank, H.A., J. Low Temp. Phys. 11, 363 (1973).

Leggett, A.J., Phys. Rev. Lett. 25, 1543 (1970).

Maradudin, A.A., Montroll, E.W., Weiss, G.H., Ipatova, I.P., Solid State Physics Supppl. 3, 1 (1971).

Maris, H.J., Phil. Mag. 16, 331 (1967).

Maris, H.J., Physical Acoustics, W.P. Mason, ed., Vol. VIII, p. 279, Academic Press, N.Y. (1971).

Maris, H.J., Phys. Rev. A8, 1980, 2629 (1973).

Maxwell, E., Rev. Sci. Instrum. 36, 553 (1965).

May, J.E. Jr., IRE Nat. Conv. Rec. 6, Pt. 2, 134 (1958).

McSkimin, H.J., Andreatch, P., J. Acoust. Soc. Amer. 34, 609 (1962).

Merkulov, L.G., Tret'yakov, V.A., Sov. Phys. Acoustics 20, 358 (1975).

Minkiewicz, V.J., Kitchens, T.A., Shirane, G., Osgood, E.B., Phys. Rev. A8, 1513 (1973).

Miyoshi, D.S., Cotts, R.M., Greenberg, A.S., Richardson, R.C., Phys. Rev. A2, 870 (1970).

Musgrave, M.J.P., Proc. Roy. Soc. A226, 339, 356 (1954).

Musgrave, M.J.P., Crystal Acoustics, Holden-Day, San Francisco (1970).

Niklasson, G., Ann. Phys. 59, 263 (1970).

Nosanow, L.H., Phys. Rev. Lett. 13, 270 (1964).

Nosanow, L.H., Phys. Rev. 146, 1, 120 (1966).

Nosanow, L.H., Werthamer, N.R., Phys. Rev. Lett. 15, 618 (1965).

Nye, J.F., Physical Properties of Crystals, Clarendon Press, Oxford (1957).

Oda, Y., Fujii, G., Nagano, H., Cryogenics 14, 84 (1974).

Papadakis, E.P., J. Acoust. Soc. Amer. 36, 414 (1964).

Papadakis, E.P., J. Acoust. Soc. Amer. 40, 863 (1966).

Papadakis, E.P., J. Acoust. Soc. Amer. 42, 1045 (1967).

Papadakis, E.P., J. Acoust. Soc. Amer. 49, 166 (1971).

Papadakis, E.P., J. Acoust. Soc. Amer. 52, 847 (1972).

Pomeranchuk, I.J., J. Phys. (U.S.S.R.) 4, 529 (1941).

Reese, R.A., Sinha, S.K., Brun, T.O., Tilford, C.R., Phys. Rev. A3, 1688 (1971).

Reich, H.A., Phys. Rev. 129, 630 (1963).

Reissland, J.A., The Physics of Phonons, Wiley, London (1973).

Rogers, S.J., J. de Phys. 33, Suppl. 4, C4-111 (1972).

Saslow, W.M., Phys. Rev. Lett. 36, 1151 (1976).

Saslow, W.M., Phys. Rev. B15, 173 (1977).

Seki, H., Granato, A.V., Truell, R., J. Acoust. Soc. Amer. 28, 230 (1956).

Sussmann, J.A., Thellung, A., Proc. Phys. Soc. 81, 1122 (1963).

Trickey, S.B., Kirk, W.P., Adams, E.D., Rev. Mod. Phys. 44, 668 (1972).

Truell, R., Elbaum, C., Chick, B.B., Ultrasonic Methods in Solid State Physics, Academic Press, N.Y. (1969).

Van Nest, J.P., Hutchison, T.S., Rogers, D.H., Can. J. Phys. 47, 1797 (1969).

Vignos, J.H., Fairbank, H.A., Phys. Rev. 147, 185 (1966).

Wanner, R., Ph.D. Thesis, University of Alberta, Edmonton (1970 - unpublished).

Wanner, R., Franck, J.P., Phys. Rev. Lett. 24, 365 (1970).

Wanner, R., Iwasa, I., Wales, S., Solid State Comm. 18, 853 (1976).

Wanner, R., Mueller, K.H. Jr., Phys. Lett. 49A, 209 (1974).

Wanner, R., Mueller, K.H. Jr., Fairbank, H.A., J. Low Temp. Phys. 13, 153 (1973).

Ward, J.C., Wilks, J., Phil. Mag. 43, 48 (1952).

Waterman, P.C., Phys. Rev. 113, 1240 (1959).

Wehner, R.K., Phys. Rev. A9, 2625 (1974).

Wilks, J. Properties of Liquid and Solid Helium, Clarendon Press, Oxford (1967).

Woodruff, T.O., Ehrenreich, H., Phys. Rev. 123, 1553 (1961).

Zener, C., Phys. Rev. 49, 122 (1936).

APPENDICES

A1 Extrapolation of Elastic Constants

Data for this extrapolation were taken from Wanner and Franck (1970), Greywall (1971) and Crepeau et al. (1971).

There are several useful relations among the elastic constants. From Franck and Wanner (1970),

$$c_{11} + c_{12} = c_{13} + c_{33}. \qquad \text{(A1-1)}$$

If (A1-1) is used in the expression for compressibility (Nye (1957)), then

$$\kappa_T = 3/(c_{33} + 2c_{13}) \ . \qquad \text{(A1-2)}$$

c_{11} was fitted to an empirical relation using all data (but especially those of Greywall which were spread over a wide volume range) to give:

$$c_{11} = 4.236\text{x}10^{11} e^{-V/3.017} \ . \qquad \text{(A1-3)}$$

Then for almost all data, c_{11} and c_{12} were found on average to be simply related according to:

$$c_{11}/c_{12} = 1.78 \pm 0.02. \qquad \text{(A1-4)}$$

From equations (A1-1) to (A1-4), the four elastic constants c_{11}, c_{12}, c_{13} and c_{33} can be calculated if κ_T is known. For this purpose the data of Jarvis et al.(1968) was found to be fitted very well by

$$\kappa_T = 4.2513 \times 10^{-12}\ e^{V/3.0703}. \qquad \text{(A1-5)}$$

In order to calculate c_{44}, we look at the Debye velocity v_D given by

$$v_D = \left[\int \left(v_L^{-3} + v_{T_1}^{-3} + v_{T_2}^{-3} \right) d\Omega/12\pi \right]^{-1/3}, \qquad \text{(A1-6)}$$

as in equation (2.4-8). Now,

$$v_D = \frac{k\Theta_o}{h} \left(\frac{4V}{3N} \right)^{1/3} \qquad \text{(A1-7)}$$

and Θ_o is given empirically by Ahlers (1970) as:

$$\Theta_o(V) = 68.56\ (V/14.208)^{-1.02}\ \exp\left[-0.083(V-14.208)\right]. \qquad \text{(A1-8)}$$

Then, using equations (2.3-9) to (2.3-12) for the sound velocities, c_{44} can be calculated on a computer once the other four elastic constants are known.

I could place a great deal of confidence in the extrapolation to 17.4 cm^3/mole because extending the extrapolation all the way to 16 cm^3/mole gave a value for

c_{33} only 7% higher than that found by Reese et al (1973) from neutron scattering (25.4×10^8 dyne/cm^2).

Some representative values for the elastic constants are given in table 2.

A2 Extrapolation of Relaxation Times

From the measurements of Hogan et al.(1969) at 85 and 126 atmospheres and the more accurate measurements of Lawson and Fairbank (1973) at 85 atm., the normal relaxation time is

$$\tau_N(T) = (2.02 \pm 0.1) \times 10^{-12} \ (\Theta_D/T)^3 \text{ sec.} \qquad \text{(A2-1)}$$

The thermal conductivity in the umklapp scattering region was fitted accurately by the expressions:

$$\kappa_\perp = A_\perp \ e^{\Theta_D/b_\perp T}$$

$$\kappa_{/\!/} = A_{/\!/} \ e^{\Theta_D/b_{/\!/} T} \ , \qquad \text{(A2-2)}$$

with $b_\perp = 2.58$ and $b_{/\!/} = 4.62$. The coefficients $A_\perp$ and $A_{/\!/}$ are functions of pressure. The data is scant in this respect. However Hogan et al.do find that $A_\perp$ (85 atm) = 112 erg/cm-sec-K, $A_{/\!/}(85) = 2310$ erg/cm-sec-K, $A_{/\!/}$ (53.4) = 0.61 $A_{/\!/}$ (85) and $A_\perp(126) \simeq 1.5\ A_\perp(85)$. We can estimate that for a melting pressure P and

TABLE 2

ELASTIC CONSTANTS

Volume (cm^3/mole)	c_{11}	c_{12}	c_{13}	c_{33}	c_{44}
	(all in units of 10^8 dyne/cm^2)				
21	4.01	2.25	1.29	4.98	1.59
20.5	4.74	2.66	1.49	5.91	1.74
20	5.59	3.14	1.73	7.00	1.92
19.5	6.60	3.71	2.01	8.30	2.11
19	7.79	4.38	2.32	9.84	2.34
18.5	9.19	5.17	2.69	11.66	2.61
18	10.85	6.10	3.12	13.83	2.96
17.5	12.81	7.20	3.62	16.39	3.33
17.4	13.24	7.44	3.72	16.95	3.43
17	15.12	8.49	4.19	19.42	3.77
16	21.06	11.83	5.61	27.28	4.93

propagation either parallel or perpendicular to the c-axis,

$$A(P) = (P/85)^{1.05} A(85) \qquad \text{(A2-3)}$$

Now,

$$\tau = 3\kappa V/C_V v_D^2 , \qquad \text{(A2-4)}$$

so we have finally:

$$\tau_U = \frac{1.73\times10^{-8}}{v_D^2} V \left(\frac{\Theta_D}{T}\right)^3 \left(\frac{P}{85}\right)^{1.05} e^{\Theta_D/2.58T} , \qquad \text{(A2-5)}$$

$$\tau_U = \frac{3.57\times10^{-7}}{v_D^2} V \left(\frac{\Theta_D}{T}\right)^3 \left(\frac{P}{85}\right)^{1.05} e^{\Theta_D/4.62T} . \qquad \text{(A2-6)}$$

Equations (A2-1), A2-5) and (A2-6) are plotted on figure 4.

The total relaxation time τ is calculated from the following relations of Hogan et al. and Guyer and Krumhansl (1966):

(a) Boundary scattering region ($v_D\tau_N >> d$, $v_D\tau_U >> d$)

$$\tau = \alpha d/v_D \text{ where } \alpha \gtrsim 1. \qquad \text{(A2-7)}$$

(b) Poiseuille flow region ($v_D\tau_N << d$, $\tau_U >> d^2/v_D^2\tau_N$)

$$\tau = \frac{5}{32}\, d^2/v_D{}^2 \tau_N . \qquad \text{(A2-8)}$$

(c) Umklapp region ($\tau_N << \tau_U$, $\tau_U << d$)

$$\tau = \tau_U . \qquad \text{(A2-9)}$$

The total relaxation time τ is shown for a cell width d = 1 cm by the dashed lines in figure 4 after interpolating equations (A2-7) - (A2-9).